INFLUENCE OF MULTI-ION SUBSTITUTION ON PHYSICOCHEMICAL AND BIOLOGICAL PROPERTIES OF HYDROXYAPATITE

Ph.D. Thesis

NIMU CHAND REGER

ID No. 2014RMT9015

Department of Metallurgical and Materials Engineering
Malaviya National Institute of Technology Jaipur

August, 2019

Influence of Multi-ion Substitution on Physicochemical and Biological Properties of Hydroxyapatite

Submitted in

fulfilment of the requirements for the degree of

Doctor of Philosophy

by

Nimu Chand Reger
2014RMT9015

Under the supervision of

Prof. A. K. Bhargava and **Dr. Vamsi Krishna Balla**

Department of Metallurgical and Materials Engineering
Malaviya National Institute of Technology Jaipur, India

August, 2019

This thesis is dedicated as tribute to my father late Shri Laxmi Narayan Reger my mother late Mrs. Shanti Devi, for their unconditional love and encouragement.....

DECLARATION

I, NIMU CHAND REGER, declare that this thesis titled, **"INFLUENCE OF MULTI-ION SUBSTITUTION ON PHYSICOCHEMICAL AND BIOLOGICAL PROPERTIES OF HYDROXYAPATITE"** and the work presented in it, are my own. I confirm that:

- This work was done wholly or mainly while in candidature for a research degree at this university.
- Where any part of this thesis has previously been submitted for a degree or any other qualification at this university or any other institution, this has been clearly stated.
- Where I have consulted the published work of others, this is always clearly attributed.
- Where I have quoted from the work of others, the source is always given. With the exception of such quotations, this thesis is entirely my own work.
- I have acknowledged all main sources of help.
- Where the thesis is based on work done by myself, jointly with others, I have made clear exactly what was done by others and what I have contributed myself.

Date: Nimu Chand Reger

CERTIFICATE

This is to certify that the thesis entitled "**Influence of Multi-Ion Substitutions on Physicochemical and Biological Properties of Hydroxyapatite**" is being submitted by me to the Malaviya National Institute of Technology Jaipur for the award of Doctor of Philosophy in Metallurgical and Materials Engineering, is a bonafide record of original research work carried out by me. The content of the thesis has been checked using software "plagiarism Detector".

I have incorporated all the suggestions/queries/changes/raised by the examiners in the thesis evaluation report

(**NIMU CHAND REGER**)

This is to certify that the above statement made by the candidate is true to our knowledge.

(**Prof. A. K. BHARAGVA**) (**Prof. Dr. V.K. BALLA**)

Ph.D. Viva-voce examination of Mr. Nimu Chand Reger, Ph.D. scholar, was held on .....in the seminar/committee hall/room of the dept of Metallurgical and Materials Engineering, MNIT Jaipur. The candidate defended the viva-voce successfully to the satisfaction of oral defense committee. The committee recommends for the award of Doctor of Philosophy (Ph.D.) degree.

Signature of Supervisors Signature of External Examiner

ACKNOWLEDGEMENTS

There are so many people that I would like to thanks for helping me to bring this thesis to completion. My bottom of heart thanks go to Mr. Prem Rawat Ji (International Peace Ambassador) for providing internal energy as and when required. My sincere thanks with deep gratitude go to my Ph.D. Supervisor Dr. A. K. Bhargava (Professor, Department of Metallurgical and Materials Engineering, MNIT Jaipur) for his supervision and guidance during the entire Ph.D. work. Further, I am also grateful to my external supervisor Dr. Vamsi Krishna Balla (Senior Scientist, CSIR-CGCRI, Kolkata) for his scientific and constructive suggestions. My heartfelt thanks go to Dr. Biswanath Kundu for providing the experimental facilities at his laboratories. A special word of thanks also goes to Prof. I. K. Bhatt (former Director, MNIT Jaipur), Prof. Udaykumar Yaragatti (Director, MNIT Jaipur), Prof. Kamal Das Gupta (Ex. Director, CSIR-CGCRI) and K. Murlidharn (Director, CSIR-CGCRI) for permitting me for research work. My honest thanks go to Prof. Upendra Pandel (Ex. HOD, MME) and Dr. R. K. Duchaniya, DPGC convener of the department for their kind support for administrative permissions.

Thanks also go to Prof. Ashok Sharma, Prof. P. R. Soni, Dr. K. L. Narang, Dr. S. K Gupta, Late Prof. R. K Yadav, Dr. N.C. Updahhya, Dr. V. K. Sharma, Dr. Krishna Kumar for their motivation during research work. Heartfelt thanks also go to DREC members, i.e., Prof. C. P. Sharama, Prof. M. K. Banerjee, Prof. R. K. Goyal, Dr. Y. V. S. S. Prasad, Dr. Vinod Kumar, Dr. Vijay N. N. for their valuable suggestions and guidance as and when required. Dr. Deep Singh (Librarian, MNIT Jaipur) is also acknowledged for his help. I would also like to acknowledge my sincere thanks to Dr. Mitun Das, Dr. Someshwar Dutta, Dr. Gangadharan, Dr. Jui Chakraborty, and Dr. Subrata Dasgupta (Senior Principal Scientist, CSIR CGCRI Kolkata) for their scientific and experimental guidance.

Technical staffs at both the places Mr. R.M. Vairagi, Mr. Vidya Sagar, Mahesh Chand Bairwa, Mr. Lal Chand Kumwat, Mr. Nathu Singh Solanki, Mr. Lala Ram (MNIT Jaipur). Mr. Susmit dutta, Ms Anuradha Jana, Itishree Ratha, and Nand Lal Dampat of CGCRI Kolkata are also acknowledged for their help.

I would like to thank some of my friends and colleagues (of both campuses) like Mr Sandeep Shekhawat, Dr. Mayur Shukla, Dr. Arnab Mahato, Dr. Bavya Devi K, Dr. Mathew Joy,

Dr. Pramod Kumar Sain, Dr. Pranav Katiyar (IIT Kanpur), Dr. Shrikant, Mr. Mukesh Choursia, Dr. Rini Singh, Miss Bhawna, Sourabh Sharma, Dr. Shashank Vyas, Mr. Vivek Yadav, Rajendra Falwaria, Nishant Chawla, Mr. Pradeep Mahawar, Divansh Agarwal who have imparted skills and supported me with their understanding, suggestions, encouragement and support.

I would also like to acknowledge the financial support provided by MHRD, Government of India (from 24 July 2014 to 24 July 2018) and TEQIP phase-3 MNIT Jaipur (from 25 July 2018 to 31 December 2018). The author also put kind thanks to Council of Scientific and Industrial Research (CSIR), New Delhi (Grant award number: ESC0103, MLP0203).

Last but not the least, I would like to express my thanks to my wife Sarla Verma, daughters Lawanya Verma and Aarghya Verma for their endless love, motivation, encouragement and kind support during this scientific learning and putting efforts in the biomaterial area for noble cause.

My heartfelt thanks go to grandfather in-law Mr. Bhom Ji Verma, my grandmother in-law Mrs Bila Devi, my Father in-law Mr. Hanuman Sahay Verma, Mother in-law Mrs Chanda Devi for taking care of me and my family during financial crises. My deep heartfelt thanks go to my brother Mr. Harkesh Kr Mourya, sister in-law Ms. Priynka, sisters Geeta-Shardha-Suman and my all brother in-laws, my aunty Ms Bhawri Devi w/o Mr. Prabhu Dayal and other family members and colleagues for all their good wishes of encouragements and support over the last few years which will always be remembered with deep gratitude.

ABSTRACT

Hydroxyapatite [HA,$Ca_{10}(PO_4)_6(OH)_2$] is the most popular among calcium phosphate (CaP) based bioceramics and it is widely used as coatings on metal implants, as bone filler/scaffolds, drug delivery systems, and bone tissue engineering due to its outstanding biocompatibility, good bioactivity and high osteoconductivity. In view of these, in the present work an attempt has been made to assess the physico-chemical, dielectric/photoluminescence (PL) and biological properties such as *in vitro* cytotoxicity, bioactivity and ion release of multi-ion doped HA. As synthesis, HA has been incorporated with Sr^{+2}, Zn^{+2}, Ag^{+} and F^{-} ions using high energy milling. In order to optimize the combination and concentration of doping elements design of experiment (DOE) based on Taguchi method has been adopted. The pure HA was synthesized by wet precipitation method. The multi-ion doping of HA with Sr^{+2}, Zn^{+2}, Ag^{+} and F^{-} was carried out successfully using high energy ball milling. Transmission electron microscopy (TEM) revealed that the particle size of both undoped and doped HA powders varied between 20 nm and 600 nm. However, few particles with size of 1.2 μm were also observed. Some nanoparticles have been observed to be single crystallite while the others with sub-grains having crystallite size as small as 8-10 nm. The values of d-spacing of doped HA crystallites were found slightly different than those of pure HA which may be attributed to the presence of dopants in the HA lattice. Energy dispersive spectroscopy (EDS) clearly confirmed the presence of doping ions in the HA structure. The % crystallinity of synthesized HA was found to increase with increasing calcination temperature which peaked to 93% at 1250 °C. It was investigated that the % crystallinity and crystallite size of HA decreased after the addition of multi-ions dopants into HA structure. Amongst the dopants used, Sr showed maximum influence on crystallinity and crystallite size of HA. DOE analysis showed clear interaction between dopants at binary level doping, while ternary and quaternary doping of elements did not exhibit any interaction. *In vitro* cytotoxicity and ion release test showed that for early culture period of 3 days, all concentrations of dopants exhibited significantly higher cell viability than pure HA, except 5 wt.% F. However, for long-term cytocompatibility the lower concentration of some dopants are found suitable in giving inhibitory effect. Strong binary interaction was found between cation dopants (Sr, Zn and Ag) than between cation and anion dopant (F). Some doped HA compositions showed up to 2-fold increase in the early-stage cell proliferation compared to pure HA. Similarly, the

composition of multi-ion doped HA to achieve excellent cell viability during initial culture period would be 5Sr-5Zn-2.5Ag and 5Sr-2.5Zn-2.5Ag with or without 2.5 wt.% F. However, for stable and positive later-stage cell proliferation on binary ion doped HA, the concentration of all dopants appears to be ≤ 2.5 wt.%. Finally, for enhanced long-term cytocompatibility the compositions of multi-ion doped HA would be 2.5Sr-2.5Zn-2.5Ag, 2.5Sr-5Zn-2.5Ag and 5Sr-2.5Zn-2.5Ag with up to 5 wt.% F. *In vitro* bioactivity experiments revealed that HA composition with high Sr and Zn concentration exhibit excellent bone-like apatite layer formation. However, high concentration of Ag and F found to have limited bioactivity. The dopants also increased the sintered density of HA and refined its grain size as well. These results can be used to tailor the composition of multi-ion doped HA to achieve desired early-stage and long-term biological performance. However, further investigations are required to evaluate their antibacterial properties followed by *in vivo* trails for potential orthopedic and dental applications. The dielectric constant of the doped HA samples (except L5) increased significantly at the frequencies below 1 kHz. However, thereafter it decreased slightly with increasing frequency. At a given frequency, its value increased from 8.5 for pure HA to 12.3 for L6 sample. From PL study, it was investigated that Sr ion increases the PL intensity gradually while the addition of Zn increases the PL intensity significantly. The addition of F and Ag ions upto 2.5 wt.% contributes more positive influence as compared to same concentration of Sr ions.

TABLE OF CONTENTS

LIST OF FIGURES

LIST OF TABLES

LIST OF ABBREVIATIONS AND SYMBOLS

HA : Hydroxyapatite

CaP : Calcium Phosphate

TJR : Total joint replacement

THR Total Hip replacement

TKR : Total Knee replacement

XRD: X-Ray diffraction

FTIR : Fourier transformation infrared spectroscopy

DOE : Design of experiments

SS : Stainless Steel

PMMA: Poly Methyl Methacrylate

UHMWPE : Ultra high molecular weight polyethylene

ASTM : American Society for testing and Materials

ELI : Extra-Low Interstitial

CpTi : Commercial Pure Titanium

PE : Polyethylene

PAN : Polyacrylonitrile

PTFE : Polytetrafluoroethylene

COF :Coefficient of fiction

M-on-PE : metal on polyethylene

C-on- C : Ceramic on ceramic

ACP amorphous calcium phosphate

TCP Tricalcium phosphate

OHA oxyhydroapatite

OA oxyapatite

MAPS : MacroPlasma Spray Technique

TTCP : Tetracalcium phosphate

Si-HA : Silicon Substituted hydroxyapatite

NMR : Nuclear Magnetic resonance

ALP : alkaline phosphatase

LPS : Lipopolysaccharides

TEM : Transmission Electron microscopy

SBF: Simulated Body fluid

E Coli : Escherichia Coli

S. aureus: Staphylococcus

nHAp : Nano hydroxyapatite

CNT: carbon nano tube

H_3PO_4 : Orthophophoric acid

ZnO : Zinc oxide

ANOVA Analysis of variance

JCPDS : Joint committee on powder diffraction standards

ICDD : International Centre for diffraction data

FWHM : Full width half maximum

KBr: Potasium Bromide

UV : Ultraviolet

SAED: selected area Electron diffraction

FBS : Fetal Bovine Serum

DMEM : Dulbecco's Minimum Essential Medium

DMSO : Dimethyl sulfoxide

FESEM : Field Emission Scanning Electron Microscope

ICP-MS : Inductively Coupled Plasma Mass Spectrometry

HRTEM High Resolution Transmission electron microscopy

Energy dispersive spectroscopy (EDS)

K_{IC} : Fracture toughness

GPa : Gega pascal

OH^- : Hydroxyl ions

X_c : % crystallinity

CHAPTER 1

INTRODUCTION

Biomaterials are manmade materials used as devices for internal reconstruction, repair or replacement of diseased or damaged bones, tissues or other body organs and function in contact with living tissues [1]. In recent past, there is great boom observed in the field of orthopedic biomaterials owing to their direct influence to the health of human on the face of this earth. Further, biomaterials can be classified into four main categories namely metals, polymers, ceramics, and composite materials. Orthopedic reconstructive surgery typically involves the use of prosthetic devices to repair or replace damaged or diseased musculoskeletal tissue in order to relieve pain and restore function for patients suffering from bone fractures, tumors, deformities, arthritis, osteoporosis, etc. [2].

Moreover, annually approximately 2.9 million joint replacement surgeries are being carried out globally that includes more than 1.4 million hip, 1.1 million knee, and over 100,000 shoulder replacements [3]. These data clearly demonstrate the potentially high demand for orthopedic implants. Typically, these implants are made of biocompatible metallic materials like 316L stainless steel, cobalt base alloys, and titanium alloys. These materials are very popular for making artificial hip and knee joints, bone plates, screws, etc. and dental implants because of excellent mechanical properties coupled with good corrosion resistance. However, metallic bioimplants are bioinert, and suffer from material loss over a period of time in biological environment resulting in toxic effects. To overcome these problems such implants are often coated with hydroxyapatite (HA) [$Ca_{10}(PO_4)_6(OH)_2$], a bioactive material. It has been demonstrated that a significantly higher number of cells adhere to HA coated implants than uncoated counterparts [4].

Hydroxyapatite is most popular among calcium phosphate (CaP) based bioceramics and is also used in maxillofacial, dental and bone substitutes due to its outstanding biocompatibility, good bioactivity and high osteoconductivity [5]. Furthermore, HA finds uses as bone filler, drug delivery systems, bone tissue engineering and scaffolds soft tissue repairs [6]. Synthetic HA is known for its ability to promote cellular functions due to its close similarity in composition to that of inorganic part of natural bone and teeth [7]. Though, synthetic HA possess good biological properties and finds numerous applications in bulk form but still it suffers from some

shortcomings such as (a) low fracture toughness (K_{IC}~0.5 MPa.$m^{1/2}$) (b) high crystallinity (which restricts its dissolution in bio environment) and (c) lack of osteoconductivity.

The osteogenic capacity of synthetic HA is considered to be inadequate for some applications as compare to that of natural hard tissue that can result in poor tissue in-growth *in vivo* [5,7]. The life of the bioactive HA coated implants still limited to about 7-10 years, vis-à-vis the need for repetition of expensive, complicated painful surgery demands research on the development of doped HA with improved properties. Many researchers have made attempts to overcome some of the limitations of HA as reviewed in [5]. A large number of comprehensive studies have revealed that doping of HA with trace ions have strong effects on physicochemical properties, dissolution kinetics as well as biological response [8] because most of these trace ions are found in natural hard tissue. Owing to these advantages, doping of metal ions into HA has received much attention as this approach can mimic natural bioapatite which contains trace ions such as Zn^{2+}, Sr^{2+}, Mg^{2+}, Ag^{+}, F^{-}, Na^{+}, K^{+}, CO_3^{2-}, etc. These trace ions play a vital role in biochemical reactions associated with the bone metabolism and subsequently in bone in-growth probably due to its amorphous nature of bone mineral caused by these trace ions.

Among the various doping ions incorporated into HA structure, Sr^{2+}, Zn^{2+}, Ag^{+} and F^{-} have been studied extensively and found very effective in enhancing mechanical properties and phase stability, imparting antibacterial properties and improved biological response [9–11]. Keeping in mind the vital role that these doping ions play in combination while enhancing biological activity of HA, a systematic study on the effect of the multi-ion dopants on physicochemical, biological and functional properties of HA seems to be interesting. So it is proposed to co-substitute Sr^{2+}, Zn^{2+}, Ag^{+} and F^{-} ions in controlled amount. Strontium ions often used for treatment of osteoporosis because of its osteoblastic stimulating effect vis-à-vis tendency to inhibit osteoclastic activity [12]. It also increases mechanical strength of bone without giving any toxic effect even when present in high amount. Presence of Zn^{2+} ions in the body helps in pathological calcification and stimulating bone formation by promoting osteoblast activities [13]. The Zn^{2+} ions also counteract the effect of toxicity arises in presence of excessive Ag^{+} ions which is commonly used as doping element to contribute to antibacterial property. Addition of F^{-} increases thermal and chemical stability of HA [14]. Most of the previous investigations have been focused on studying the influence of single, binary and ternary ion doping into HA on physicochemical, biological and functional properties. Studies on multi-ion

doping of HA are in sparse though multi-ion doping of HA can impart multifunctional properties to HA and can compensate for any deleterious effect of a particular dopant. Report on quaternary co-doping of HA evaluating their influence on physicochemical, biological and functional properties of HA is hardly found so far.

Therefore in the present work, four doping elements namely, Sr^{2+}, Zn^{2+}, Ag^{+} and F^{-} have been incorporated into HA to evaluate their influence on physicochemical, biological and functional properties. The phase purity, crystallinity (%) and crystallite size have been assessed using x-ray diffraction (XRD). Functional group analysis was performed using Fourier transformation infrared (FTIR) spectroscopy. The hardness and density measurements of the sintered pellets were carried out to get information about hardness and soundness, respectively, of the samples. Electron microscopy was used to find the morphology and size of synthesized undoped and doped HA powder. The functional properties (dielectric and photoluminescence) and *in-vitro* biological properties were also evaluated. In order to optimize the combination and concentration of these doping elements design of experiment (DOE) based Taguchi method, L9 orthogonal array, was adopted. Using DOE the present investigation enable identification of individual, binary, ternary and quaternary effects of ion doping on physicochemical, biological and functional properties of HA. Based on these effects one can manipulate the composition of HA with desired combination of properties such as strength, bioactivity and degradation to suit variety of implant applications. This thesis consists of five chapters. The chapter 1 is focused on background, overview, and objectives of the work. The chapter 2 is devoted on exhaustive literature review giving studies on influence of substituent ions in HA on physicochemical, biological and functional properties. It also gives insight into clinical performance of doped HA and HA coated implants. Chapter 3 is describing the materials and methods used for synthesis and characterization of pure and multi-ion substituted hydroxyapatite. Chapter 4 gives the findings of the work and discussion. The last chapter 5 consists of conclusions of the work carried out and suggestions for future work.

CHAPTER 2

LITERATURE REVIEW

Among different biomaterials, ceramic biomaterials were introduced quite late in the 1970s for orthopedic applications when failures of metallic materials namely, 316L stainless steel (SS), Co-Cr-Mo alloy, titanium and its alloys and polymers (poly methyl methacrylate, ultra high molecular weight polyethylene etc.) have been reported worldwide [15]. Consequently concentrated efforts have been initiated to develop ceramic materials specifically calcium phosphates (CaPs) in an attempt to find good alternatives with excellent bone in-growth properties and bioinertness. In the category of bioceramic materials both bioactive and bioinert ceramics have been used in biomedical field. A bioinert material, is one which does not illicit a reaction with the surrounding physiological tissue upon implantation. However, bioactive materials allow tissue in-growth and induce specific biological response (the so called osteoconductivity) at its interface, thus enabling the formation of bridge between the tissues and artificial biomaterial.

Hydroxyapatite (HA) a special calcium phosphate (CaP) based bioceramic material that is used extensively to improve the integration of femoral implants of total hip replacement. HA appears to be the most promising biomaterial due to its outstanding biological properties such as no cytotoxicity, lack of inflammatory response and absence of immunological reactions. The chemical composition and biocompatibility of HA resemble those of natural bone. Consequently, when HA comes in contact with physiological fluids, a chemical reaction towards the production of newly formed bone takes place, i.e. the process also termed as osteoconductive. Bioactivity is related to a modification of the surface of a material with formation of naturally induced; biologically equivalent HA as a result of dissolution, precipitation and ion exchange reaction with the physiological environment.

2.1 Historical developments of biomaterials

There are many kinds of materials with different application potential. In this perspective, biomaterials stand out because of their ability to remain in contact with the human tissues. The use of biomaterials to help repair and augment the body has been documented for thousands of years[16–18]. Before the 20th century, naturally-derived materials were used. For example,

shaped wood was used as structural replacements for tissues lost during trauma or disease, whilst in ancient Egypt, seashells were used as teeth replacements [19]. In the early 20th century, synthetic polymers, metallic alloys and ceramics found to replace naturally-derived materials. Rapid advancements in the technology and increased efficacy led to wide range of applications of these materials as dental restoratives, artificial hip joints and contact lenses. Advancements in molecular biology in the 1970s, genomics in the 1990s and proteomics in the 2000s contributed significantly to the design and development of current range of biomaterials. Biomolecular enhancement of biomaterials refers to their bioactive components, which utilize well-established molecular pathways to elicit a biological response. A commercially example is the INFUSE Bone Graft device marked by Medtronic, which combines bone morphogenetic protein along with synthetic components [17].

The historical development of bone-related biomaterials, with a focus on weight-bearing, total joint replacement implants, is described here in brief. Arthroplasty, a surgical replacement of joints [20], initially made use of SS for load-bearing TJR implants. 316L SS (ASTM F138) comprising a ferrous matrix alloyed with carbon, molybdenum, nickel and chromium, was used primarily for temporary devices such as hip nails, fracture screws and plates. However, with the rise in TJR surgery, it became evident that the very high modulus of SS was not suitable due to problems such as stress-shielding and corrosion. Cobalt-chromium-molybdenum (Co-Cr-Mo) alloys (ASTM F75 and F799) were then developed, but high modulus and biocompatibility issues of this material is still a major concern for load-bearing applications. Bone cements were used to fix the implant into bone. In order to resolve issues regarding the adverse effects of bone cement wear particles that may ultimately require revision surgery [21], the concept of uncemented implants was developed in the 1960s [22,23]. Uncemented implants rely on biological fixation using natural bone cells of the body. Bioactive compounds, such as CaP or HA , when coated on metallic implants, were found to increase bone cell attachment and proliferation [24]. Research on the positive effects of silicon (Si) on bone metabolism resulted in the development of Si-substituted calcium phosphates in the 1990s [23]. Backtrack to the mid-1970s, Ti-alloys started to gain popularity due to their low modulus, being closer to that of bone, combined with good levels of specific strength, biocompatibility, superior osseointegrative ability and higher corrosion resistance. Commercially pure titanium (CpTi; ASTM F67) was the first Ti product used for these implants due to its naturally-occurring surface passivation oxide

film which provides corrosion resistance and reduces the risk of metal ion release [3,25,26]. Commercial pure Ti (CpTi), however, exhibits limited specific strength and hence its uses are limited to dental implants, pacemaker cases and hip cup shells.

The need to improve on strength for load-bearing applications, such as for TJR, led to the development of an alloy originally developed for aerospace applications, *i.e.* Ti-6Al-4V extra-low interstitial (ELI) alloy (ASTM F136) made from Ti with 6 wt% Al and 4 wt% V. It exhibits an elastic modulus of ~ 110 GPa which is half that of 316L SS. Whilst it has been used successfully for TJR, it was found that V is cytotoxic and causes adverse tissue reaction. Therefore, iron and niobium were introduced in place of V, with the development of Ti-6Al-7Nb and Ti-5Al-2.5Fe alloys. Other alloys were also developed incorporating Al additions, such as Ti-15Mo-2.8Nb-3Al and Ti-15Mo-5Zr-3Al. However, further studies revealed that both V and Al ions released from these alloys into the body could cause long-term health problems, such as osteomalacia (softening of the bones), Alzheimer's disease (a type of dementia) and peripheral neuropathy (peripheral nerve damage). These circumstances led to developments of new and improved orthopaedic implant materials [15,20,27]

2.2 Current materials used in implants

So far four major classes of materials, *i.e.* polymeric, metallic, ceramic and composite, have been used as biomaterials [28]. Current advancements in nanotechnology [29–31], tissue engineering [32] and biology allow for more flexibility and creativity in biomaterial design and the generation of new composites. Materials can now be enhanced biologically in order to exploit particular, well-established, molecular pathways. For example, bio molecule-based surface modifications may be performed on nitinol, a nickel titanium metallic alloy that exhibits shape memory effect, with the aim of increasing its efficacy for osseointegration [33]. In the field of tissue engineering, three-dimensional scaffolds with tailored architecture may be made using artificial (bioactive glass) or natural materials (biodegradable polymers) to control the proliferation and differentiation of premature osteoblasts [17,20,32,34]. Further, polymers are commonly used as inter-positional cementing materials between bone tissues and implant surfaces and can act as articulation bearing surfaces because they exhibit appropriate creep resistance, wear rates and yield strength. In these applications, certain high density polymers exhibit low wear rates and low coefficients of friction, making them particularly suitable as bearing surfaces. As a fixative for a structural interface, they can be cured *in vivo* and moulded

into shape [35]. Even though there are hundreds of orthopaedic applications and numerous specialties, only a few types of materials dominate the market [16]. Metallic alloys were developed initially to replace long bones as load bearing members and as fracture fixation devices due to their excellent combined properties of biocompatibility and ductility [28]**.** Indeed, the metals and alloys cited in "Historical development of biomaterials" are still in use today, *e.g.* Ti-6Al-4V, Co-Ni-Cr-Mo (ASTM F562) and Co-Cr-Mo (ASTM F75 and F76). Table 2.1 provides a brief overview of biomaterials currently in use and their functions.

Table 2.1 Overview of biomaterials and biomedical implants [34]

Implant	Material
Skeletal system Joint replacements e.g. hip, knee Bone cement Bony defect repair Bone plate for fracture fixation Dental implant	Polyethylene, 316LV (stainless steel; SS), Titanium (Ti), Ti-6%Al-4%V (Ti64 or Ti6Al4V) alloy Poly(methyl) methacrylate (PMMA) Hydroxyapatite (HA) Cobalt-chromium (Co-Cr) alloy, 316LV (stainless steel; SS) Calcium phosphate, polyethylene, Ti, Ti-Al-V alloy, SS
Cardiovascular system Catheter Blood vessel prosthesis Heart valve	Silicone rubber, Teflon, polyurethane Polyurethane, Dacron, Teflon Carbon, reprocessed tissue, SS
Organs Heart-Lung machine Artificial kidney (hemodialyser) Artificial Heart Skin repair template	Silicone rubber Hydrogel e.g. Cellulose, polyacrylonitrile Polyurethane Silicone-collagen composite
Senses Corneal bandage Cochlear replacement Contact lens	Hydrogel, Collagen Platinum electrodes Hydrogel, Silicone-acrylate

2.3 Load bearing implants

There has been significant growth in the science and applications of biomaterials particularly in load bearing total joint replacements (TJR) such as total hip replacement (THR) and total knee replacements (TKR) over the past five decades [36]. Stringent requirements are placed on materials for its use in the biological environment. For orthopaedic applications an ideal material must possess an elastic modulus similar to that of bone, high resistance to mechanical damage, high corrosion resistance, low toxicity, excellent biocompatibility, appropriate wear resistance and thermodynamic stability within the body. Among metallic materials titanium and its alloys (Ti-6Al-4V) have demonstrated their closest fit to the above criteria, being especially true for long-term orthopaedic implantable devices [36,37]. Knee joint is the most common and movable type of joint in the body as illustrated in Fig. 2.1a.

There is a joint cavity present between two smooth articulating bone surfaces surrounded by a body fluid called synovial fluid, which helps to absorb shock and reduce friction during movement of articulating surfaces. This joint gains movement through the contacting point with the surrounding bones, which is common among most of the other joints. The main difference between the synovial joints and others is the presence of the capsule around the surface of the synovial joint, along with the presence of the lubricating fluid (Fig.2.1b). These joints are complex in nature and function under severe cyclic loading conditions. When such natural joints are broken or damaged due to disease, they often need to be replaced totally by an implant device.

For the successful implementation of biomedical implants the interface between tissue and implant surface plays an important and crucial role. Although it has been reported that current implants materials have 10-15 years lifespan in service but still it needs to improve (increase) as a result of more and more young patients need TJR due to change in lifestyle globally [38]. It has been estimated from the data collected on total joint replacements surgery that by the end of 2030, the number of total hip replacements will rise by 174% (572,000 procedures) and total knee replacement is projected to grow by 673% from the present rate (3.48 million procedures) [39].

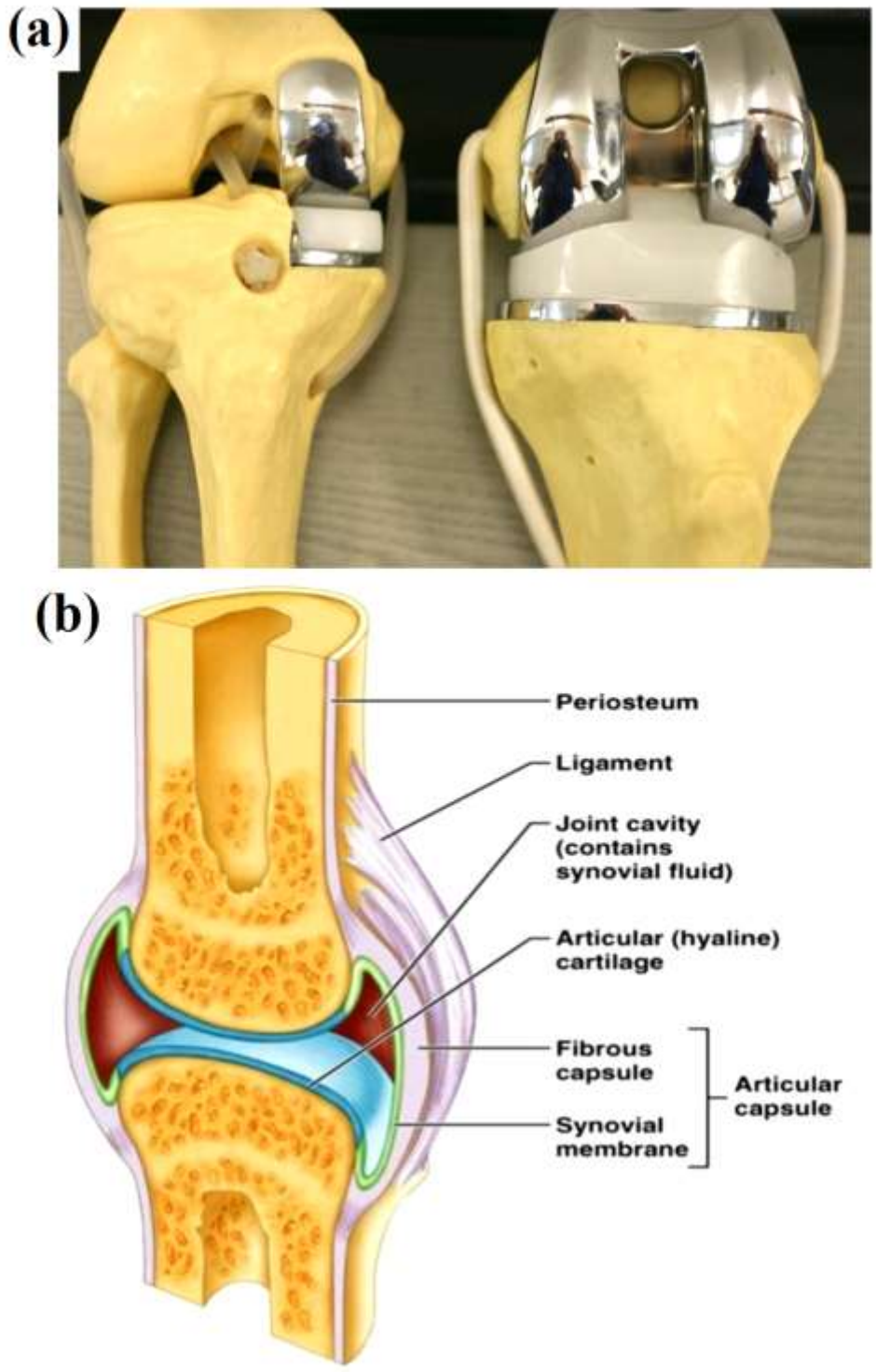

Fig. 2.1 (a) artificial metallic knee implant (b) illustration of synovial joint [40]

2.3.1 Basic structure and composition of bone

Precise knowledge of the physical, chemical, and mechanical properties of natural human bone is critical for the development of bone-like materials. The study of biological apatite (that is, human bone mineral) has been widely investigated in order to understand its chemical composition. Despite significant research, science is still far from producing biomaterials that can entirely substitute for natural apatite. Synthetic HA is a type of calcium phosphate that exhibits similarities to the mineralized mammalian tissues, such as bone and tooth. In this section, the structure and growth of bone are described, with focus on the proliferation and mineralization of bone cells during the early stages of growth. The skeletal system consists of ligaments, cartilage, tendons and bone, accounting for ~ 20% of the body's weight. It functions to protect and support the soft organs of the body, support the body against the pull of gravity, and works with muscles to facilitate body movement. Bone is a mineralized hard tissue found in mammalian bodies. Its structure consists of a framework of collagen fibers, essentially all type I; a mineral matrix, primarily calcium hydroxyapatite; and a small quantity of organic phase composed of mucopolysaccharides and protein polysaccharides, collectively referred to as ground substance or cement.

A Except structure, all bones have nearly the same properties depending upon the relative proportions of the three phases: organic, mineral, and void. *In vivo*, the void phase is filled with cells, cell processes, and fluid. These have not been shown to contribute to either the static or dynamic properties of fully wet bone. Dry bone, of course, has considerably different properties, but these are not relevant to either tissue mechanics or to the selection of materials to augment or replace bone. Bone is a complex, highly structured porous matrix and specialized hard tissue. It is a natural composite material composed of organic component collagen (20 wt%), Carbonate-hydroxyapatite, an inorganic nanocrystalline solid (65 wt%) intimately bonded with collagen and 9 wt % water [16,41–43].The carbonated apatite crystals and organic matrix provide stiffness to the bone, ability to withstand pressure and elasticity and resistance to stress, bending and fracture [34,42]. Besides calcium phosphate, the other minor negatively charged group such as carbonate (CO_3^{2-}), citrate [$(C_6H_5O)^{4-}$], Fluoride (F^-) and hydroxyl ions (OH^-) are also present. Bone has a hierarchical structure (Fig. 2.1) and is inconsistently dense. From the macroscopic point of view, bone can be depicted into two terms. Firstly, Compact (cortical) bone refers to the solid mass of bone, *e.g.* femur which functions to carry a significant share of the skeletal load. Secondly,

Spongy (cancellous) bone is less dense and hence lighter than compact bone. Figure 2.2 represents hierarchal structure of natural bone and this explain how bone regeneration strategy is conducted by the synergistic effect of cells and scaffolds [42].

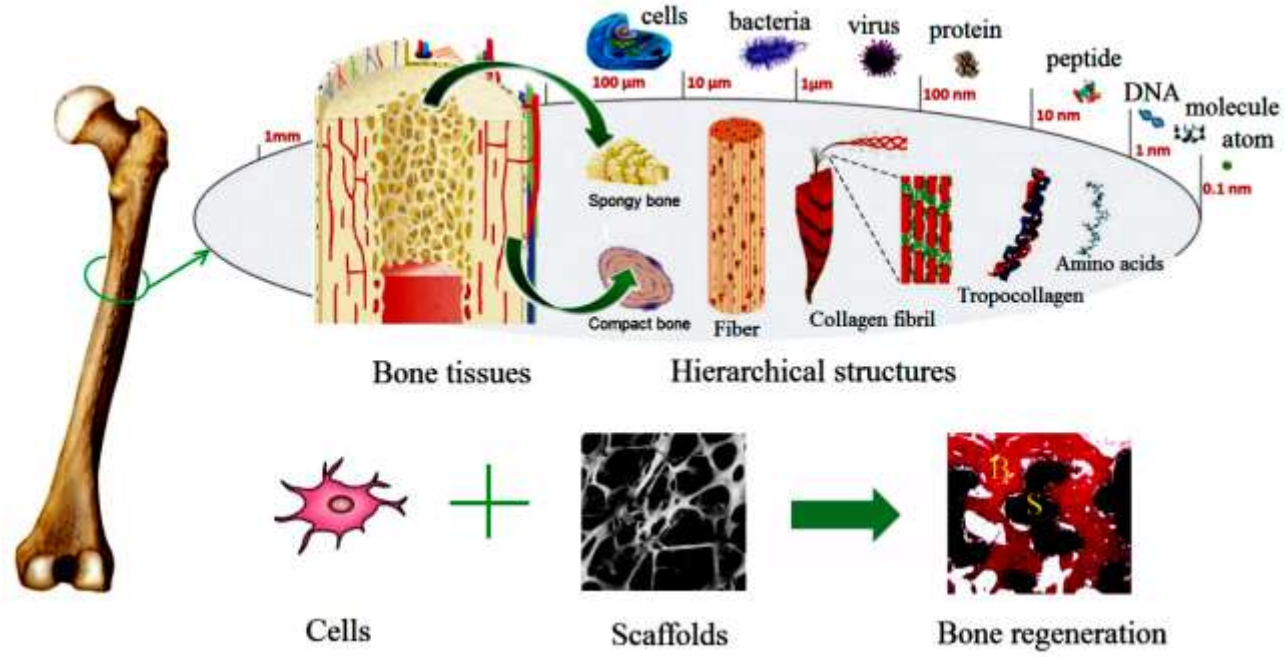

Fig. 2.2 Hierarchal structure of natural bone [42]

The functions of the bone are to give supporting strength and flexibility whilst providing the ability to generate bone marrow. From the microscopic point of view, bone is made up of the basic building blocks called osteon embedded into collagen fibril as shown in Figure 2.2. Each osteon consists of lamellae that are formed by bundling fibers, which are built up by numerous collagen fibrils in an array, as indicated in Figure 2.2. Bone structure is hierarchically organized shown in Figure 2.2, which means that bone displays different structural entities at different length scales or levels such as macrostructure, mesostructure, microstructure and nanostructure, respectively. Further these structures are also denoted in previous research reports by continuum level (or level 0), tissue level (level 1), cellular level (level 2) and molecular level (level 3) respectively [44,45]. The composition of the mineral phase of normal adult human being is shown in Table 2.2.

Table 2.2 Composition of the mineral phase in human bone [46]

Mineral Component Constituents (wt. %)	Chemical Formula	Enamel	Bone
Calcium	Ca^{2+}	36.0	24.5
Phosphorous	P	17.7	11.5
Ca/P molar ratio		1.62	1.65
Carbonate	CO_3^{2-}	3.2	5.8
Sodium	Na^{+}	0.5	0.7
Magnesium	Mg^{2+}	0.44	0.55
Potassium	K^{+}	0.08	0.03
Chloride	Cl^{-}	0.30	0.10
Fluoride	F^{-}	0.01	0.02

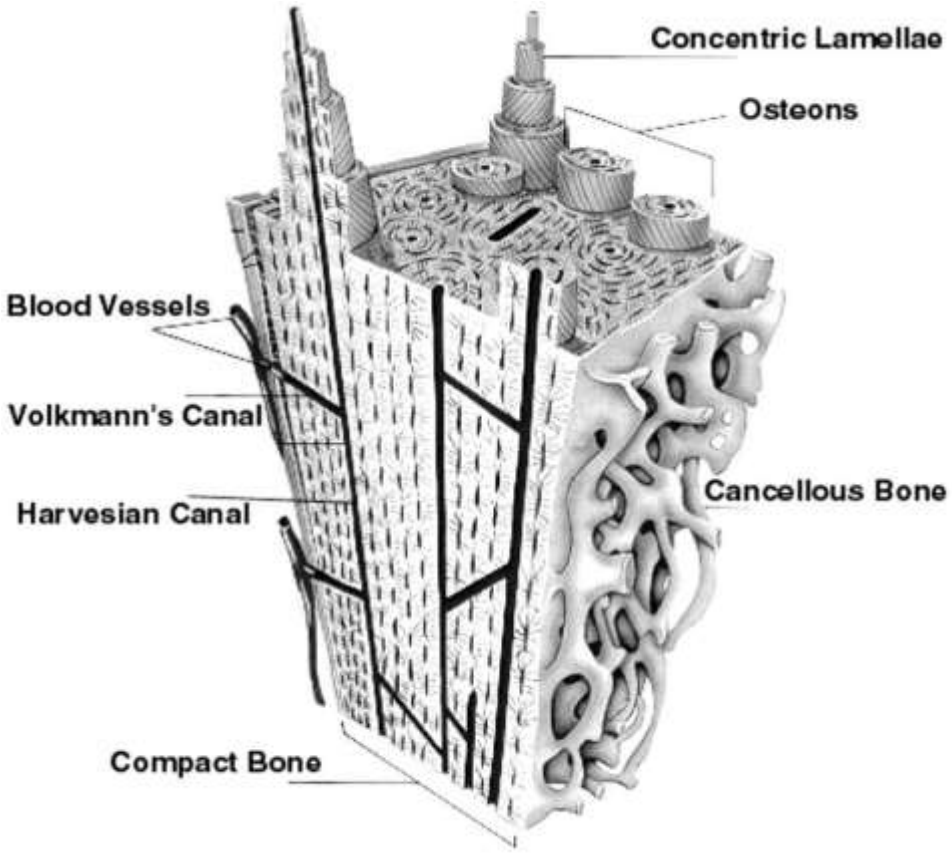

Fig. 2.3 Schematic presentation of compact bone cross-section [37].

Macrostructure (Level 0): generally, bone structure at continuum level the scale of 5 mm and higher, i.e., cortical bone and trabecular bone which can be seen by naked eye without help of any microscope or magnify glass. Porosity of bone also play important role in case of load bearing applications i.e. knee and hip natural bones and cortical bones have a porosity ranging between 5 to 10 % and it is usually found along the exterior shaft of the bone in contrast to this trabecular bone has a porosity ranging from 75 to 95 %. Cortical bone accounts for about 80% of the total skeletal mass while trabecular bone constitutes some 70% of the skeletal volume and a schematic presentation of compact bone cross-section is shown in Fig. 2.3. Cortical bones are comparatively stronger and tougher than trabecular bone forms the outer shell around the trabecular bone in joint and in vertebrae. Trabecular bone found, at the end of the long bones (i.e. femur), flat bones (i.e. pelvis) and cubicoidal bones (i.e., vertebrae). The anisotropic structure of bone exhibits extraordinary mechanical directional properties, displaying both viscoelastic and semi-brittle behavior [47]. The hierarchical structure, length scale and constituents of bone are displayed in Table 3.

Mesostructure (level 1 or tissue level): this type of bone structure at tissue level, the scale bar ranging from 100 μm to 1 mm that cannot seen by naked eyes in contrast to that of cortical and trabecular structures. Cortical bone is composed of osteon (150 to 300 μm in diameter and up to 3 to 5 mm in length) or Haversian systems. These osteon are embedded in a matrix of lamellar bone known as interstitial lamellae [8]. The central cavity inside an osteon is known as the Haversian canal. Haversian canals are typically 40 to 50 μm in diameter and run along the long axis of a bone. Normally blood vessels (15 μm in diameter) as well as nerve terminations are found inside Haversian canals. Volkmann‘s canals are short transverse channels connecting the Haversian canals. These canals also contain blood vessels and probably nerves. The mesostructure of trabecular bone is composed of plates and struts called trabeculae. Sometimes trabeculae appear organized into orthogonal arrays, but they are often more randomly arranged. Each trabecula is about 200 μm thick. Rarely, it is possible to find trabeculae thick enough to contain a blood vessel and some osteon-like structure. Within a trabecula, one can find trabecular packets, which are the product of new tissue formed after remodelling. A typical trabecular packet is about 50 μm thick and 1 mm long [36,47].

Table 2.3 The hierarchical structure, length scale and constituents of bone [16]

Hierarchical Structure	**Length Scale**	**Constituents**
Whole bone	cm-m	Cortical (compact) and cancellous (spongy) bone
Microstructure	10-500 μm	Single trabeculae, osteons, Haversian systems
Sub-microstructure	1-10 μm	Lamellae
Nanostructure	few hundred nanometers - 1 μm	Embedded apatite mineral and fibrillar collagen
Sub-nanostructure	< few hundred nanometers	Molecular structures of constituent elements such as collagen, non-collagenous organic proteins and mineral

Microstructure: generally the structure of bone at cellular level or level-2 is found in the range of 5 to 50 μm further this level of structure can be divided into 2 categories: woven bone and lamellar bone. Woven bone is a poorly organized tissue and may usually be found in adults post fracture injuries. With maturation, the woven bone is converted into lamellar bone. The lamellae are bands or layers, 3 to 7 μm thick, forming an anisotropic matrix of mineral crystals and collagen fibers. Trabecular packets and osteons are formed of lamellae and attached to the bone matrix by cement lines which are favorable for bone formation (osteoblast) and bone resorption(osteoclast) reactions [48]. The mechanical properties of various natural bone parts are shown in Table 2.4.

Table 2.4 Properties of bone [38]

Tissue	**Direction of test**	**Modulus of elasticity (GPa)**	**Tensile Strength (MPa)**	**Compressive Strength (MPa)**
Leg Bones				
Femur	Longitudinal	17.2	121	167
Tibia	Longitudinal	18.1	140	159
Fibula	Longitudinal	18.6	146	123
Arm Bones				
Humerus	Longitudinal	17.2	130	132
Radius	Longitudinal	18.6	149	114
Ulna	Longitudinal	18.0	148	117
Vertebrae				
Cervical	Longitudinal	0.23	3.1	10
Lumbar	Longitudinal	0.16	3.7	5
Spongy bone	Longitudinal	0.09	1.2	1.9
Skull	Tangential	-	25	-
	Radial	-	-	97

Nano structure: bone structure at nano scale level in the range of few nano meter to 100 nm describe under nanostructure level-3. At nano structure three main materials of importance, such as biologic apatite crystals, collagenous and non-collageneous organic proteins. The mature crystals are not needle-shaped, but plate-shaped. Plate-like biological apatite crystals of bone

occur within the discrete spaces within the collagen fibrils, thereby limiting the possible primary growth of the mineral crystals, and forcing the crystals to be discrete and discontinuous. The mineral crystals grow with a specific crystalline orientation in the *c* axes of the crystals are roughly parallel to the long axes of the collagen fibrils. The average lengths and widths of the plates are 50 x 25 nm [36,49].

2.3.2 History of the total joint replacement (TJR)

The development of materials for orthopedic surgery has evolved thorough centuries of research and interdisciplinary cooperation between surgeons and material scientist or engineers. The history of artificial joints and internal fixation of fractures is already very long and documented in various research reports worldwide. In London in 1822 Anthony White (1782–1849) from Westminster Hospital performed the first excision joint arthroplasty [50]. The first surgical principles and techniques for bone fracture treatment developed in the eighteenth and nineteenth century. The first fixation plate was made by Hansmann from Hamburg in 1886 [51]. Professor Themistocles Glück (1853–1942) from Berlin implanted the first artificial knee in 1890 and manufactured and implanted the first artificial hip in 1891 as well. The ivory head was fixed to the bone with a nickel plate and screws [52] . He is also credited for introducing the term arthroplasty in 1902. In 1893 the French surgeon Pean implanted the first artificial shoulder joint. The implant, made of natural, biological materials, lasted for 2 years which is almost incredible [53] . Before Charnley's "low-friction arthroplasty," hip implants were predominating, and most of the development was also concerning the hips. Typically the implants were used as an interposition arthroplasty and made from various materials with unpredictable results. The pioneer of these surgical procedures was renowned American surgeon of Norwegian origins, Marius Smith Petersen (1886–1953). With the introduction of Vitallium interposition implant (Co-Cr-Mo alloy), he achieved the first predictable and lasting results of this type of surgery [54]. In this period surgeons experimented with real bone-joint replacements from various materials. The acrylic implant from brothers Robert (1901–1980) and Jean (1905–1995) Judet from Paris achieved the greatest popularity. It was introduced in 1948. This implant holds the current world record in the implant in vivo durability 51 years [55]. Artificial knees were developed in the same period but they were less successful if compared to hip implants. The reason for the inferior results was probably not in the implants but resulted from inadequate

surgical technique. Contemporary principles of mechanical axis balance and the importance of joint stability evolved only in the mid-1980s. Following the example of Smith-Petersen, Boyd introduced Vitallium (Co-Cr alloy) femoral coating. Similar implants for femoral and tibial part were tested also by others, including Smith Petersen, but without success [56] . In 1957 Walldius published his comparison of hinge knee endoprostheses and resection arthroplasties (Fig. 2.1a). Good results of the hinged knee implant opened a new era of total knee replacements, which prevailed for the next 30 years, in some centers almost to the present days. The study was a landmark for another reason. It was the first one with pain as the indication for the implantation of an artificial joint [57]. Until then, limited range of movements was virtually the only appropriate indication. Following the example of J. Charnleya, in Wrightington Hospital Gunston was the first to used polyethylene against metal in his knee replacement which represented the predecessor of the contemporary condylar type of knee replacements [58] .

Gunston devoted considerable attention to the kinematics of the knee but neglected efficient fixation, which made his implant unsuccessful. Only in 1974, following the example of Freeman's implants, Insall introduced the first successful total condylar knee replacement and developed a surgical technique that was indispensable for this type of knee replacement to function effectively [59] . In the same fashion, implants for other joints were developed. These are, however, much less frequently used today, although the incidence is increasing, especially for the shoulders. Further development of the implants was based on the introduction of new materials, different ways of fixation, advances in implant design, properties and coatings, and new, less invasive surgical techniques [60] . Today the list of materials used for production of artificial joints is very extensive.

Indian history indicates the use of biomaterials dates back in Vedic period. A study of the Rig Veda, for example, shows that Rudra and Marut could straighten the bodies of the crippled, and could provide metallic legs after amputation. The Athrava Veda explains healing of fracture. Sushruta(1000 BC) was considered as the father of Indian surgery. The Indian history also shows the availability of methods of fracture reduction and reduction of dislocations. The records of Charak Samhita (3000 BC) also indicate extensive use of a variety of suture materials for wound repair. Unfortunately this knowledge was forgotten for long period until the advent of modern era when use of gold wire was made as suture material in 1550 and subsequently, the use of gold plate prosthesis for cleft plate in 1565 [1].

Natural Joints

When two or more bones come together at some region and allow one bone to move relative to the other it is called a joint. Joints or articulations are essential parts of skeleton system which impart mechanical support and in most of the cases provide mobility in stiff skeleton. Joints are broadly classified into two groups namely structural (based on structural composition, i.e. interlinked tissue, joint capsule) and functional. The structural and functional joints are further sub-classified into three groups as shown in Fig. 2.4.The structural joints include fibrous joints, cartilaginous joints and synovial joints.

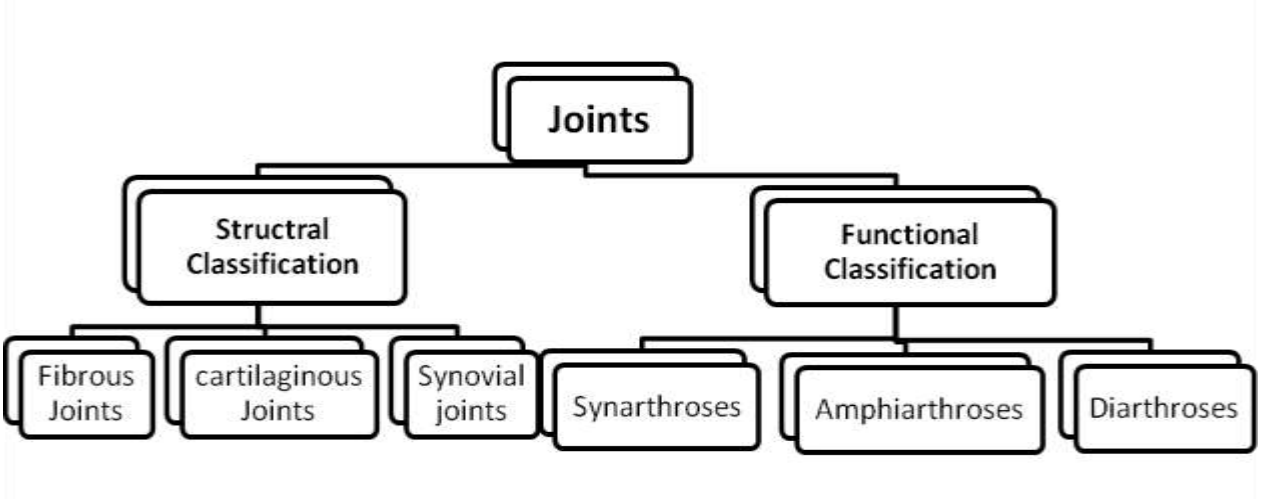

Fig. 2.4 Classifications of natural joints [61]

(a) Fibrous joints

These joints are also called "fixed" or "immovable", because they exhibit no or slight movement. There is no joint cavity and the joints are connected via fibrous connective tissue so these are called fibrous joints.

I. ***Cartilaginous joints*** – These joints are connected entirely by either hyaline cartilage or fibro-cartilage, there is no joint cavity. These joints exhibit little more movement than fibrous joints between bones.

II. ***Synovial joints*** – This joint is the most common and movable type of joint in the body. There is a joint cavity present between two smooth articulating bone surfaces surrounded by a body fluid called synovial membrane (Fig. 2.5.) that helps to absorb shock and reduce friction during movement.

(b) Functional Joints

I. ***Synarthroses*** – This type of joint permits very little or no movement under normal conditions. Here bones are in more or less direct contact and connected through fibrous connective tissue. A typical example of this type of joint is Fibrous joints made of a thin layer of dense fibrous connective tissue that unites skull bones.

II. ***Amphiarthroses*** – In these joints bones are connected by cartilage allowing slight movement. Example - spinal column, rib cage where the ribs connect to the sternum.

III. **Diarthroses** – These joints are also called synovial joints and exhibit free movement. Universal (Ball and socket) joints such as hip joint, knee joint, shoulder joints, elbow joints allow all movements except gliding.

Diarthrodial or synovial joints are found at the articulations of the long bones of the skeleton (hip, knee, shoulder, fingers, etc.). Fig. 2.5 shows typical structure of specific synovial knee joint. Diarthrosis refers to the degree of movement allowed by the joint: freely movable articulations as opposed to either amphiarthroses (slightly movable articulations) or synarthroses (immovable articulations). Synovial refers to the structure of the joint: articular surfaces covered with hyaline cartilage, connected by ligaments and lined by a synovial membrane to create a joint cavity filled with synovial fluid.These synovial joints allow relative motion of the bones. The bone ends meet within a fibrous enclosure termed the joint capsule. The joint cavity is filled with synovial fluid which is viscous and pale yellow in colour. The lubricating factor that allows the relative motion of the bones is believed to be contained within the synovial fluid. Daily use of the synovial joints of the lower limbs - the hips, knees and ankles, involves large ranges of relative motion in multiple directions experiencing loads often as high as six times the body weight during a normal walking cycle. The loads experienced by synovial joints are complex and variable, exceeding 100 million cycles within a lifetime (approx 70 years) without failure**.** Cartilage rubbing on cartilage has extremely low coefficients of friction (COF), μ in the range of 0.003- 0.024, this is much lower than the values attained using any synthetic bearing materials in equivalent situations, the best of which is Teflon (PTFE) rubbing against Teflon which gives a value for COF of 0.04 [62].

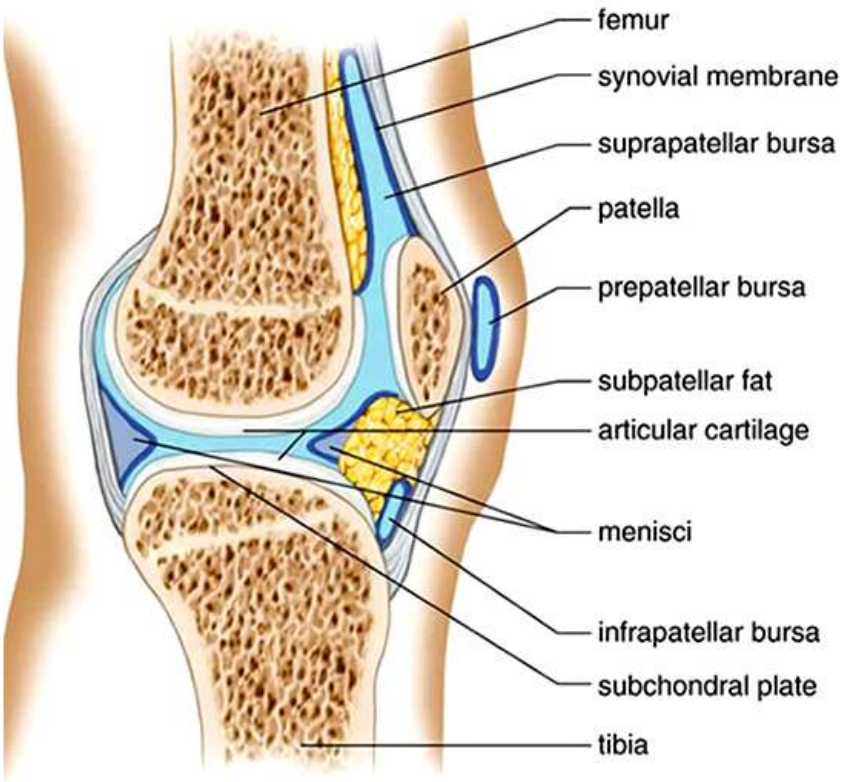

Fig. 2.5 Typical structure of synovial knee joint (lateral view) [40]

The synovial joints are the majority moveable joints in human body and work under grave situations of loading. Due to changes in the life style, increase in the number of road accidents and increased life expectancy, joints' related tribulations increases many fold day by day world-wide. Joints suffer from degenerative (Osteoarthritis) and inflammatory diseases (Rheumatoid Arthritis) that lead to pain or loss in function. The degenerative diseases lead to degradation of the mechanical properties of the bone due to excessive loading or absence of normal biological self-healing process. Among different joints, knee and hip joints are most commonly affected by osteoarthritis. Orthopedic procedure adopted to replace these dysfunctional or arthritic joints with artificial material implants is known as arthroplasty or TJR. Nowadays worldwide apart from total joint replacements revision of these surgeries also increasing tremendously some of possible reasons are displayed in flow chart shown in Fig. 2.6.

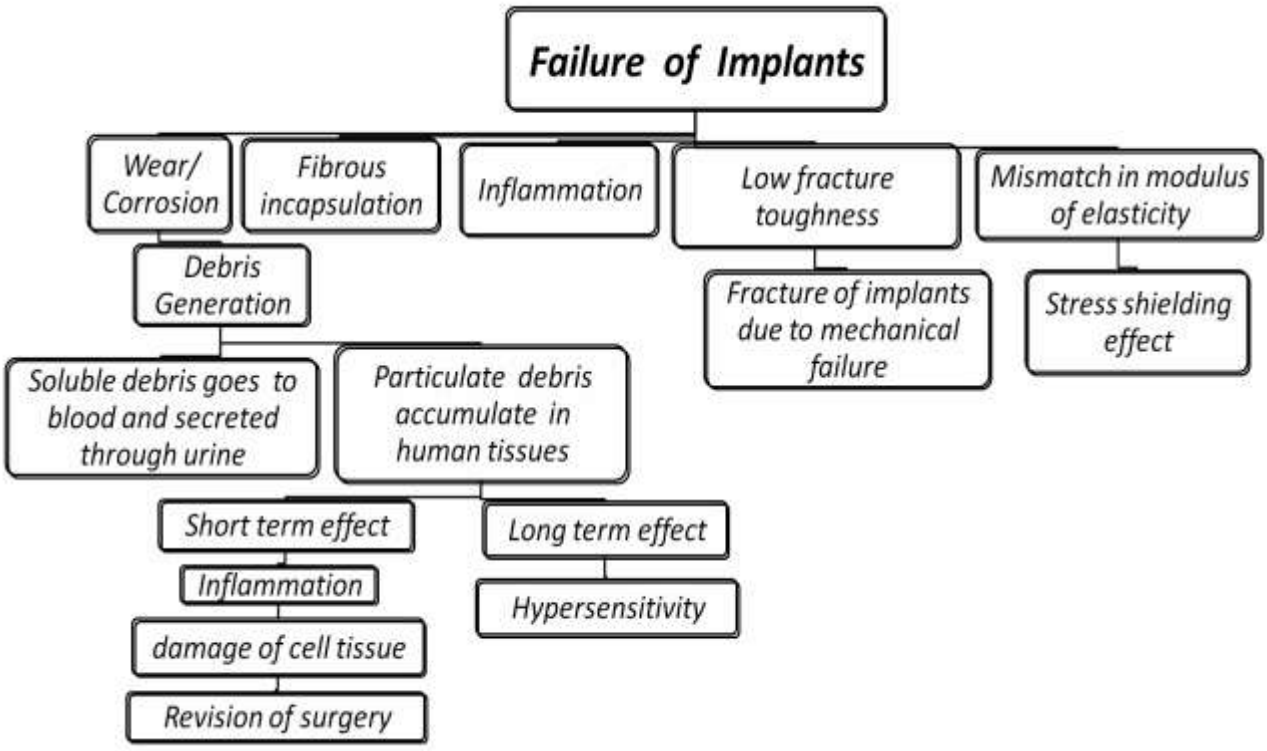

Fig. 2.6 Causes for failure of implants leading to revision of surgery [3]

Total knee replacement surgery done in 1974, following the example of 'Freeman' implants shown in Fig. 2.7 revealed that implants failed due to instability which are confirmed by the X-ray diffraction images. As the number of successful operations has increased, orthopaedic surgery techniques have become standardized and the average age of those receiving hip replacement has reduced. As a result, this magnified the problems of implant failure due to wear and other possible causes are mention in flow chart shown in Figure 2.6. Thus for long term survival there are variety of bearings in different combinations are used to overcome the fewest complications are mention in Table 5.

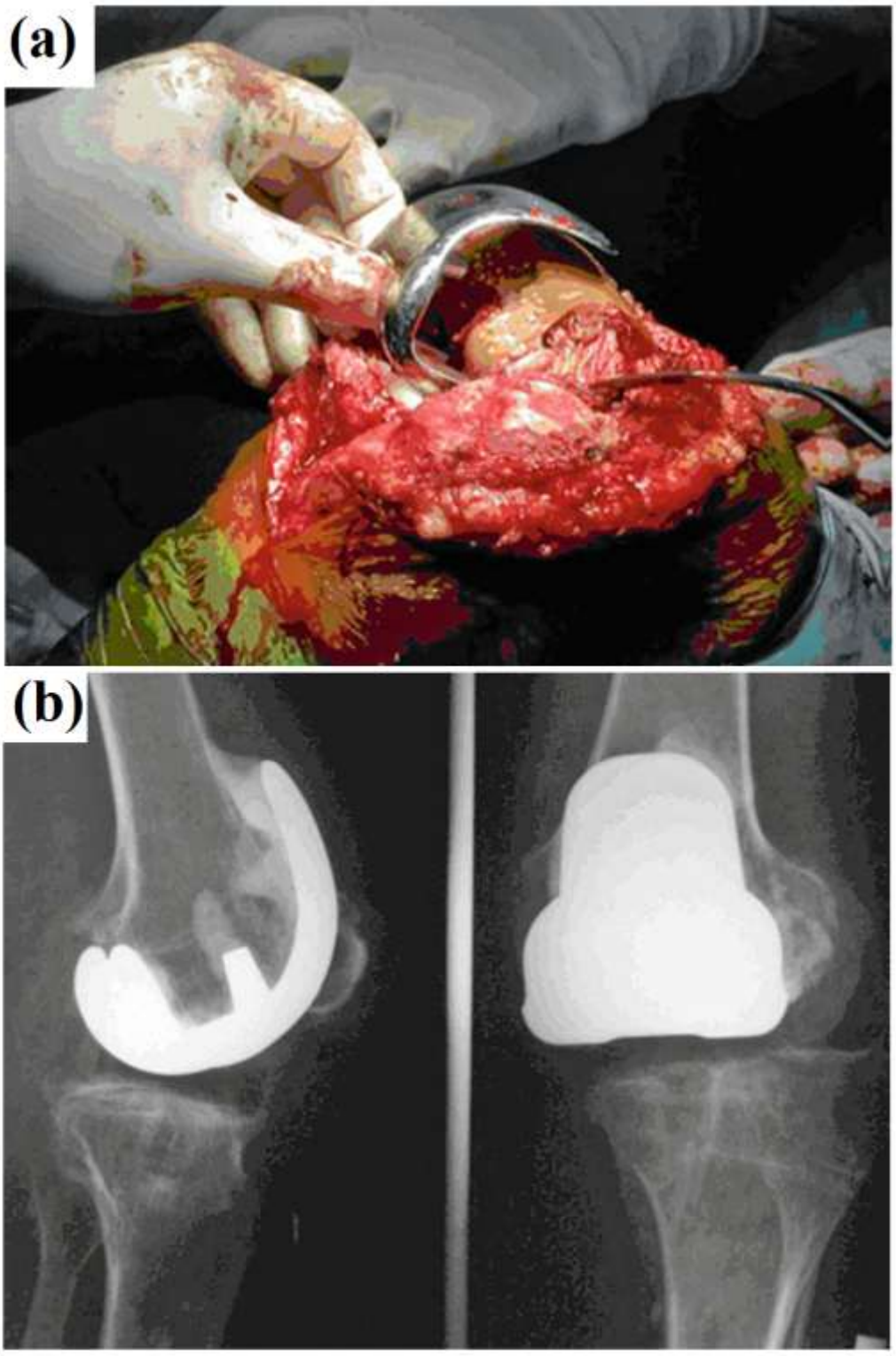

Fig. 2.7 (**a**) Revision of a ‘Freeman’ total knee arthroplasty 20 years after implantation that failed due to instability. (**b**) X-ray of the same knee before implantation

Table 2.5 Comparison of materials used in total hip arthroplasty [63]

Prosthesis	Advantages	Disadvantages
Metal-on-polyethylene	Large volume of evidence to support use predictable lifespan cost effective	Polyethylene debris leading to aseptic loosening
Metal-on-metal	Potentially longer lifespan than polyethylene due to reduced wear larger femoral head –therefore lower dislocation rate	Metallosis potential carcinogenic effect of metal ions
Ceramic-on-ceramic	Low friction Low debris particles	Expensive require expert insertion to prevent early damage can produce noise on movement

Metal-on-polyethylene*:* metal-on-polyethylene (M-on-PE) bearings are the popularly used and rigorously followed up of all the prostheses, making up the majority of THA undertaken in the UK today. These got recognition by the early success of the Charnley prosthesis in the 1970's, polyethylene-based implants almost completely displaced all other bearing surfaces. So much so that a large proportion of research was aimed at developing design and improving implantation techniques purely for the M-on-PE prosthesis. Currently the M-on-PE bearing provides a safe, predictable and cost-effective bearing for the majority of patients, and for many represent the gold standard in THA. The main concern for M-on-PE prosthesis is PE debris which creates per prosthetic osteolysis by the release of cytokines and proteolytic enzymes - ultimately leading to implant failure. PE wear debris is cited as the ultimate cause of most total joint arthroplasty failures today, leading to an increased frequency of hip revision due to aseptic loosening. Although debris may be minimized through the irradiation of PE with gamma particles, greatlyimproving the materials wear resistance, implant failure has led to renewed interest in metal-on-metal bearings [64–66].

Metal-on-metal: Metal-on-metal (M-on-M) prostheses are experiencing a revival after falling out of favour in the 1970's. Previously, concerns were raised of the bearings potential to generate metal ions (metallosis), which had a theoretical carcinogenic risk, as well as associated hypersensitivity reactions and prosthetic loosening. It is now thought that the cause for aseptic loosening in first generation models was due to poor design and improper implantation technique rather than the M-on-M bearings themselves. Prosthetic wear in M-on-M has been reported to be

60 times less than expected with conventional M-on-PE prostheses. In addition, as the metal femoral heads are less brittle than other materials they can have a larger diameter, increasing joint stability, and therefore the incidence of dislocation in these arthroplasties is lower. M-on-M implants also reduce osteolysis and peri-prosthetic inflammatory tissue compared to its polyethylene counterpart. An unknown entity in M-on-M bearings is the long-term effects of metal ions liberated, with cobalt and chromium ion blood levels tending to be 3-5 times higher than those patients with M-on-PE prostheses, Furthermore, many patients who receive M on-M implants are younger (due to its wear characteristics), therefore potentially increasing the total length of the exposure to these metal ions over their lifetime. But such a carcinogenic risk from these metal ions remains theoretical, with only a few case reports of malignancies (mainly sarcomas) in publication to date. There is currently insufficient clinical follow- up to draw firm conclusions about the current new generation of M-on-M implants. Studies into the long-term outcomes are currently being conducted and results eagerly awaited [67–70].

Ceramic-on-Ceramic: First introduced by the French surgeon Pierre Boutin in 1970, half of the hip arthroplasties in central Europe use ceramic heads, but there is a much lower usage in the UK and USA (<10%). Developed to address the problems of friction and wear reported in other materials, the ceramic used in orthopaedics consist of either alumina or zirconia. The benefits of ceramic-on-ceramic (C-on-C) bearings are its high level of hardness, scratch resistance and the inert nature of debris compared to metal or PE versions. Furthermore these hydrophilic prostheses create improved lubrication, therefore resulting in a lower coefficient of friction and excellent wear resistance. Hence C-on-C bearings are a good choice of implant in young, active patients due to reduced wearing. However, the cost of ceramic implants is significant and for this reason these bearings are used infrequently in NHS orthopaedic units. The risk of fracture in first generation alumina ceramic bearings was highly published. Chipping of the contact surfaces caused on insertion of the prosthesis, or as a result of dislocation due to the small femoral heads used in the ceramic implants, can lead to devastating third body wear so excellent surgical insertion technique is vital [69,71,72].

Hybrid prosthesis: A hybrid hip prosthesis is formed from a cemented femoral stem and acetabular cup fixed in place with cementless techniques. This is an option for young, active patients as it prevents pelvic bone loss, to aid revision, yet still providing solid fixation and good

usage. A major study in Norway showed that the use of hybrid systems offer better survivorship than a cemented socket in younger patients. It is though a technique seldom used in the UKgiven the poor clinical data for long-term follow- up [73].

Cementless techniques: Cementing hip arthroplasties was first described by Glück in 1891, using methacrylate bone cement to improve prosthetic fixation, but it was Charnley in the late 1950‘s that popularized this technique with a cement taken from dentists. Between these dates cementing often failed and attention was placed in the development of cementless techniques. The role of cement is to act as a grout rather than a glue to improve the fit of the prosthesis – and theoretically its survival. Cementless prosthesis have a specialized coating, hydroxyapatite, that allows in-growth of bone and thus fixation of the prosthesis. Cementless techniques allow for easier planning of hip revision surgery, particularly in the younger patients, with greater preservation of bone tissue. However, better short to medium-term clinical outcomes were found for cemented over uncementless techniques, with no radiological differences seen. Long-term comparison is difficult to make due to lack of large randomized controlled trials [74].

Computer-assisted surgery: Entering its second decade of use, computer assisted total hip replacement utilizes digital image systems to map the position of surgical instruments in relation to anatomical landmarks, helping to obtain reproducible and accurate placement of implants. Computer navigation may improve the accuracy of prosthesis positioning but, despite its obvious advantage with respects to reducing asymmetric wear, this has not yet been shown to have a clinical benefit. In actuality navigation leads to increased surgical time, elevated costs and operative complexity. On the other hand it is a useful tool in order to conduct research into prosthesis positioning and clinical outcome. Some discussion as to whether the combination of computer assisted surgery with a minimally invasive approach can help to improve outcomes is ongoing – but at present greater quality designed studies and the mastering of this surgical technique is required before such techniques can be formally analyzed [75,76].

2.3.3 Bone cell growth on implants

Osseointegration elicits a specific biological response at the interface of the implant materials which results in attachment and growth between the tissue and material. Osseointegration is generally affected by surface properties of the implant i.e. surface roughness, surface chemistry and surface topography. The remodeling of bone (i.e. growth, repair and development) depends on homeostasis process. Three major building blocks of bone namely osteoblasts (bone forming cells), osteoclasts (break down or resorb bone) and osteocytes (Mature bone cells) regulate the process of homeostasis. In particular the role of osteoblasts cells, located within the matrix actively participate to manufacture the organic components of extracellular matrix as well as cortical and cancellous bone. Osteogenesis (Ossification) is another alternative term for the process of formation of new bone by cells called osteoblasts.

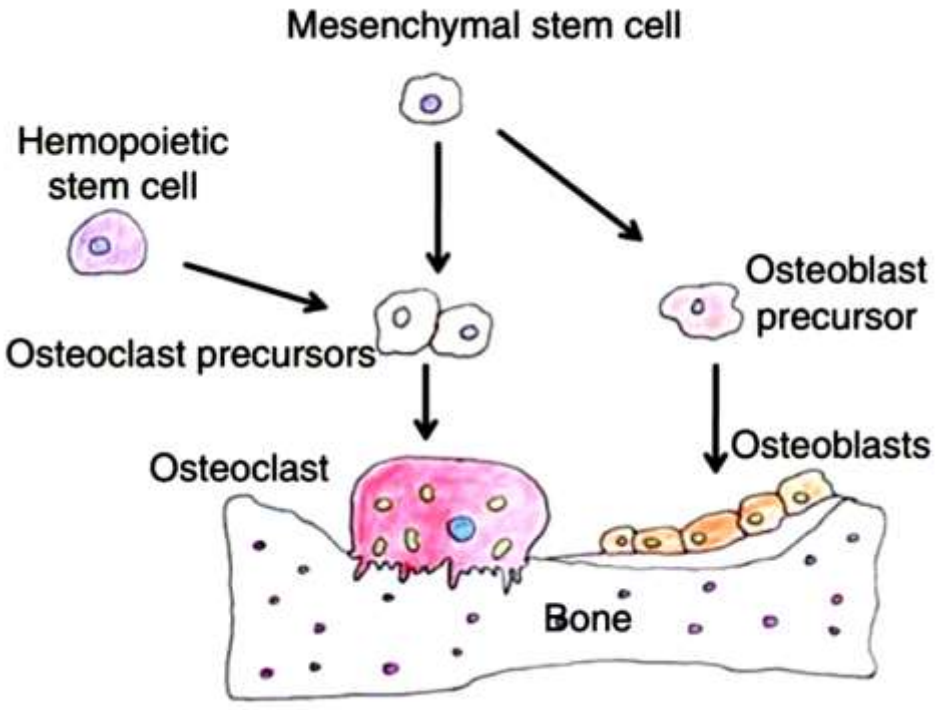

Fig. 2.8 Schematic diagram showing evolution of osteoblasts and osteoclasts in the formation of bone [77]

Basically three steps are involved in the osteogenesis process (Fig 2.8) (i) Synthesis of extracellular organic matrix, collagen, glycoproteins and proteoglycan. (ii) Matrix mineralization

leading to the formation of bone (iii) Remodeling of bone by the process of resorption and reformation. After replacement of hard tissue the bone healing process, at the cellular level, involves many cells, a signal transduction pathway, hormones and growth factors; all of which have been described in detail at somewhere else [77]. The surface of an implant determines its ultimate ability to integrate into the surrounding tissue. The combined effect of surface energy, composition, roughness, and topography plays a major role during the initial biological reactions onto the implant surface, such as protein adsorption and cellular adherence, as well as during the later and more chronic phases of the response. For bone, the successful incorporation (and hence rigid fixation) of an alloplastic material within the surrounding bony bed is called osseointegration. Fig 2.9 is a flow diagram showing how implant surface energy gets affected by various surface properties which leads to change in different biological responses.

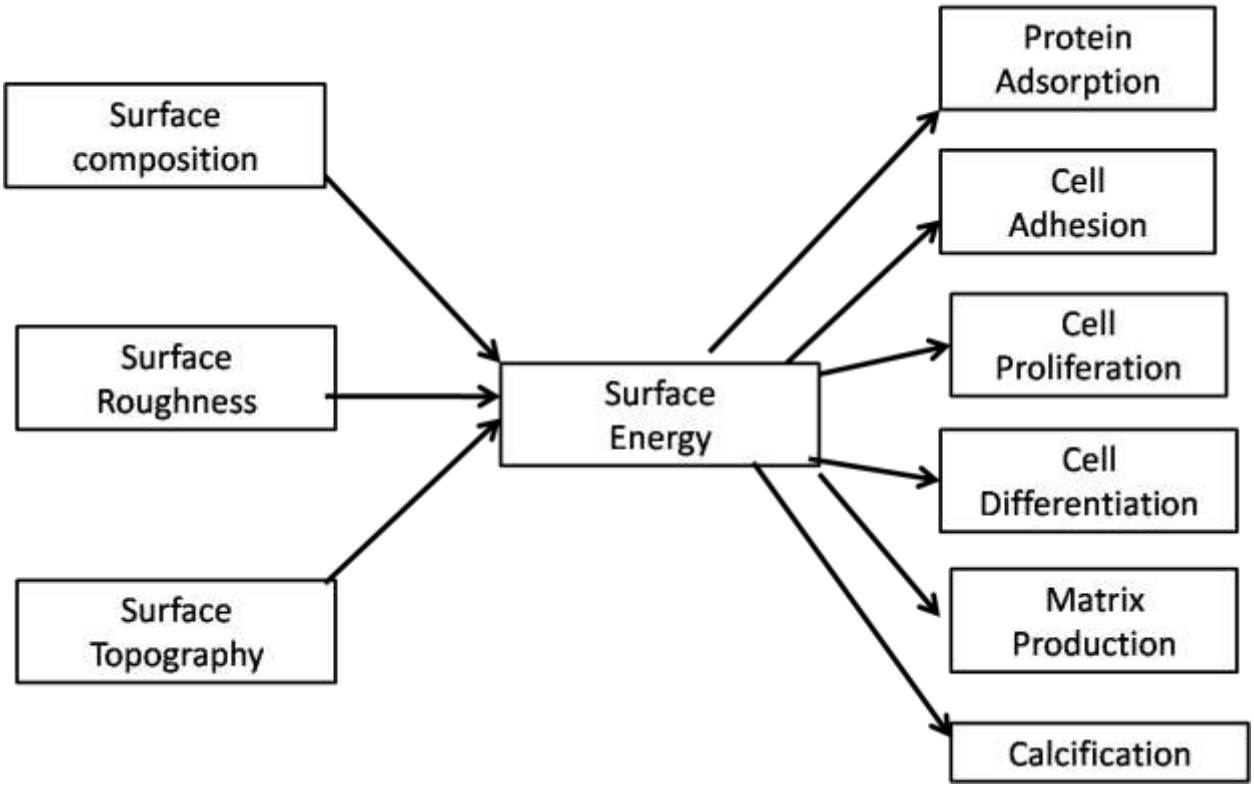

Fig 2.9 Schematic flow diagrams shows how implant surface energy get affect by various surface properties and ultimately leads to change different biological responses

2.4 Calcium Phosphates

Calcium phosphates (CaPs) have been widely used in the form of bone. This kind of material is used for fabrication of various forms of implants, as well as in the form of coatings on metallic implants. The major properties for which CaPs find applications in biomedical field include their reasonably good biocompatibility and osteoconductivity which in turn are associated to their chemical composition which is similarity to that of natural apatite. Though there are many kinds of CaPs but the major ones are: amorphous calcium phosphate (ACP), α- and β-tricalcium phosphate (TCP, $3CaO.\ P_2O_5$), oxyhydroapatite (OHA, a OH^- deficient product), oxyapatite (OA) and hydroxyapatite (HA). Among these, HA is the most stable *in vivo*. The order of dissolution or biodegradation of these CaPs in body fluid is given by Eq. 2.1 [78]

$$\text{ACP} > \alpha\text{-TCP} > \beta\text{-TCP} >> \text{OHA/OA} >> \text{HA} \quad \ldots\ldots\ldots\ldots \quad (2.1)$$

In this work, we have focused on undoped and doped HA. Therefore, crystal structure and properties of HA is discussed in subsequent section.

2.4.1 Structure and properties of hydroxyapatite (HA)

Pure HA is a stoichiometric apatite phase with a Ca/P molar ratio of 1.67 is the most stable CaP ceramic. The HA has two type crystal structures; hexagonal and monoclinic. Hexagonal form of HA is most frequently used for biomedical applications and has $P6_3/m$ space group symmetry. The lattice parameter of HA structure are a=b=0.9432 nm and c=0.6881 nm; $\alpha = \beta = 90^{\circ}$ and $\gamma = 120^{\circ}$.The crystal structure of HA is complex and its simplest form is represented in Figure 2.10.

Ten Ca^{2+} ions are distributed in two markedly different sites called Ca(I) and Ca(II) in two columns parallel to c-axis. Four Ca^{2+} ions per unit cell occupy Ca(I) position and are surrounded by nine oxygen atoms of phosphate groups in column parallel to c-axis. Remaining six Ca^{2+} ions per unit cell are located in another column and are surrounded by remaining oxygen atoms of phosphate group at Ca(II) position. These six Ca^{2+} ions are arranged in two equilateral triangles parallel to column axis. The two anions (OH^-) are also located in this column. Therefore, this column is also popularly known as anion channel [79].

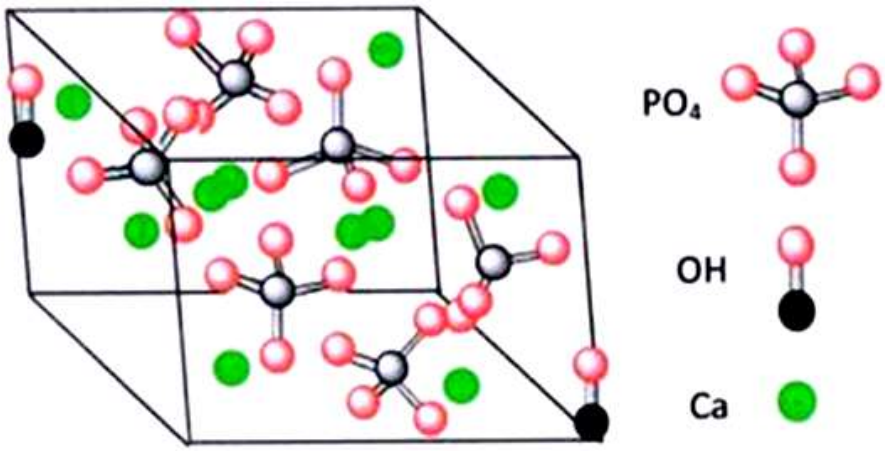

Fig. 2.10 Unit cell of HA [79].

The good biocompatibility of synthesized HA has been confirmed in several studies [38,80,81] carried out on HA coated implants. The dissolution behavior of HA is greatly affected by its composition and degree of crystallinity. Presence of impurities such as F^- and Mg^{2+} ions, defect structure, porosity, the amount and type of impurity phase (such as CaO, and TCP) also affect biodegradation of HA. In addition, dissolution rate of HA may also be affected the concentration and pH of the environment of *in vitro* study. HA having high crystallinity is most stable in physiological environment having pH of about 7.4. The other CaPs are less stable (Eq. 2.1) in physiological environment. Though the mechanism of dissolution is not very clear, the process believed to be physicochemical [82]. In this process, the particles are ingested by osteoclast-like cells attached to the surface and that intracellular dissolution of these particles takes place. Further, it is believed that the process preferentially occurs at imperfections such as dislocations and grain boundaries [83]. Ducheyne et al. [80] compared the clinical performance of uncoated and phosphate coated implants and found that phosphate coated implants allow greater degree of bone in growth than uncoated implants.

The *in vivo* behavior of HA coating with different degree of crystallinity has been examined by Porter et al.[84] They observed that implant with HA coating having crystallinity of 70 ± 5% demonstrated bone growth (formation of plate-like biological apatite) occurred after 3 h whereas the implant with HA coating having crystallinity 92 ± 1% (achieved after annealing) did not exhibit similar bone-growth even after 10 days. This study therefore clearly demonstrates good biocompatibility and osteoconductive property of HA. HA coatings on metallic bioimplants

are very commonly produced by high power macroplasma spray technique (MAPS) due to high deposition rate and economic advantages [38,85]. However, these HA coatings are invariably associated with one or more of the impurity phases such as TCP, tetracalcium phosphate (TTCP), CaO and even sometimes ACP which have high dissolution rate in aqueous solutions and biofluids thereby making HA less stable. In order to achieve fixation of implant with surrounding bone and a long life, HA coating must have limited dissolution after implantation. The crystallinity of HA produced by MAPS usually lies below 70% [86]. To improve crystallinity applications of post heat treatment to as sprayed HA coatings is very common. Alternatively, microplasma, i.e. low power plasma (1-4 Kw) has also been used to produce HA coatings on implants with crystallinity of about 90% with invariably introduced porosity of about 18% [87]. This high level porosity is reported to be beneficial as pores permit tissue in-growth and thus anchor the prosthesis to the surrounding bone, thereby preventing the loosening of implant [88].

Since synthetic HA is relatively less soluble while TCP is more soluble, a mixture of these two phases, i.e. the biphasic HA is expected to display improved osteoinductive potential [89]. Increased amount of TCP in HA can also improve osteoinductivity of HA due to TCP's ability to introduce pores as it dissolves, as well as to promote calcification. Apart from the good biocompatibility and osteoconductivity, synthetic HA suffers from some drawbacks such as brittleness and low mechanical strength, in particular, the fatigue strength required for load bearing implant applications in bulk form, inadequate degradation rate because of its high stability and lack of targeting and labeling. There is still potential to improve biocompatibility and osteoconductivity of synthetic HA. Because of the lower mechanical properties HA is widely employed as coatings on implants and used for non-load bearing biomedical applications. From the point of view of biomedical applications, the main strength of HA is its excellent biocompatibility and osteoconductive properties because of its composition similar to natural bone apatite. Apart from the good biocompatibility and osteoconductivity, synthetic HA suffers from some drawbacks such as brittleness and low mechanical strength, in particular, the fatigue strength required for load bearing implant applications in bulk form, inadequate degradation rate because of its high stability and lack of targeting and labeling. There is still potential to improve biocompatibility and osteoconductivity of synthetic HA. Because of the lower mechanical properties HA is widely employed as coatings on implants and used for non-load bearing biomedical applications.

2.4.2 Clinical performance of HA

One of the most important and wide spread applications of HA is in the form of coating on bioinert metallic implants because of its good biocompatibility coupled with good bioactivity. Therefore, most of the clinical studies on HA have been carried out on HA coatings on bioimplants. Clinical studies on HA coated implants are generally performed by surgeons in order to get approval from the Food and Drug Administration. The surgeons who perform arthroplasties of HA coated implants, study its clinical performance. To investigate clinical performance a surgeon looks for the following queries: (i) whether HA coating will enhance bone in-growth or on growth, (ii) whether HA will increase wear of polyethylene or increase the possibility of osteolysis, (iii) if HA disappear, then how implant fixation will be maintained intact. Capello et al. [90] have reported that 436 HA coated (thickness = ~ 50 μm) femoral components including hips, stems and cups were implanted in 380 patients of several sites in United States during 1988 to 1999 (11 years). Extensive clinical studies showed that few patient's stems and cups were revised before the minimum 6 years. Clinical tests revealed that HA coated hip components enhanced both bone in growth or on growth with no increased evidence of osteolysis for as many as 10 years [91–93].

Interestingly, the clinical investigation has shown no deterioration of femoral component fixations even up to about 10 years. Moreover, the survival rate of HA coated stems and HA coated threaded cups was reported 100% and 99%, respectively, at 6-years minimum follow up [94] Bony growth over some area of HA coating has also been noticed after 2 years of implantation. According to, McPherson et al. [95] HA coated stems exhibited accelerated bone remodeling (cancellous hypertrophy) as compared to porous coated stem at all follow up intervals of 3 years. Retrieval studies on HA coated stem components implanted in animals revealed progressive improvement of bone in-growth from 1-20% of the surface at 3 weeks, 48% after 12 weeks and 32 - 78% at 5 to 25 months. These clinical studies clearly confirm the osteoconductive property of HA. Bone in growth is suggested to stabilize prostheses mechanically. Moreover, an animal study showed that HA coating inhibited the migration of wear debris of the polyethylene (PE) along the bone-implant interface as compared to uncoated implants and there was no evidence that HA coating leads to PE wear or an increased incidence of osteolysis [96].

2.5 Necessity of doping ions into HA structure

The composition of natural apatite and synthetic hydroxyapatite (HA) differs in terms of elemental compositions and lattice parameters as reviewed by [8]. Typically synthetic HA is not an ideal material for use as a bone substitute in load bearing implants, due to certain shortcomings such as brittleness and lack of desired mechanical properties, higher degree of crystallinity and consequently higher structural stability. This results in a lower rate of biodegradation and hence poor response as an orthopedic implant material. Hence, it is essential to improve these properties for its use as a monolithic material in implant/tissue engineering applications. In the last two decades, researchers found that the sites of implantation of different parts of our body require different chemical and physical properties. Bioactivity of HA mainly depend on its surface reactivity and composition and by modifying these, improvement of the system can be possible. The physical, chemical and mechanical properties of HA may be modified to some extent by one or more of the methods such as (i) altering the grain size and/or (ii) changing the surface morphology/topography and/or (iii) incorporating metal trace elements into HA structure. Generally, a combination of two or all of these methods is preferred to improve the properties of HA and also to overcome the draw backs of HA mainly the slow dissolution rate and inadequate osteoconductivity [5].

Recent studies in literature suggest that ionic dissolution products from inorganic materials are keys to understand and assume the behavior of HA in *vitro and in vivo*. Many trace metal ions such as Ag^{+}, Zn^{2+}, $Cu^{2+,}$ Fe^{2+}, Ba^{2+},Mg^{2+} and Sr^{2+}(which are the part of bioapatite) are chemically related to Ca^{2+}ions and their substitutions for Ca^{2+} ions can modify solubility, crystallinity, morphology and lattice parameters of synthesized HA [8,10]. Moreover, minerals and traces of metal elements not only improve its mechanical strength but also accelerate bone formation [13] and resorption on bone cells or bone mineral in vivo and in vitro [97]. The release of these ions after exposure to a physiological environment tends to improve the bioactive activities of the implant related to both osteogenesis and angiogenesis. Thus, recent trend has been to incorporate different ions into the composition of HA to enhance its physical characteristics and therapeutic benefit. This substitution of one or more than one ions in the composition of HA is called doping and it is very essential for production of functional material, in particular, coatings on bioimplant. By definition, a doping element is a supplementary substitution in the main composition at a very low concentration compared to the major

constituents ranging from a few ppm to a few percent. Investigations carried out on doping or co-doping of elements in HA revealed that the functionality of the material is directly influenced by doping elements. Further, it is also found that doping may improve surface characteristics of the implant or the physical attributes of it.

2.5.1 Influence of silicon (Si) substitution in HA

Silicon (Si) is another essential element for bone and cartilage formation and is present in the areas of osteoblastic activity during bone growth. This element is essential for normal development of the glycosaminogly can network in the extracellular matrix and increasing bone collagen content. Si also appears to inhibit macro phase and osteoclast activity. Small levels of ionic substitution by Si in hydroxyapatite (HA) have been shown to have significant effects on thermal stability, solubility, osteoclastic and osteoblastic response both *in vitro* and *in vivo*. Thus, silicon substituted hydroxyapatite (Si-HA) presents enhanced bioactivity *in vivo* than pure HA, showing beneficial effects in the early stages of bone formation. Several reports have suggested that Si-HA would be essential for the metabolic processes associated with biomineralization process. Therefore, Si-HA is widely being used in the field of bioactive bone substitutes and bone tissue engineering. Doping of HA with Si also play important role on the differentiation, proliferation and collagen synthesis of type I osteoblasts (MG63 cell line) cells *in vitro*.

The favorable effects of Si substitution in HA have been explained by considering passive and active mechanisms as material solubility increase, topographical changes, grain size reduction, surface charge modifications and ionic release of Si and Ca, which directly act on bone cells. Gibson et al. produced phase pure Si-HA by an aqueous precipitation of a calcium containing solution and a phosphate containing solution at high pH by using silicon acetate as the source of silicate ions . Patel et al. [98]studied the *in vivo* behavior of HA and Si-HA granules prepared by aqueous precipitation method followed by sintering at 1200 $^{\circ}$C for 2 h. They found that sintered granules did not show any toxicity (inflammatory) to cells and well accepted by host tissue. The *in vivo* results from this study concluded that the bioactivity of Si-HA improved significantly over undoped HA. Porter et al. [99]compared *in vivo* dissolution process of both pure HA and Si-HA. However, the mechanisms by which silicate improve bioactivity *in vivo*is still a challenge for many researchers. They proposed that incorporation of silicate ions into HA leads to an increase rate of dissolution of Si-HA. The Ca, P, and Si ions subsequently diffuse through the ceramic grains to the bone-HA interface (i.e. grain boundaries and triple junction

points). The increased concentration of Ca, P and Si ions at the HA-ceramic interface accelerated the precipitation of biological apatite and induced bone apposition at the surface of ceramics. Leventouri et al. [100] performed comparative study of heat treated pure HA and (0.4 wt %) Si-HA prepared by aqueous precipitation method. High resolution NPD measurements and Rietveld refinement methods have confirmed that doping Si into HA results in change in lattice parameters marginally. This substitution has no significant effect on the interatomic distances in the phosphate tetrahedron. However, the angles between the phosphorus/silicon and the oxygen atoms of the phosphate tetrahedron are distorted from the ideal value of 109.47°.

The Si-HA structure corresponds to substitutions of phosphate ions (PO_4^{3-}) by silicate ions (SiO_4^{4-}) in HA crystal structure has been confirmed by Botelho et al. [101] X-ray photoelectron spectroscopy (XPS). Decrease in net surface charge and isoelectric point of Si-HA determined by Zeta potential measurements may lead to faster *in vitro* apatite formation in SBF testing. XPS data collected for Si-HA revealed that Si seems to first leached out onto the surface of Si doped HA to take part in dissolution reaction (i.e. improve bioactivity) in tris-buffer using dynamic system. Gasquers et al. [102] demonstrated that solid state Nuclear Magnetic resonance (NMR) is a powerful tool for investigating structural changes that occur due to doping of Si as compared to conventional (indirect) method such as infrared spectroscopy and diffraction based methods. This NMR technique has precisely measured the isotropic chemical shift of silicate anions inside the HA structure. Moreover, the structural modifications taken place during the heat treatment of Si-HA have been safely monitored by 29Si MAS NMR spectroscopy. Si-HA powder prepared by hydrothermal technique was analysed by XRD, and FTIR by Aminian et al. [103] and detected only a single crystalline phase, similar to stoichiometric HA but with slight change in lattice parameters. They further observed that the presence of Si reduced the crystallinity and increased the solubility of the prepared powder. These authors also found that Si-HA significantly contribute to increase in proliferation, good biocompatibility and improved bioactivity as compared to undoped HA. Zhang et al. [104] produced Si- HA coating on Ti-substrate by using biomimetic technique. Si in Si-HA coating existed in the form of SiO_4 group which in turn is observed to be responsible for improved shear (adhesion) strength of Si-HA/Ti as against that of HA/Ti. In order to examine the effect of nanosize structure *in vitro* study of crystalline and nanocrystalline Si-HA has been carried out by M desilva et al [105] for 7 days on both osteoblasts and osteoclast activities.

2.5.2 Influence of magnesium substitution in HA

Magnesium is also an important trace element present in bone and teeth and play a significant role though exist in small quantity from about 0.5 to 1.5 wt%. In the body it stimulates osteoblast proliferation, especially during early part of osteogenesis process and thus improves bone metabolism [106]. Its deficiency causes bones to become fragile and degrade [107]. Magnesium (Mg^{2+}) is a divalent cationic substitute for calcium (Ca^{2+}) in the HA lattice. Such substitution often inhibits crystallization, increases solubility, and lowers the temperature at which conversion of HA into β-TCP occurs which possibly related to the much smaller Mg cation with radius (0.65 Å) substituted for larger cation of Ca (0.99 Å) in the HA structure [108]. The large difference in radii of Mg^{2+} and Ca^{2+} limits the substitution of Mg for Ca in HA because lot of distortion of HA lattice will result leading to reduced crystallinity. Lower degree of crystallinity is favourable for solubility and biodegradability of magnesium substituted hydroxyapatite (Mg-HA) in physiological environment.

Yasukawa and co-workers [109] reported various effects of Mg on the crystallite size of apatite and prepared Mg-HA solid solutions with Mg/Ca molar ratio ranging from 0 to 0.5 by wet method, using the reagents of $Mg(NO_3)_2 \cdot 6H_2O$, $Ca(OH)_2$, and H_3PO_4. They observed that the crystallite size of apatite increased with increasing Mg/Ca ratio from 0 to 0.31 [109]. In contrast, crystallite size has been observed to decrease with increasing Mg/(Mg+Ca) ratio from 5 to 15 mol% in Mg-HA nanocrystals synthesized by wet precipitation method at 90 °C [110]. Mehrjoo et al [111] found that the effect of different amounts of Mg^{2+} ions on biological properties of samples were assessed using cellular proliferation, alkaline phosphatase (ALP) activity and gene expression. The cellular behavior of MG-63 cells was improved in Mg^{2+} incorporated samples. Finally, the results indicated that the high amounts of Mg^{2+} in HAp, could improve the cellular behavior in comparison with pure HA. This destabilization tendency of HA may be counteracted by co-substitution with other ions such as CO_3^{2-} in the structure of HA doped with Mg [112].

2.5.3 Influence of strontium (Sr) substitution in HA

Li et al. [113] prepared Sr-HA by wet precipitation method under alkaline condition (pH11) at 25 °C with Sr content of 0.3, 1.5 and 15 mol%. HA doped with Sr up to 1.5 mol% yield single phase structure similar to pure HA without affecting crystallinity. However, crystallinity drastically reduced from 33% in HA to 5% in 15 mol% Sr-HA probably due to the associated formation of $CO_3^{2-}$and HPO_4^{2-} [113,114] as revealed by FTIR examination. The CO_3^{2-} is expected to form due to pick up of CO_2 from the atmosphere during synthesis reaction carried out under alkaline condition. The substitution of CO_3^{2-} ions in HA structure is probably due to larger structural strain caused by large size Sr^{2+} ions (ionic radius 0.113 nm) substituted for smaller size Ca^{2+} ions (0.099 nm) in the structure [115]. The observed extensive structural strainis in agreement with increased lattice parameters (both "*a"* and "*c"*) [113] .

Mardziah et al. [116] synthesized Sr-HA nanopowder (30 to 150 nm) by sol-gel method with 2, 5, 10 and 15 mol% Srand found that crystallinity of doped and calcined(at 900 °C) HA powder decreases steadily with increase of Sr concentration. It was also found that 2 mol% Sr doped HA exhibits a dual phase mixture of HA and β-TCP even after 900 °C calcination. An increase in "*a"* lattice parameter but decrease in "*c*" parameter was observed which is in contrast to the finding of [113], in which both "*a"* and "*c*" parameters of Sr-HA were found to increase with increasing Srconcentration.The % crystallinity(70.2%) of Sr-HA was found to decrease compared to that of undoped HA(79.2%) [117]. Boanini et al. [118] reported decease in both crystallinity and crystallite size of Sr-HA for low concentration of Sr doping whereas both are increased for higher concentration. A marked reduction in crystallinity and crystallite size by Sr doping (0.61, 2.53 and 2.97 wt%) with increasing concentration has also been reported for nano-HA synthesized by surfactant mediated approach [119]. Decrease of crystallite size from 33.5 nm for pure HA to 19.7 nm for Sr-HA has also been reported in [113].

HA containing lower concentration of Sr exhibits higher solubility. The dielectric constant has been observed to increase with increasing doping concentration of Sr because of increased ionic polarization [119]. Hence, Sr-HA is expected to be more beneficial for bone growth, repair and regeneration [120]. Tank et al. [119] further found that maximum dielectric loss (tanδ) for all composition of Sr-HA occurs at 20 kHz and thereafter, it decreases at higher frequencies. The ac conductivity was observed to increase gradually with increasing frequency

and it was also increased with increasing Sr content, particularly at higher frequencies. Wafi and coworkers [121] synthesized Sr-HA by sol-gel method for various x ratios of Sr (x = 0.1, 0.2, 0.3, 0.4 and 0.5) and calcined the nano-powder at 800 °C for 2h. It was found that the value of dielectric constant initially decreased at x = 0.2 and thereafter it was increased with dopant concentration. The change in dielectric constant is due to ionic polarization caused by Sr doping and therefore it is controlled by Sr concentration. Wafi et al. also suggested that Sr-HA can be used for dielectric device applications [121]. Incorporation of Sr into HA not only influence the physicochemical and biological properties but also influence mechanical properties. Landi et al. [122] synthesized Sr doped HA by wet co-precipitation method in the powder form with molar ratio of Sr/(Sr+Ca) in the range 0.5 to 3 mol%. Porous (45 vol% porosity) Sr-HA scaffolds were prepared by sintering powder at 1250 °C to perform compression test. The porosity mimic the pore size and the distribution of spongy bone so as to use the biomaterial as bone substitutes and drug delivery system, especially to a patient with Sr deficiency. The compressive strength of 4.52 ± 1.40 MPa was obtained which is reported to fall within the range of natural bone [122]. Vickers hardness was found to increase from 5.2 GPa for the undoped HA to 5.5 GPa for 8 mol% Sr doped HA [123]. Kaygili et al.[124]substituted Sr into HA (Upto max 2.25 at %) by using sol-gel technique. It was found that presence of Sr at low levels and soaking in SBF influenced crystal size, degree of crystallinity, lattice parameters and volume of the unit cell of the HA. Biphasic polycrystalline structure composed of HA (> 95%) and β-TCP phase (< 5%) was detected in this study.

2.5.4 Influence of zinc (Zn) substitution in HA

Zinc (Zn) doped HA has shown antibacterial and antifungal effects against E. Coli, Staphyloccus aureus and pathogen yeast candidaalbicans in solid and liquid media [125]. The substitution of Zn in HA decreases grain size while increases the solubility of HA [126,127]. It has been investigated that a considerable amount of Zn can be incorporated into HA structure [128,129] but higher amount (i.e., > 9.1 wt%) of Zn in HA tends to change crystalline apatite to amorphous apatite like phase [128,130]. The high concentration (up to 15-20 mol%) of Zn^{2+} doping tends to inhibit HA phase formation [129,131]. The addition of Zn into HA affects its cytotoxicity, therefore Ito and coworkers [130] suggested that low concentration of Zn^{2+} doping is favourable to avoid cytotoxicity effects. Addition of Zn has been reported to decrease lattice parameter 'a' of pure HA [132]. Though Zn^{2+} ions are positively charged and are expected to

replace positively charged Ca^{2+} ions in the lattice of HA, Tang et al. [133] suggested that Zn^{2+} ions can be placed into 3-probabale positions in the structure of HA. These are Ca (I), Ca (II) and P positions. The Ca (I) atoms formed octahedral structure with surrounding O^{2-} ions [134] while Ca (II) atoms formed tetrahedral structure with O^{2-} ions. Tetrahedral structure requires less energy of formation [135]. Like Ca (II) atoms, P^{5-} ion also forms tetrahedral structure but a vast difference in ionic sizes as well as the difference of charges (positive on Zn ion and negative on P ion) make Zn ion preferable to replace Ca^{2+} ion in the lattice of HA. Between two sites, Ca (I) and Ca (II), Zn^{2+} will prefer to replace Ca (II) ion due to less energy for formation associated with tetrahedral structure [133,135]. If it is true, then Zn^{2+} is likely to reduce the 'a' and 'c' parameters and unit cell volume also [136]. Miyaji et al. [128] reported a decrease in 'c' parameter with increasing Zn concentration, but 'a' parameter increases at higher concentration of Zn (> 5 mol%). In contrast, Tang et al. [133] reported an increase in 'c' parameter with increasing Zn content in HA. Some other studies [131,137] demonstrate that as a consequence of Zn^{2+} ion doping into HA, 'a' parameter initially decreases with a Zn concentration up to 10 mol% and thereafter this parameter begin to increase with further increase of Zn concentration. Crystallinity and crystallite size of Zn-HA affect dissolution and bioactivity of HA. Crystallinity has been reported to reduce with addition of Zn in HA particularly at low concentrations (< 6 mol%). The crystallite size of the Zn-HA decreases with increase of Zn content into the HA structure [138,139].

2.5.5 Influence of silver (Ag) substitution in HA

One of the rare but critical problems in orthopedics and dentistry is implant associated infection. Silver has been used for years in the medical field for antimicrobial applications because of its antimicrobial properties. Silver doped HA (Ag-HA) shows promising antimicrobial properties, but the concentration of released silver ions has to be controlled to avoid cytotoxic effects. Mirzaee et al.[140] synthesized silver-doped hydroxyapatite ($Ca_{10-x}Ag_x(PO_4)_6(OH)_{2-x}$) and deposited on anodized titanium (Ti) using electrophoretic technique. The FTIR, XRD and TEM analysis of Ag-HA coating showed that the Ag particles are of nano size and homogenous in the composition, while a lower value of contact angle in SBF, determined by the drop test, proved its better wettability compared to the HA coating. XRD analysis confirmed the formation of hexagonal structure of HA annealed at 600 °C with a small shift in the major peak position toward lower angles due to presence of silver. XPS spectra

confirmed the formation of the chemical states of Ag^{2+} Ag^{+} and Ag^{0}. Findings of antimicrobial study indicated that antimicrobial efficiency of the Ag-HA is a function of concentration of silver ions. Ag-HA samples with low silver content have excellent activity against E. coli and S. aureus. The corrosion tests also indicated that the silver doped HA coatings have effective corrosion resistance. Therefore, silver doped HA with X=0.05 could be a better choice especially to prevent device associated infections [141]. Investigation on Ag-HA nanoparticles demonstrated the effectiveness of Ag in protecting macrophages from LPS induced cytotoxicity in RAW 264.7 macrophage thereby suggesting that Ag-HA might have potential applications. The use of $Ca_{10-x}Ag_x(PO_4)_6(OH)_2$ with X_{Ag}=0, X_{Ag}=0.05 and X_{Ag}=0.4 for medical purposes requires considering the effects of these materials on different types of cells (including macrophages) in order to avoid unwanted immune reactions of the human body. Thus, gaining solid knowledge of the optimal doses allowing for equilibrium between the positive effects of $Ca_{10-x}Ag_x(PO_4)_6(OH)_2$ with X_{Ag}=0, X_{Ag}=0.05 and X_{Ag}=0.4 and their possible adverse consequences is a matter of prime importance [142]. According to Yanovska et al. [143], the HA–Ag and HA–Ce–Ag antibacterial coatings were formed by co-deposition in aqueous solutions. It was concluded that the HA–Ag (modified) and HA–Ce–Ag coatings obtained via the thermal substrate method exhibited better cohesion between HA-crystals due to the organic component of the coatings and better adhesive strength to the substrate surface. The HA–Ag coatings deposited on modified and unmodified Ti–6Al–4V substrates exhibit the antibacterial activity against infection strain of E. coli as compared with the HA coating without Ag, and can be used for development of coatings for implant protection against infection. Good antibacterial properties of Ag-HA nanoparticles (synthesized via accelerated microwave processing) against E-coli and S-aureus bacteria has also been demonstrated by Rameshbabu et al. [144].

2.5.6 Influence of fluorine (F) substitution in HA

Bakhsheshi-Rad et al.[145]coated fluorine doped hydroxyapatite (F-HA) on the surface of biodegradable Mg alloys using electrochemical deposition technique. They found that a nano-F-HA coated sample presents nano like structure which is oriented perpendicular to the surface of the substrate with denser and more uniform layer. Crystallite size of F-HA found to be in the nano (nm) range. The corrosion behavior of F-HA determined by polarization, immersion, and H_2 evolution tests indicated a significant decrease of corrosion rate and induced passivation as compare to uncoated samples. F-HA coated Mg alloys observed to exhibit accelerated bone-like

apatite layer formation with a significant decrease of the dissolution rate as compared to that shown by uncoated Mg alloy. In an investigation carried out by Tredwin et al. [146]on F-HA prepared by sol-gel technique and assessed for ion release (Ca and PO_4) and biocompatibility it has been found that the dissolution rate decreased with increasing F dopant into apatite structure. The dissolution rate has been found to decrease further with increasing the sintering temperature up to 1000 °C of F-HA as compared to undoped HA. The tendency of cell proliferation i.e. biocompatibility increased with increasing the levels of fluoride substitution into apatite structure. Nathanael et al. [147] produced fluorine-doped hydroxyapatite with varied concentration of substituted anions via hydrothermal method. The F-HA so produced was found to be nanocrystalline in nature. The doping of fluorine ions has been found to change the morphology, aspect ratio, degree of crystallinity appreciably. The increased crystallinity was assessed by a combination TEM, XRD and Raman spectra analysis. Further, F has been observed to decrease 'a' parameter while 'c' parameter was not much affected. The enhanced crystallinity of HA by F substitution is explained by Nathanael et al. in terms of substitution of F^- for OH^- ions in the structure [147]. Once the OH^- ions are partially substituted by F- ions, the existing O atoms of OH^- group are tightly bound to the nearby F- anions due to hydrogen bonding. This is because of the great affinity of F with O. This results in a well ordered apatite structure. The increased degree of crystallinity due to F addition enhanced the orientation dependent growth and accordingly the aspect ratio. So F substituted HA displayed nanorods. Biological study of F-HA revealed an enhanced osteoblast proliferation which can be attributed to the high specific surface area of F-HA nanoparticles. The mechanical and cell compatibility analysis revealed that the F substituted HA nanorods are the promising candidate for the bone analogue materials for biomedical application. F substitution in HA has also been found to increase thermal stability of HA, particularly with increasing F concentration [148].

2.5.7 The role of multi-ionic substitutions into HA

The strength of bone depends on the presence of Ca, vitamin K and vitamin D. Moreover, it is influenced by certain trace ions such as Mg^{2+}, Sr^{2+}, Zn^{2+}, F^-, Mn^{2+}, Na^+, K^+, and B. A deficiency of these trace ions slows down the bone mass and thus, resulting in risk of bone fracture [149]. Biological behaviour of the natural apatite arises because of its chemical composition, low crystallinity, lattice dimensions and off-stoichiometricity. Natural apatite exhibits the crystallite size of about 8-10 nm [150]. The chemical composition and crystal

structure of the natural apatite is similar to that of synthetic apatite, i.e., both are made of calcium phosphate with hexagonal structure. However, natural apatite (or bioapatite) also consists of several foreign ions such as Mg^{2+}, Sr^{2+}, Zn^{2+}, F^{-}, Mn^{2+}, Na^{+}, K^{+}, and B [151], and it has predominantly nonstoichiometric and amorphous phase. In contrast, synthetic apatite (or HA) is stoichiometric and highly crystalline (crystallinity may be as high as 92%) phase. The high degree of crystallinity is responsible for slow rate of dissolution of pure HA. Synthetic HA has good biocompatibility but it is inadequate in osteoconductivity from the implantation point of view. In addition, its mechanical properties required for load bearing applications are low. In order to improve the mechanical properties and to have required dissolution rate, ionic doping or substitution is carried out with the ions present in bone. In view of above, one of the approaches to improve mechanical properties of HA coupled with good biological response is to substitute cation and/or anion into HA structure with one or more of those ions existing in bone mineral or even the others which influence biological response of HA in the right spirit. For instance, reports confirmed that incorporating the foreign ions such as Zn^{2+} , Sr^{2+}, and Mg^{2+} into calcium phosphates can have beneficial effects with respect to crystallinity, dissolution in physiological fluids, and surface charge under SBF conditions [138]. Sr is nontoxic and even when injected in human body in large doses; it does not cause any toxicity. "Namardha Devi et al. also reported non-toxic behavior shown by Sr-substituted calcium deficient HA (CDHA) nanoparticles synthesized via accelerated microwave processing [152]. The toxicity of as synthesized nanoparticles was evaluated against human periodontal ligament fibroblast (HPDLF) cells. These authors further demonstrated the antimicrobial activity of Sr substituted CDHAs against E-coli and *S-aureus* bacteria".

In this context, numerous attempts have been made by investigators on single, binary, ternary or even multi-ion doping into HA and evaluated physicochemical, mechanical and biological properties as discussed in previous sections, though majority of studies are confined to single ion doping. Ionic substitution can alter crystallinity, crystallite size and lattice parameters of HA and thus affect its solubility. As the crystallinity decreases dissolution rate also increases. Codoping is often done for tailoring the properties of HA. For example, one doping ion (e.g. Sr^{2+} and Zn^{2+}) reduces the crystallinity of HA and thus, improves dissolution while the other ion (e.g. F^{-}) enhances the crystallinity and thus, reduces dissolution. Moreover, Zn^{2+} ion enhances antibacterial and antifungal effects against E Coli, S. aureus and pathogen yeast

candiadaalbicans. Codoping of HA with Zn^{2+} and F^- also improves mechanical and biological properties [153]. Therefore, a proper combination of co-doping elements/ions and their proportions may lead to desired degree of crystallinity in HA and hence, the dissolution rate. Excessive dissolution is not advisable for the implant to be used for long life. Similarly, for good bioactivity a reasonable degree of dissolution is needed. The doping of Ag ions in HA enhances antibacterial property [154] but its high concentration increases cytotoxicity [155,156]. To counteract cytotoxicity effect of excessive Ag, Sr and/or Zn may be added into HA [157] Excessive concentration of Zn doping into HA also results in cytotoxicity [130]. Sr is nontoxic and even when injected in human body in large doses; it does not cause any toxicity. It offsets the potential toxicity of Ag ions in HA. Therefore, Sr appears to be a preferred co-doping element for HA containing Ag. Low to moderate concentration of Sr into HA decreases its crystallinity and improves dissolution rate. Sometimes an excess concentration of a doping ion may destabilize HA and may result in the formation of some impurity phase in small amount. For instance, doping of Mg^{2+} into HA beyond certain limit leads to formation of β-TCP. Co-substitution of CO_3^{2-} into HA is expected to have counter effect on destabilization of HA[106]. Similarly, the addition of a small concentration of Zn^{2+} along with Ag^{2+} into the structure of HA counteracts the effect of cytotoxicity (arises due to excessive Ag^{2+}) and strengthens the antibacterial effect of Ag. In addition, Zn^{2+} into HA is expected to promote bone formation around HA coated implant and decreases the inflamentary response [158]. The substitution of F^- ion into HA improves strength and hardness approximately 2 and 4 folds, respectively because of increased crystallinity of HA. It may also improve biological properties including cell attachment, proliferation, and functionality of the HA. It also improves thermal and chemical stability. However, its higher concentration decreases hardness and elastic modulus. The small concentrations of Cu^{2+} and Zn^{2+} ions are essential for various metabolic processes in most of the living organisms, while their higher concentrations are potentially toxic. Zinc has shown a stimulatory effect on bone formation in-vitro and in-vivo. In antimicrobial activity, metal ions bind to proteins deactivate them and interact with microbial membrane, which causes structural change and permeability. Finally, these ions interact with microbial nucleic acids and thus, preventing microbial replication [125]. Turkoz et al. [159] synthesized co-doped (Ag^+ and F^- ions) hydroxyapatite using precipitation technique and sintered for 1 hr at 1100 °C. Both dopants combined in trace amounts showed high in densities. Hydroxyapatite was the predominant phase

with a minor amount of β-TCP in all the samples. Presence of fluoride and small amount of TCP was verified with all characteristic FTIR bands of hydroxyapatite for most of the samples. Compared to the pure hydroxyapatites, much higher microhardness values were measured in samples co-doped with Ag^{+} and F^{-} ions. Antibacterial activity of the material is related to Escherichia coli were also observed in hydroxyapatite samples with high amount of Ag+ ions. Ramya et al. [160] prepared co-doped nanocrystalline hydroxyapatite (nHAp) with Fe^{+3} and Zn^{+2} ions using wet chemical technique assisted to ultrasonicator. XRD confirmed the pristine nHA phase and Fe^{+3} and Zn^{+2} co doped HA phases. IR spectroscopy confirmed all the functional groups of the apatite structure, indicating that iron and zinc ions were doped into the HA lattice. From TEM studies they found that spherical and rod like particles at higher concentrations of Fe^{+3} and Zn^{+2} ions with a considerable reduction in the average particle size. The enhancement of dielectric properties of co-doped HA can be correlated with their ionic polarization due to negative Zeta potential obtained. The super magnetism properties found after doping of Fe^{+3} and Zn^{+2} ions into HA as compare to undoped nHA might be used for magnetic drug delivery applications and hyperthermia treatments. From hemocompatibility test results it was shown that the samples are appreciably hemocompatible. Further it was found from *in vitro* bioactivity tests that co-doped nHA samples showed excellent growth of apatite on the surface of samples immersed into simulated body fluid.

2.5.8 *In-vitro* biological clinical relevance of doped HA

Several in vitro investigations have been carried out on HA incorporated with two or more doping ions to evaluate any improvement in biological properties as well as physicochemical properties. In this section principally the influence of co-doping (binary, ternary and multi-ion) on biological properties of HA investigated previously has been narrated. The addition of Zn^{2+} ions into HA increased microhardness but decreased fracture toughness. However, co-substitution of both $Zn^{2+}$and F^{-} increased microhardness as well as fracture toughness of the HA. In addition, in-vitro biological properties were also improved by co-substitution of Zn^{2+} and F^{-} ions into HA. About 2 mol% Zn^{2+} ion into HA improved cell proliferation and ALP activity of the cells both at 7 and 15 days which was further enhanced by co-doping with 1 mol% F^{-}. The improved ALP activity was attributed to the finer grain structure (grain size of 0.176 μm) exhibited by 2 mol % Zn-1 mol % F-HA samples. In fact, these samples

have shown the best biological response among all other combinations of Zn-F-HA studied. It is interesting to note that the ALP activity of the HA decreased with an increasing concentration of F^-[153]. The *in vitro* hemocompatibility of the HA incorporated with Zn^{2+} and Fe^{3+} ions using wet-chemical precipitation route has been studied. The addition of Zn^{2+} ions into HA improved antimicrobial properties and osteoclast differentiation and promoted osteoblast activity [160]. Further, Fe^{3+} ion doped HA nanoparticles exhibited strong ferromagnetic properties. The hemocompatibility of the pellet samples was carried out in a mixture of acid citrate dextrose (ACD) and fresh human blood. It was investigated that co doped HA is highly blood-compatible. This was attributable to the presence of Fe^{3+} and Zn^{2+} ions in HA.

The in vitro bioactivity test performed by immersing samples in SBF solution showed a deposition of apatite on the surfaces of the samples. The super-paramagnetic property coupled with good antimicrobial property exhibited by Fe-Zn-HA samples demonstrated that the material is a potential candidate for magnetic drug delivery applications and hyperthermia treatments [118,160–162]. The Eu^{3+} doped HA has been considered as a promising fluorescent probe for *in vivo* imaging applications. Additionally, substitution of Ca^{2+} with Fe^{3+} in HA structure may endow the capability of producing heat upon exposure to a magnetic field. Thus, Eu-Fe-HA material has been considered an effective biodegradable and biocompatible drug/gene carrier in biological applications [163].

According to Bodhak et al. [164], *in vitro* cell-material interaction study revealed that the codoping of Mg^{2+} and Sr^{2+} ions into the HA structure significantly improved the initial day osteoblast response and activities on a negatively charged surface. The MTT results indicated that due to the early stage stimulation, the binary (i.e., combined Mg^{2+} and Sr^{2+}) ions doped HA samples showed cell viable density highest compared to those of pure HA or single ion (i.e.Mg^{2+} or Sr^{2+}) doped HA samples. They suggested that binary ions doped HA can potentially be useful in designing bone graft materials for tissue in-growth for HA based orthopedic implants [164]. Ternary ions such as Si^{4+} (56 ppm), Sr^{2+} (87 ppm), and F^- (190 ppm) co-doped HA produced by hydrothermal method was studied *in-vitro* to evaluate biocompatibility [8]. The Si-Sr-F-HA exhibited enhanced biocompatibility and osteoconduction than pure HA. However, cell culture test for 6 h and 12 h indicated that the amount and density of distribution of MG63 cells adhering to Si-Sr-F-HA surface was significantly higher than that of the pure HA surface. This finding suggested that Si-Sr-F-HA is more favorable to adhesion of osteoblasts on the surface of

materials. In addition to osteoblastic adhesion, cell proliferation has also been reported to enhance with culture time. The cell viability detected by MTT Assay revealed that cells grow well adhering to the wall with polygonal shapes. This indicated that the multi-ion doped HA is biocompatible and useful for promising implant applications [165]. The biocompatibility of the multi-ion (M = Ag-Zn-Mg-Sr-HA) doped and electrolytically deposited HA coatings on Ti-alloy (Ti-6Al-4V) substrate were investigated after two weeks cell (MG-63 cell line) culture test in DMEM medium. The cell viability values were found to increase significantly for both HA and multi-ions doped-HA (M-HA) samples (i.e., 78 % and 85 % after 2 days and 81 % and 90 % after 2 weeks respectively) compared to bare Ti-alloy substrate. It was clearly found that the biocompatibility and bioactivity properties of Ag-Zn-Mg-Sr-HA are higher than that of pure HA. ALP expression has been reported to be higher by about 25% and 30% for pure HA and M-HA coatings respectively for 6 and 14 days of culture as compared to uncoated Ti-alloy sample. However, the electrochemical potentiodynamic measurements revealed that corrosion resistance of both HA and M-HA was lower than that of the substrate material.

Compared to pure substrate, the low resistance to corrosion for the coated substrate has been attributed to porous structure of the deposited layers [166]. Gopi and coworkers [167] investigated the corrosion behaviour (in SBF solution) and in vitro human osteoblast (HOS) MG-63 cell culture measurements of CNT reinforced single ion (Sr^{2+}, Mg^{2+} and Zn^{2+}) and multi ion (Sr^{2+}+ Mg^{2+} + Zn^{2+}) doped-HA composite coatings on Ti substrate to evaluate corrosion resistance and biocompatibility of coatings. The composite coatings were produced by electrodeposition technique. The samples for cell viability test were incubated at 37° C for 1, 4 and 7 days. The results have shown that cell proliferation occurred on all the composite coated samples and he cell viability better than CNT/single ion doped HA composite coatings. This demonstrated that M-HA enhances bioactivity of the HA coating while the reinforcement of CNT played no role in enhancement of bioactivity of HA coating. The multi-ion doped HA/CNT composite coating exhibits superior corrosion resistance than single ion doped HA/CNT composite coatings [167].

2.5.9 Effect of multi-ionic substitutions on dielectric constant and PL properties

Out of the typical fractures such as hip, spine, wrist, and ribs, the hip and vertebral fractures require long-term care. Bone growth was found to enhance on polarized HA plates, both at the negatively and positively charged surfaces [168]. The dielectric properties are exploited to screen, diagnosis, and in the overall management of bone treatment. Moreover, clinicians use electrical currents to stimulate bone growth for several decades. The dielectric properties have been used to provide useful information about the overall bone health (osteoporosis and monitoring osteogenic response to treatment) extensively up to 5 MHz [169]. The dielectric properties of biological cells and tissues typically display frequencies dependent behavior, i.e., the dielectric constant decreases from a very high value at lower frequency to a lower value at higher frequency. The frequency dependent dielectric constant permits identification and investigation of a number of completely different underlying mechanisms. Therefore, dielectric studies of biomaterials have long been important in electrophysiology and biophysics [170]. The dielectric constant of the HA varies with frequency, porosity and moisture [171] The doping of ions such as cadmium (Cd) [172] iron (Fe) and zinc (Zn) [160] into the HA structure increases the dielectric constant of HA due to increase in ionic polarization. This assists the calcification and mineralization of osseous tissue at the fracture site and helps in healing the fractured bone [171]. It has been reported that single or multi-ion substituted HA nanostructures which exhibit PL properties have received vital importance for *in vivo* observations when implanted in the body [173,174]. The substitution of some ions into HA structure, which are not present in bone mineral, impart some functional properties in the HA. For example, rare earth elements (such as La^{3+}, Eu^{3+} and Gd^{3+} ions) are getting popularity in improving biological properties. The Eu^{3+}/Gd^{3+} ion doped HA samples have shown a sustained/controlled release of drug (i.e. IBU) compared to undoped HA. Moreover, the PL intensity of Eu^{3+} doped HA increases with increasing concentration of Eu^{3+} while emission spectra remained unaffected. They also reported that the Eu^{3+}/Gd^{3+} doped HA are effective for *in vivo* dual mode luminescence imaging, implantation and clinical use, drug release and targeted drug delivery applications [175–177]. Mahabole et al. [178] investigated the effect of incubation in modified SBF (m-SBF) solution on PL property of Sr doped HA. The pure HA, Sr-HA and Sr-HA incubated in SBF fluid have shown intense blue emission spectra at 476 nm (for excitation at 409 nm). The PL relative intensity increases with incubation time.

It is concluded that m-SBF incubated samples exhibited superior performance than other samples. However, the luminescence phenomenon suggested to be not due to Sr doping rather it may be due to some impurities present in the HA lattice [178]. Gonzalez et al. studied the luminescent properties of HA containing carbonate impurities [179]. They observed high PL intensity and very broad emission spectra covering the visible region. The broad emission spectrum is expected to be due to recombination of defects which introduced energy levels within the band gap. The luminescence decay time was of the order of *ms* instead of *ns* range.

2.6 Research gap

An extensive literature review revealed that doping of cations (Sr^{+2}, Zn^{+2}, Ag^{+}) and anions (F^{-}) in HA can significantly enhance not only structural and mechanical properties but also alter or improve required biological properties as a single and binary combination. However, studies related to ternary and quaternary doping of HA appears to be extremely rare. So study the effects and optimize the concentration of these dopants is very crucial and is primary goal of this current research. In order to optimize the combination and concentration of these doping elements design of experiment (DOE) based on Taguchi method, L9 orthogonal array, was adopted. DOE based on Taguchi method systematically assesses the interactive effects of various single, binary, ternary and quaternary dopants HA properties and enable identification of optimized compositions to alter physico-chemical and biological properties of HA. Optimization of functional properties such as dielectric constant and photoluminescence (PL) on Ternary and quaternary ion doped HA has not been reported so far.

2.7 Aim and Objectives

I. To synthesis HA following wet precipitation route and addition of dopants (Sr^{+2}, Zn^{+2}, Ag^{+}, and F^{-}) using high energy planetary ball milling.

II. To study the influence of these dopants on (1) Physico-chemical, i.e., Phase purity, crystallinity, crystallite size (2) Functional groups (FTIR) (3) Mechanical property: hardness (4) In-vitro biological studies: Cell proliferation, Bioactivity, metal ion release, antimicrobial sensitivity (5) Functional properties : dielectric constant and photoluminescence (PL).

III. To propose the optimum compositions of multi-ion doped HA exhibiting the desired combination of physicochemical and biological properties as well as functional properties using Taguchi method of design of experiments.

CHAPTER 3

EXPERIMENTAL PROCEDURE

The following sections consist of selection of materials, procedure adopted for preparation of hydroxyapatite (HA) with and without doping and their characterization. In this, designing of the experiments using Taguchi L9 orthogonal method is described to optimize doping concentrations and combinations of various dopants to achieve desired properties. Crystallinity, crystallite size, hardness, density, bioactivity, metal ion release, self-proliferation and cytotoxicity and antimicrobial behavior, dielectric and photoluminescence behavior of undoped and doped HA have been evaluated.

3.1 Materials

All chemicals used in this investigation were of analytical grade supplied by Sigma-Aldrich, India. Calcium hydroxide [$Ca(OH)_2$with 96.00% minimum assay] and ortho-phosphoric acid [H_3PO_4, with 88.00% minimum assay] were used as precursor reagents for HA synthesis. Precursors for substituents were $SrCO_3$ (99.0 % minimum assay), ZnO (99.0 % minimum assay), Ag_2O (99.0 % minimum assay), and CF_3CONH_2 (97% minimum assay),for Sr^{2+}, Zn^{2+}, $Ag^{+}$and F^{-} ions, respectively. The concentration of each dopant was selected at three levels: 0, 2.5 and 5.0 wt. %.The process adopted for preparation of HA powders without and with doping ions is described in section 3.2.

3.2 Synthesis and preparation of HA Powder

3.2.1 Synthesis of pure HA powder

The detailed procedure adopted for synthesis of HA powder is shown in the flow diagram **(**Fig. 3.1). Wet precipitation method was used for synthesis of HA. The aqueous solutions of precursor reagents containing calcium hydroxide and ortho-phosphoric acid were prepared separately. To prepare calcium hydroxide aqueous solution, 2 liter ultra-pure distilled water was taken in a 5 liter capacity beaker and placed on a hot plate cum magnetic stirrer. Temperature of water was raised to 75±5 ^{o}C and maintained until bubble formation. Once bubbles start forming, 155.6 g of calcium hydroxide powder (77.8 g/lit calculated from mol%) was added in hot water

and stirred vigorously. Similarly phosphoric acid solution was prepared by mixing 76.38 ml H_3PO_4(at the rate of 38.18 ml/lit calculated in the same manner as calcium hydroxide) with distilled water contained in a round flat bottom flask of 2 liter capacity. The mixture was well shaken to achieve complete mixing. Ortho-phosphoric acid solution was taken in a separating funnel and then added drop wise at slow rate into calcium hydroxide solution. Concurrently stirring was continued and the temperature of the solution was maintained at 80 °C. The pH of the solution was maintained at11 by adding ammonium hydroxide solution. The solution was continued to stir for 30 min. at 80 °C. The reaction at this stage that results HA precipitation is as follows:

$$10Ca(OH)_2 + 6H_3PO_4 \longrightarrow Ca_{10}(PO_4)_6(OH)_2 + 18H_2O \ldots\ldots\ldots\ldots 3.1$$

The fine HA precipitates remained in the suspension and therefore it was allowed to settle for 24h. Subsequently, the HA precipitate was filtered by suction pump and washed with distilled water to get whitish cake of HA. The cake was cut into small pieces and dried overnight at 80^oC in an air oven. The dried cake was crushed and ground to powder using pastel mortar and subsequently sieved to 50 mesh (300 μm) size powder.

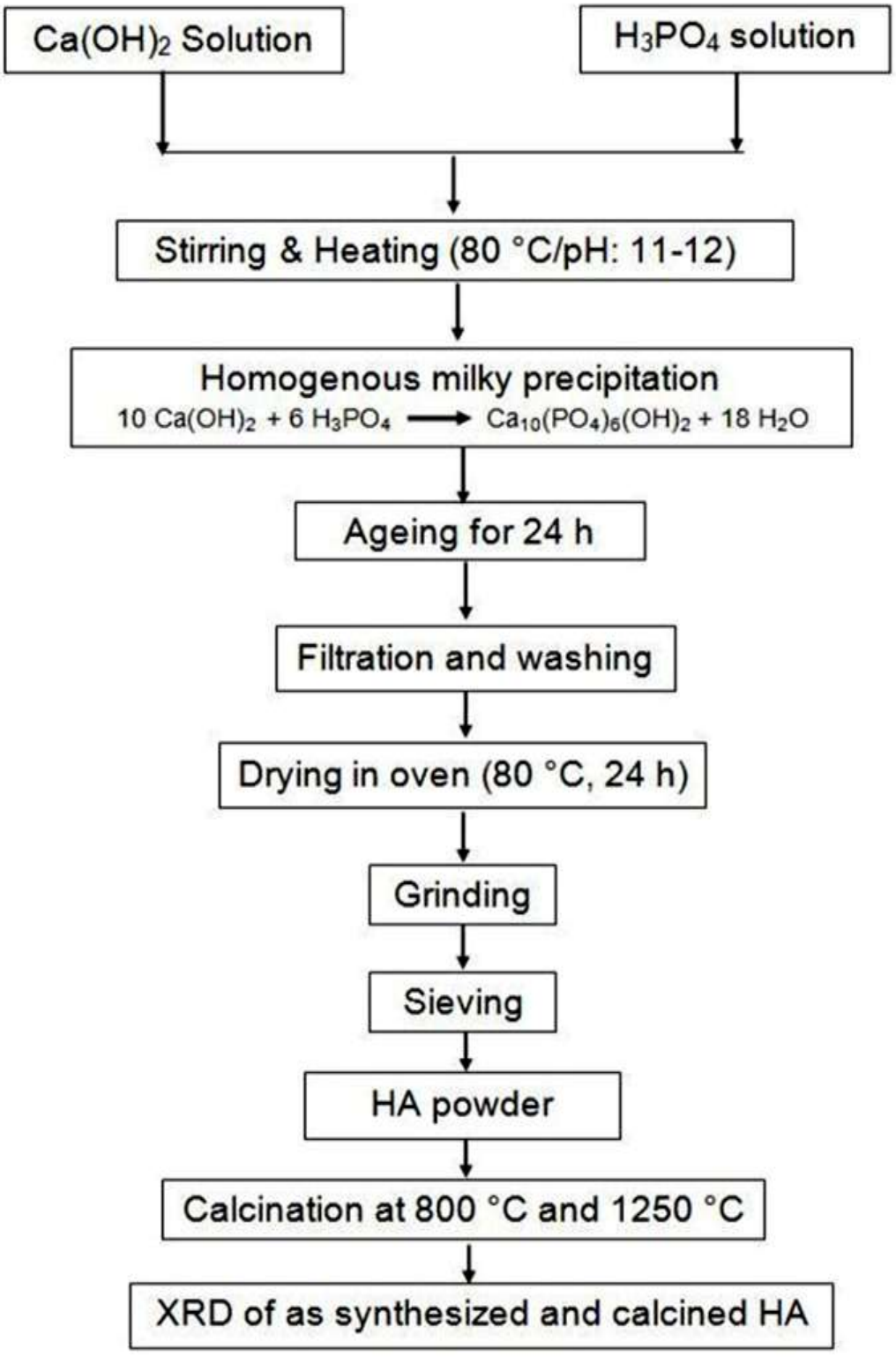

Fig. 3.1 Schematic flow diagram for the synthesis of HA by wet precipitation technique and characterization

3.2.2 Synthesis of multi-ion doped HA powder

In order to investigate substituted HA (S-HA), nine different compositions (**Table 3.1**) containing different concentrations of Sr^{2+}, Zn^{2+}, Ag^{+} and F^{-}in the form of $SrCO_3$, ZnO, Ag_2O, and CF_3CONH_2, respectively were used as precursor materials. To prepare S-HA, as-synthesized HA powder and respective precursor compounds in appropriate proportions were mixed using high energy planetary mill (PM/400 Retsch GMBH, Germany**) (Fig. 3.2**). The milling was carried out in ZrO_2 lined pots with ZrO_2 balls and with the ball-to-charge ratio of 2:1. Ethanol was used as liquid medium. The milling was performed for 72h at 200rpm. During milling a pause of 15 min was given after each hour to avoid excessive heating. The direction of milling was reversed after each pause. Since ethanol was used as medium, the substituted HA was in the wet condition and therefore it was dried in an air oven at 60^{o}C for 24 h. After being dried the cake was crushed and ground again in pastel mortar and sieved to less than 50 mesh size.

Table 3.1 The L9 orthogonal array describing experimental compositions (wt%)

Composition	Sr	Zn	Ag	F
L1	0.0	0.0	0.0	0.0
L2	0.0	2.5	2.5	2.5
L3	0.0	5.0	5.0	5.0
L4	2.5	0.0	2.5	5.0
L5	2.5	2.5	5.0	0.0
L6	2.5	5.0	0.0	2.5
L7	5.0	0.0	5.0	2.5
L8	5.0	2.5	0.0	5.0
L9	5.0	5.0	2.5	0.0

Undoped and doped HA (L1 to L9) powders were used to make disc shaped pellets of 12 mm diameter and 2 mm thickness. Each sample was prepared by cold compaction under a load of 800 N using a Simpliemet-2 press. Subsequently, the pellets were sintered in air at 1250 ^{o}C for 2h using a constant heating rate of 5 ^{o}C/min, and cooling at the same rate.

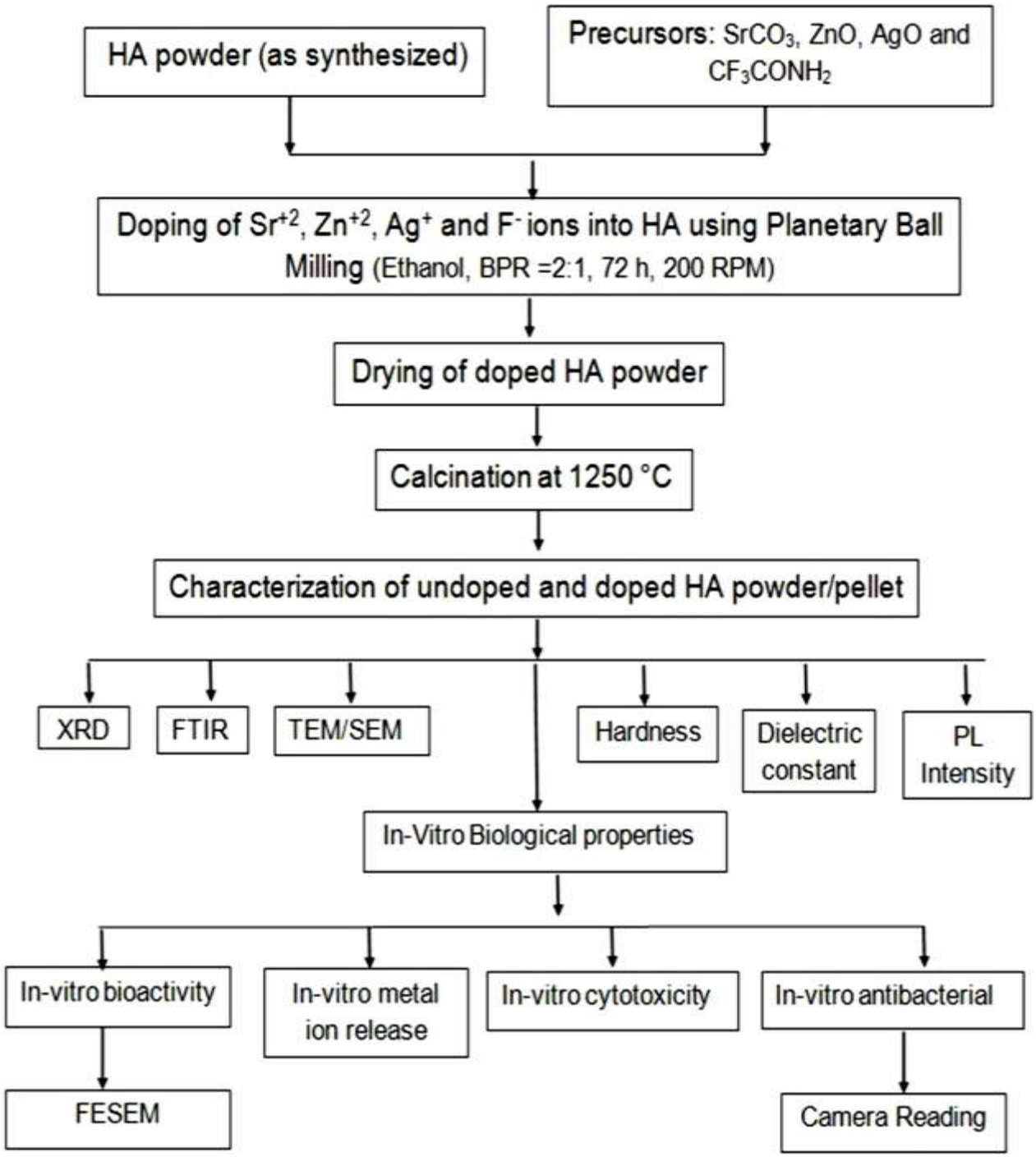

Fig. 3.2 Schematic flow diagram of doping of HA with multi-ions and subsequent characterization

3.2.3 Calcination of HA and S-HA powders

The HA powder synthesized by wet precipitation is mostly amorphous. The crystallinity can be increased by thermal treatment known as calcination. The undoped and doped powders were placed in Al_2O_3 crucibles which were kept in the programmable furnace (Naskar and Company Ltd., India). The samples were calcined at 800 °C and 1250 °C for 2h with a heating rate of 5 °C/min.Calcination of HA resulted in agglomerated powder which was crushed to powder and used for further characterization and testing.

3.3 Design of experiments

In this study, the effect of multi-ion substitution on structural, phase, mechanical and biological characteristics of HA was evaluated using Taguchi design of experiments (DOE). Apart from individual effects of dopants on properties, the interactive effects of multiple dopants on these properties have been assessed to identify the optimal composition to achieve desired properties. In the present investigation, doping elements, namely Sr, Zn, Ag and F are considered as four factors at three concentration levels (wt.%) (Table 3.2). Throughout the thesis, the concentration of substituents is in wt.% unless otherwise specified. When process parameters are more in number and large number of experiments is to be performed to optimise parameters, Taguchi suggested an experimental plan in terms of orthogonal array that reduces number of experiments to perform. This method gives different combinations of parameters and their levels for each experiment. The L9 orthogonal array [34] along with the details of S-HA compositions investigated in the present work are summarized in Table 3.3.

Minitab 17 statistical software was used for both Taguchi design of experiment and ANOVA analysis in terms of individual effects and their interaction. While Taguchi method is an effective tool in optimizing main doping effects and their interactions, the ANOVA method is useful in quantitatively evaluating the contribution of individual dopants. The calcined undoped and doped HA powders were characterized for physicochemical and biological properties in section 3.4.

Table 3.2 Factors (dopants) and levels (concentration) of each factor investigated in this research.

S. No	Factors	Level of each factors		
		Level 1	Level 2	Level 3
1	Strontium (Sr)	0	2.5	5.0
2	Zinc (Zn)	0	2.5	5.0
3	Silver (Ag)	0	2.5	5.0
4	Fluorine (F)	0	2.5	5.0

Table 3.3 Experimental layout using the L9 orthogonal array evaluated in this investigation.

Composition	Sr	Zn	Ag	F
L1	1	1	1	1
L2	1	2	2	2
L3	1	3	3	3
L4	2	1	2	3
L5	2	2	3	1
L6	2	3	1	2
L7	3	1	3	2
L8	3	2	1	3
L9	3	3	2	1

3.4 Characterization and Testing

3.4.1. Physicochemical Properties of HA powder

3.4.1.1 Phase, Crystallinity and Crystallite size

X-Ray fluorescence (XRF) spectrometer (PANalytical) was used to measure quantitatively chemical composition (in wt %) of undoped and doped HA samples. X-ray studies of undoped and doped HA were carried out using X-ray diffractometer (D500 Kristalloflex,Siemens) with Cu K_α radiation in order to evaluate the phases present, fraction of crystallinity and crystallite size. The XRD data were collected over 2θ range of 10 to 90° with

step size of 0.028 and step time of 2s. X'Pert High Score Plus software X-Pert Pro was used to identify the constituent phases and corresponding hkl values.

Phase identification was performed by comparing XRD patterns of the samples with the Joint Committee for Powder Diffraction Standards (JCPDS) files of the HA (JCPDS, Card No. 9-432) supplied by the International Centre for Diffraction Data (ICDD). The X-Pert Pro analytical software was used to match experimental peaks and hkl values with JCPDS data. The fraction of crystalline phase of the powder was determined using the Eq. 3.2.

$$Xc = \left(1 - \frac{V112/300}{I300}\right) \ldots\ldots\ldots\ldots\ldots\ldots\ldots\ldots\ldots\ldots\ldots\ldots 3.2$$

where, $V_{112/300}$ is the intensity of shoulder between the planes (112) and (300) reflections and $I_{300}$is the intensity of (300) reflection [124]. Figure 3.3 shows typical XRD pattern of HA exhibiting mainly 211, 112, 300 planes and, I_{300} and $V_{112/300}$ are also marked on the pattern.

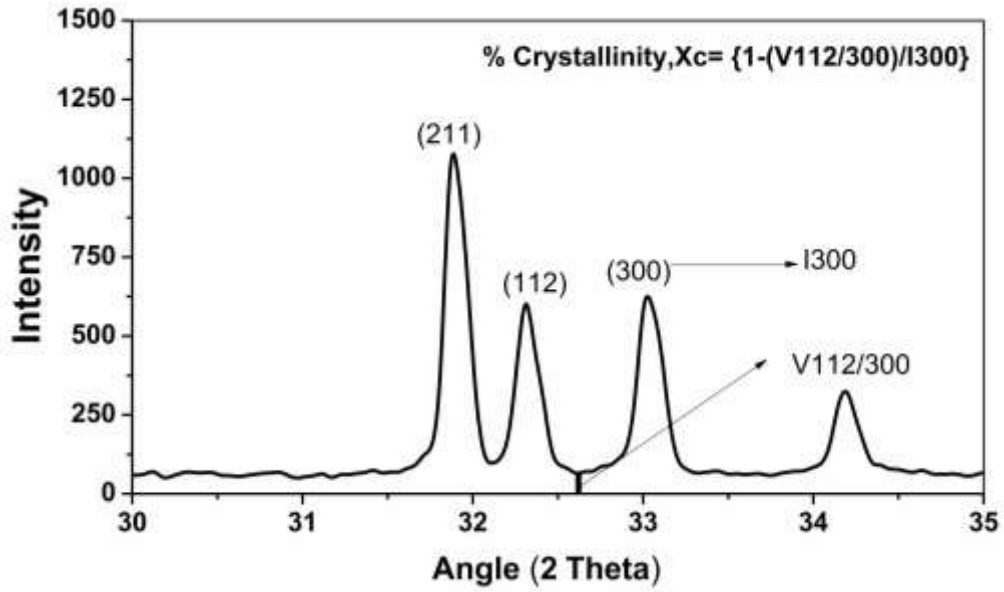

Figure 3.3 XRD pattern of undoped HA

The average crystallite size of the powder was estimated using Scherrer‘s formula, as given in Eq. 3.3.

$$D = 0.9\lambda/(FWHM.\cos\theta) \qquad \ldots\ldots\ldots\ldots\ldots\ldots\ldots\ldots 3.3$$

where, *D* is the crystallite size (nm), λ is the wavelength of monochromatic X-ray beam (0.15406 nm for Cu Kα radiation), FWHM is the full width at the half maximum of the diffraction peak under consideration (in radians), and θ is the diffraction angle [124].

3.4.1.3 Density Measurement

Densities of the sintered pellet samples of both undoped and doped HA were determined by the Archimedes method. Relative density of the materials was calculated by dividing the measured density with theoretical density of pure HA (3.156 g/cm^3).

3.4.1.4 Hardness Measurement

Hardness measurements of all the HA pellets were recorded using Vickers microhardness tester (UHL-VMHT 002, Walter Uhl, techscheMikroskopie GmbH & Co., KG, Germany) at 50 g load with dwell time of 15 s. Average of 10 measurements at different locations on each sample is reported.

3.4.1.5 Analysis of Functional Group

The functional group (such as OH^-, CO_3^{2-} and PO_4^{3-}) analysis of undoped and doped HA powders was done using Fourier-transforms infrared spectroscopy (FTIR, Spectrum 100, Perkin Elmer, USA). FTIR measurements were performed in mid IR region (4000-400 cm^{-1}). The pellets were prepared by mixing powder samples of undoped HA and doped HA with Potassium bromide (KBr) powder at room temperature. The ratio of HA/doped HA powder to KBr was 1:150 (by wt.). Spectra were obtained by averaging 16 successive signal scans and the average results are reported.

3.4.1.6 Microstructural Study

Sintered samples were polished using diamond paste and then examined for grain size measurement and bioactive test using Field Emission Scanning Electron Microscope (FESEM) (Supra 35 VP, Oberkochen, Germany) operated at 15 kV. The samples surfaces were coated with a very thin gold coating to minimize charging effect. High-resolution transmission electron microscopy (HR-TEM,Tecnai^{TM} G^2 20, FEI Company Japan) images of the powder were collected for analyzing crystallite size and presence of crystal defects. Particle size and morphology were also evaluated by TEM. For TEM analysis, powder sample was prepared by dispersing 1 mg of powder sample of each composition in absolute ethanol (concentration in ppm level) and ultrasonicated for about 30 min to break down the aggregates of HA. One drop of

the well dispersed powder was dropped onto a carbon coated copper grid with the help of micropipette. The Cu grid with sample was dried in a UV lamp. Finally, the dried sample was examined using TEM under bright-field image mode for analysis of particle size, crystallite size and their morphology. Selected area electron diffraction (SAED) pattern was also obtained to confirm crystallinity of HA.

3.5 Biological responses

3.5.1 *In vitro* cell culture

In vitro cytotoxicity experiments were performed using mouse embryonic fibroblast cell line (NIH3T3). Sterilization of sintered pellets was done at 120°C, 15 psi for 20 min using an autoclave.Each sample (n = 3), placed in a 24-well plate, was seeded with 5×10^3 cells. The cells were allowed to adhere to the sample surface for 2-3 h and then 1 mL milliliter of Dulbecco's Minimum Essential Medium (DMEM) supplemented with 10% Fetal Bovine Serum (FBS) was added into each well. The culture plates were incubated for 3, 5 and 7 days in an incubator (37°C,95% humidified air atmosphere + 5% CO_2).After every 2-3 days the culture media of the wells was replaced with fresh media. After desired incubation the samples were removed for MTT [3-(4,5-dimethylthiazole-2-yl)-2,5-Diphenyltetrazolium Bromide] assay. To prepare MTT solution 5mg of MTT reagent (Sigma- Aldrich,USA) was added to 1 mL of PBS. MTT solution of 200 µl was added to each well and after 4 h of incubation at 37˚C, 5% CO_2 the MTT solution was removed and 1 mL of DMSO (dimethyl sulfoxide) was added. A 100µl of resulting supernatant was transferred to each well of a 96-well plate and the absorbance was measured using ELISA reader (Bio-Rad Instruments, USA) at 595nm. At least three readings from each of the triplicate samples, pure HA and doped HA, were obtained. Cell adhesion morphology of dried samples after sputter coated with gold was examined under the scanning electron microscope (SEM, Phenom ProX, Neteherland).

3.5.2 *In vitro* bioactivity tests

To assess the bioactivity of present HA samples, in terms of apatite forming tendency, immersion experiments were performed using simulated body fluid (SBF).The samples were immersed in 50 mL SBF solution at 37 ± 1°C upto 14 days. The samples were removed from the SBF solution, after 7 and 14 days of immersion, and carefully rinsed with 50 mL double distilled water followed by 20 mL ethanol and then dried at room temperature. FESEM was used to study

the morphology of the bone-like apatite layer/ precipitates formed on the samples' surface. The Ca/P ratio of the apatite layer was determined using energy dispersive X-ray spectroscopy (EDX). The concentration of ions released during SBF immersion study was measured using inductively coupled plasma mass spectrometry (ICP-MS, 7700, Agilent Technologies Inc., USA).

3.5.3 Analysis of Chemical Composition by ICP

Inductively coupled plasma mass spectrometry (ICP-MS, 7700, Agilent Technologies Inc., USA) was used to determine the composition of the samples after metal ion release. An amount of 2.0 g of HA and S-HA powder was digested in 1.0 N HNO_3 for better accuracy and system adequacy prior to ICP analysis.

3.6 Dielectric and PL study of sintered HA

3.6.1 Dielectric Properties

The dielectric constant provides information about the charges stored inside the material. The dielectric properties were measured using precision impedance analyzer (Wayne Kerr Electronics 6515B, UK) at frequencies varying from 1 kHz to 120 MHz at room temperature. For this, both the opposite surfaces (i.e. cross-sectional area) of pellets were coated using silver paste. From the values of capacitance, the dielectric constants were calculated using standard the Eq. (3.4) and the dissipation factor was noted directly from the instrument [160].

$$\varepsilon = C.t/ \varepsilon_o. S \quad \ldots\ldots\ldots\ldots\ldots\ldots\ldots\ldots\ldots\ldots 3.4$$

where, $\boldsymbol{\varepsilon}$ is the permittivity of the sample, C the capacitance, ε_o (8.854×10^{-12} F/m) the permittivity of free space, t the thickness and S the surface area of the sample.

3.6.2 Photoluminescence (PL) properties

The photoluminescence (PL) measurements of HA and Doped HA carried out by using a (STR-500 Confocal Micro Raman Spectrometer, AIRIX corporation, Japan) by using He-Cd laser source at 325 nm wavelength at room temperature.

3.7 Design of experiments using Taguchi method

In this study, the effect of multi-ion doping on structural and phase, hardness, porosity characteristics, biological responses such as cell proliferation, functional properties such as dielectric and photoluminescence of HA and doped HA were evaluated using Taguchi design of experiments (DOE) [180,181]. Apart from individual effects of dopants, we have assessed the interactive effects of multiple dopants to identify optimal composition to achieve desired aforesaid responses. In the present investigation, four factors namely doping elements Sr, Zn, Ag and F at 3 concentration levels have been used. The L9 orthogonal array along with the details of HA compositions investigated in the present work are summarized in Table 3.1. The Taguchi method is systematic application of design and analysis of experiments for the purpose of designing and improving product quality. In recent years, the Taguchi method has become a powerful tool for improving productivity during research and development so that high quality products can be produced quickly and at low cost. Optimization of process parameters is the key step in the Taguchi method in achieving high quality without increasing cost. This is because optimization of process parameters can improve quality characteristics and the optimal process parameters obtained from the Taguchi method are insensitive to the variation of environmental condition and other noise factors. Basically, classical process parameters design is complex and not easy to use. Especially, a large number of experiments have to be carried out when the number of process parameters increases. To solve this task, the Taguchi method uses a special design of orthogonal arrays to study the entire process parameter space with a small number of experiments. A loss function is then defined to calculate the deviation between the experimental value and desired value. Taguchi recommends the use of the loss function to measure the deviation of the quality characteristics from the desired value.

Usually, there are three categories of the quality characteristics in the analysis, i.e. lower is best (better), higher-the-better (best), and the nominal-the-better (best) detailed calculation and discussions can be read elsewhere [182–184]. A statistical analysis of variance (ANOVA) is performed to see which process parameters are statistically significant. The optimal combination of the process parameters can then be predicted. Table 3.3 gives the selected process parameters and their levels in the current study.

In the present investigation, all the process parameters or factors were set at three levels. This enables initial screening of the influential process parameter with a lower number of

experiments. To suit the process variables and their levels, L9 orthogonal array was chosen. Minitab 17 statistical software was used for Taguchi design of experiment and ANOVA analysis in terms of individual dopant effects, their interaction and contribution towards changing the various physicochemical, hardness, density, *in-vitro* biological responses, dielectric constant, and PL intensity of HA with and without doping.

CHAPTER 4

RESULTS AND DISCUSSION

In this chapter, the results of the various experiments and material characterization conducted as part of current research are presented and discussed. Firstly, the results from physico-chemical and structural characterization of HA samples are presented. Following this, the results from the various i*n-vitro* biological characterizations/properties of undoped and doped HA samples are discussed. Thirdly, the results of the functional properties i.e. dielectric constant and photoluminescence intensity investigation experimental work are discussed. Taguchi method part of design of experiments was used to optimize the doping concentration of various dopants (Sr, Zn, Ag, and F) at main or individual effect level, binary, ternary and quaternary in combinations to affect the essential responses for various biomedical applications. *In-vitro* bioactivity, metal ion release and antimicrobial studies are also presented and analyzed.

4.1 Phase, crystallinity and crystallite size

The diffraction patterns of as-synthesized and calcined HA are presented in Fig. 4.1.The XRD peaks of all samples were well matched with stoichiometric HA (JCPDS file No. 00-009-432). Few peaks, though identified as HA, were not indexed in Fig. 4.1 to ensure clarity. No secondary phases, such as tricalcium phosphate (TCP) and precursor materials were detected in these samples. The absence of secondary phases or impurities is attributable to the purity of the precursor materials used for synthesis. Purity of HA also depends on the rate of addition of orthophosphoric acid to calcium hydroxide during synthesis process. It is also well known that slow and controlled addition of reactants is necessary to achieve phase pure HA. In the present work, controlled addition of H_3PO_4not only avoids local compositional inhomogeneity, but also maintains a relatively high pH of 10-11.

The pH of the solution can decrease drastically to less than 7 if the rate of acid addition is high. In the present work, the addition of orthophosphoric acid to calcium hydroxide solution was maintained at 100 ml/min to achieve a pH of 11 during synthesis. In addition to slow addition of acid to alkaline solution, simultaneous controlled stirring also helped in maintaining high pH and thorough mixing of the solution leading to no residual reactants. High pH is aimed to achieve high crystallinity as well as fine particle size [185]. The crystallinity(~52%)of as-

synthesized powder estimated from XRD data was higher by 20 % than the value reported elsewhere [186]. Further, the rate of reactant addition also control the rate of HA nucleation during synthesis [187]. A slow rate ensures discrete nucleation and thus forms fine precipitated particles. Crystal growth proceeds through arrangement of HA molecules from the solution on to the nucleated particles. During ripening process, the crystallites can grow freely on the surfaces of the precipitates in all directions and longer ripening time is expected to result in large crystallite size.

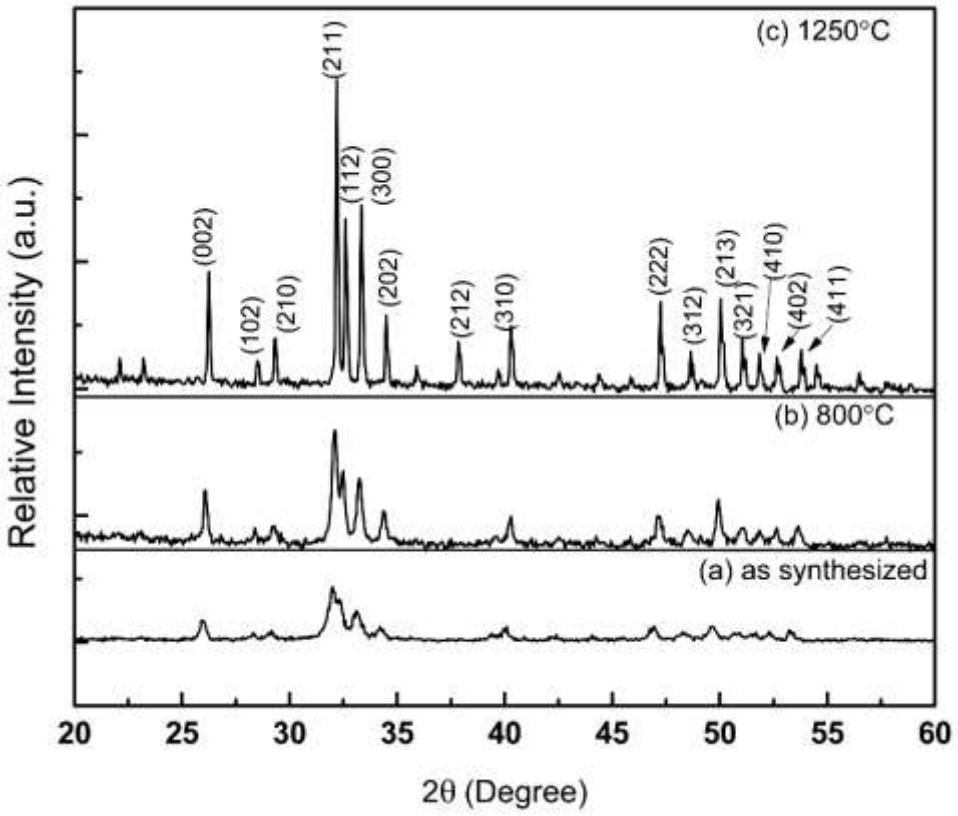

Fig. 4.1 XRD patterns of pure HA powder of (a) as synthesized, (b) calcined at 800°C and (c) calcined at 1250°C.

A comparison of XRD traces represented in Fig. 4.1 shows that the peaks are relatively more sharp and intense in HA powder calcined at 800°C and 1250°C compared to as synthesized powder. This suggests that the degree of crystallinity increases with increasing calcination temperature. The % crystallinity estimated from experimental XRD traces was found to be 52%, 77% and 91% for as-synthesized, calcined at 800°C and calcined at 1250°C, respectively.

Overall, the crystallinity of as synthesized HA increased by 140% and 176% after calcination at 800°C and 1250°C for 2h, respectively. The observed increase in the crystallinity of calcined HA can be correlated to crystallization of HA from amorphous HA in as synthesized powder during calcination. It is well reported that thermal treatment promotes the crystallization of HA and also increases the crystallite size [186]. The mechanical properties of HA are also expected to improve due to the increased crystallinity of calcined powder. The increase in the crystallinity and crystallite size with increasing calcination temperatures has also been reported earlier [188].

The XRD patterns of undoped (L1) and doped (L2 to L9) HA powders, calcined at 1250°C for 2 h, are presented in Fig. 4.2a.Predominant peaks correspond to HA phase (JCPDS file no. 00-009-0432, 01-070-1464, 01-073-1731) in all samples. The peak corresponding to β-TCP (JCPDS file no 00-09-0169) was also observed in samples L2, L4 and L8.The formation of β-TCP can be attributed to the difference in the ion size of Ca and other substituted elements in these doped samples. Interestingly these three compositions (L2: Sr-0, Zn/Ag/F-2.5; L4: Sr/Ag-2.5, Zn-0, F-5.0; L8: Sr-5.0, Zn-2.5, Ag-0.0, F-5.0) contain F doping which is known to assist formation of β-TCP in HA [189]. Similarly, L4 and L8 composition containing Sr becomes less stable when calcined above 900°C leading to formation of small amount of β-TCP[116]. A weak peak corresponding to some residual ZnO (JCPDS file no. 01-077-2414) was noticed in the XRD traces of L3, L6, L8 & L9 samples. Similarly, low intensity peaks of precursorAg_2O were also found in some samples.

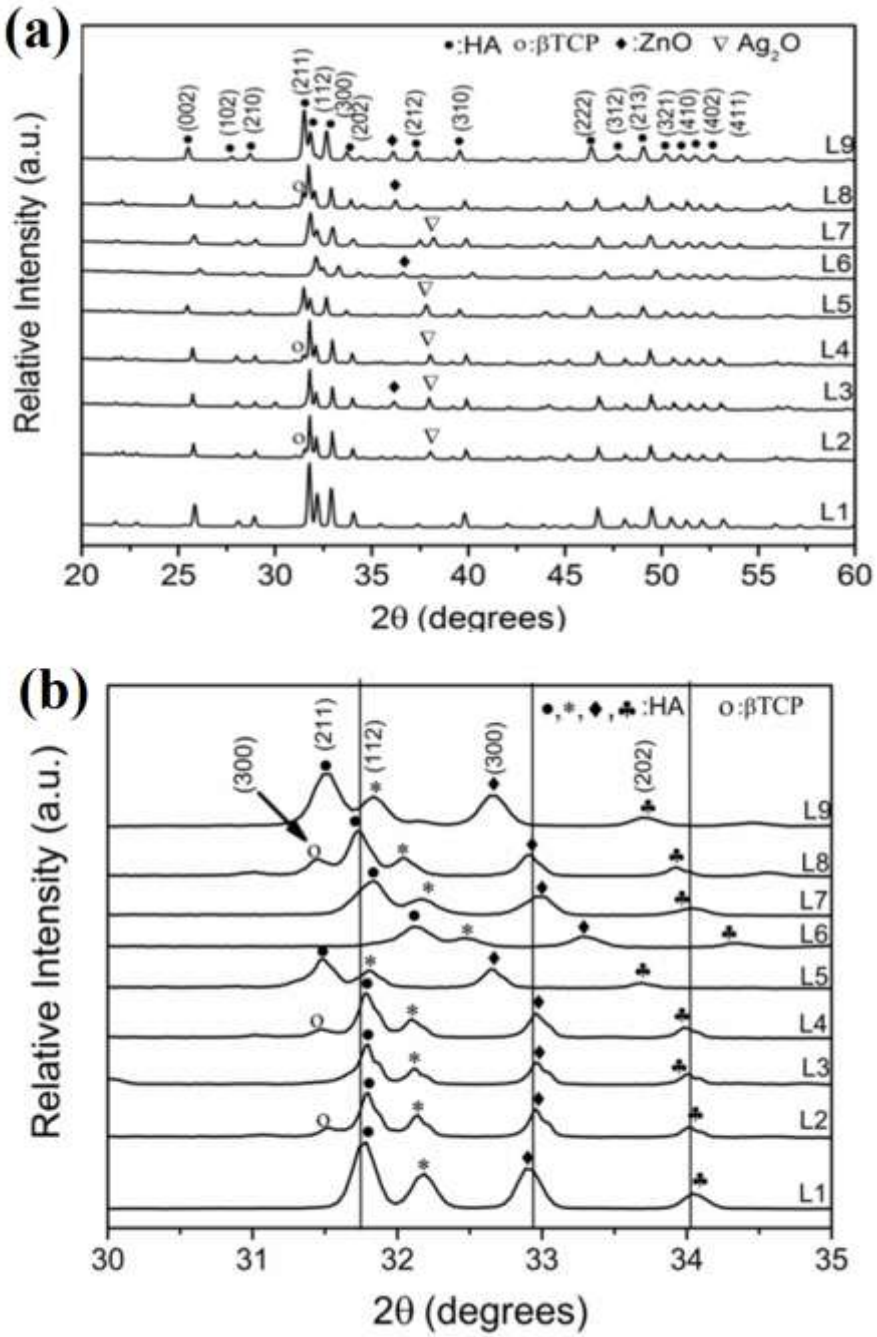

Fig.4.2 (a) XRD patterns of doped (L2-L9) and undoped HA (L1) samples, (b) Enlarge view of XRD patterns (of Fig.4.2a) showing the peak broadening and shifting due to multi-ion doping

The influence of different dopants on the XRD peaks in terms of their intensity, broadening and shifting with reference to pure HA (L1 sample) is presented in **Fig. 4.2b**, which clearly indicates the substitution of doped ions into parent HA lattice. The decrease in the peak intensity and peak broadening of characteristics peaks such as (211), (300) and (202) of doped

HA samples can be correlated with decrease in their crystallinity compared to pure HA. Broadening of the peak indicates nano size of the powder and incorporation of dopants into the HA structure. Compared to undoped HA sample (L1) the doped samples L2, L3, L4, L6 and L7 showed shifting of all characteristics peaks such as (211), (300) and (202) of towards higher angles, which could be attributed to the lattice contraction due to doping. In the case of L5 (2.5Sr-2.5Zn-5.0Ag-0.0F) and L9 (5.0Sr-5.0Zn-2.5Ag-0.0F), the characteristic peaks are shifted to lower angles which indicate expansion of the HA lattice. The shifting in observed peak scan be attributed to the incorporation of dopants into HA structure. The crystallinity (%) and crystallite size (nm) calculated from XRD data is summarized in Table 4.1.These results show that doping reduces the crystallinity of HA and the extent of reduction depends on the composition of HA. For example, samples containing highest Zn content (L6 with 5 wt.%) with 2.5 wt.% Sr and F showed lowest crystallinity (71%) among all compositions. Among the doped samples L2 with moderate concentration of Zn, Ag and F found to have highest crystallinity of 87%, which is only 5% less than pure HA (L1). Similarly, L3 and L4 compositions also exhibited marginal decrease in the crystallinity compared to pure HA. The crystallite size of L6 and L7, containing Sr and F, found to be smaller than pure HA, while the compositions without Sr, L2 and L3, found to exhibit considerable increase in the crystallite size.

Table 4.1 Crystallinity and crystallite size derived from XRD analysis of different HA compositions.

	L1	L2	L3	L4	L5	L6	L7	L8	L9
Crystallinity (%)	92	87	84	85	81	71	81	82	83
Crystallite size (nm)	44	58	56	52	55	32	33	43	40

4.1.1 Main effect of dopants on crystallinity and crystallite size

The crystallinity and crystallite size are important characteristic of HA that commands its strength, stability and *in vivo* dissolution for various bone replacement applications. Therefore, these two parameters have been considered as response parameters to assess the influence of different dopants on HA. An “analysis of means” (ANOM) or main effect plot was used to determine the effect of individual dopant on mean response in terms of crystallinity and

crystallite size of HA. During ANOM the main effects of dopants on crystallinity (%) and crystallite size (nm) of HA were determined using *'nominal is best'* and '*smaller is better'* condition [190], respectively. The criterion of selecting 'nominal is best' for the crystallinity is based on previous findings, The high crystallinity can decrease the dissolution/interaction with surrounding bone while too low crystallinity of HA can degrade it faster. On the other hand, 'smaller is better' condition for crystallite size is intuitive due to enhanced mechanical and biological properties with decreasing crystallite size of HA. The effect of different dopants, thus determined, on mean crystallinity and crystallite size is presented in Fig. 4.3 (a) and (b), respectively.

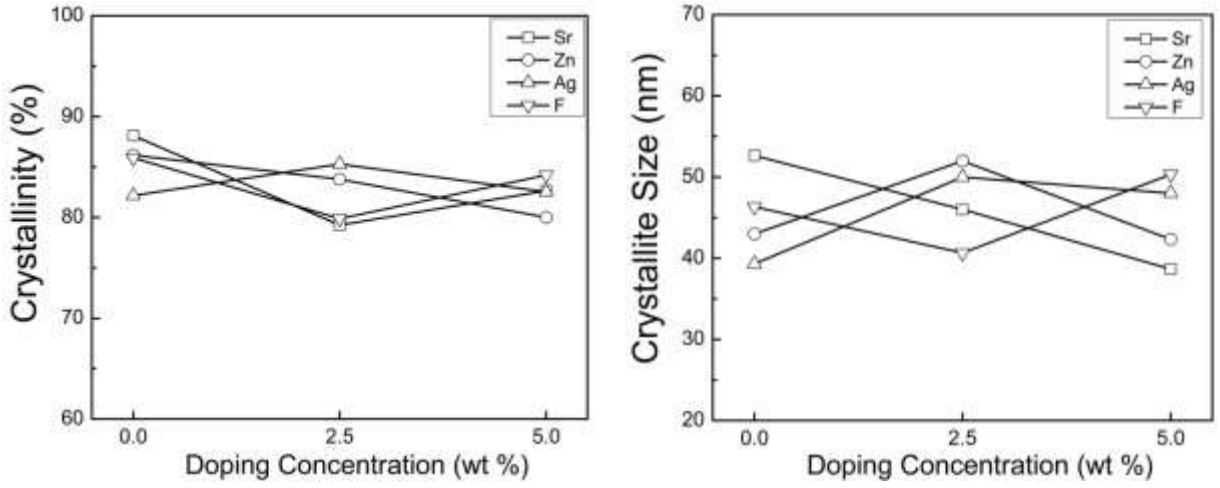

(a) **(b)**

Fig. 4.3 Main effect of different dopants and their concentration on (a) crystallinity, and (b) crystallite size of HA.

From Fig. 4.3a**,** it can be seen that, in general, all doping elements reduced the crystallinity of HA and the amount of reduction is limited to ~ 10% (max.) depending on the type of dopant and its concentration. Among the dopants studied, only Zn appears to decrease the crystallinity with increasing concentration from 0 to 5%. In contrast, Sr or F doping resulted in initial decrease in crystallinity (up to 2.5 wt. %) and then it increased slightly at 5 wt. %. The addition of Ag to HA revealed increase in the crystallinity up to 2.5 wt. % and thereafter the crystallinity decreased marginally. From these results, it can be said that the concentration of Sr, Zn, Ag and F up to 2.5% is appropriate to achieve nominal crystallinity in doped HA. The

observed reduction in crystallinity with Sr and Zn doping in HA is in line with early studies [191,192].

The size of the doping cation/anion is different from that of the host ions, which results in distortion in the HA structure. Therefore, the distorted structure partly loses its long-range periodic arrangement leading to decrease in the crystallinity [193]. However, it is not clear how the crystallinity increased, although marginally, with increase in the concentration of Sr and F from 2.5 to 5%.HA doped with F was found to have higher crystallinity compared to undoped HA [147] but the present results show that the change depends on its concentration. The effect of different dopants and their concentration on mean crystallite size of HA is illustrated Fig. 4.3b. Gradual decrease in the crystallite size was observed, from 54 nm to 40 nm, with increase in the concentration of Sr from 0 to 5%. Similarly, F addition, up to 2.5%, appears to be beneficial in achieving smaller crystallite size, but further increase resulted in coarsening of crystallites. HA doped with Zn and Ag exhibited mixed results with increase in the crystallite size up to 2.5 wt.% followed by small decrease at 5 wt.%. Based on the individual effects smaller crystallite size can be achieved with high concentrations of Sr, Zn, and intermediate concentration of F and low concentration of Ag. Table 4.2 shows the % contribution of different dopants towards the observed change in the crystallinity (nominal the better) and crystallite size (smaller the better). The data show that Sr had maximum influence (45.6%) on crystallinity of HA followed by Zn (26.5%) and F (19.97%). Minimum effect on crystallinity was exhibited by Ag. The contribution of these elements on crystallite size was different from that observed on crystallinity, except Sr, which showed maximum influence on the crystallite size as well. The influence of Ag and Zn found to be almost close. The contribution of F in achieving smallest crystallite size was very small among the dopants studies. The main effects of individual dopants and ANOVA analysis clearly suggest that HA with Sr from 0 to 5 %, Zn/Ag/F upto 2.5 % can achieve nominal crystallinity and smaller crystallite size.

Table 4.2 Contribution (%) of each doping element towards change in crystallinity and crystallite size (results obtained using standard ANOVA).

Doping element	Contribution to Crystallinity	Contribution to Crystallite size
Sr	45.60	38.06
Zn	26.50	21.71
Ag	7.93	23.26
F	19.97	16.98

4.1.2 Effect of multi-ion doping on crystallinity

The important benefit of DOE, used in the present investigation, is its ability to identify the interaction between different dopants in changing the crystallinity and crystallite size of HA. For example, as shown in Fig. 4.3, the crystallinity and crystal size of HA decreased with increase in the concentration of Zn and Sr, respectively. However, it is difficult to know the effect of Zn on crystallinity in the presence of Sr. Similarly the crystallite size may not decrease with increasing Sr concentration when Zn is added to HA along with Sr. Therefore, the effect of binary, ternary and quaternary ion doping on crystallinity and crystal size of HA was evaluated using DOE analysis.

4.1.3 Binary ion doping

The effect of binary doping on HA crystallinity is shown in Fig. 4.4. Generally, in the interaction plots parallel lines indicates [194] no interaction and crossing lines indicates the presence of interactions between the two parameters. In this work, the interaction is between doping elements in changing the crystallinity or crystallite size. Majority of lines in the plots shown in Fig. 4.4 are not parallel which indicates clear interaction between binary dopants and crystallinity, i.e., the relationship between individual dopants and crystallinity depends on the concentration of second dopant in HA. The interaction plot of Zn and Sr doping for crystallinity, shown in Fig. 4.4a, indicates that the relationship between Sr doping and crystallinity depends on the concentration of Zn only when Sr is more than 2.5%. The individual effect of Zn on crystallinity, Fig. 4.3a,show that the crystallinity decreases with Zn concentration. However, due

to positive influence of 5% Sr (Fig. 4.3a), the crystallinity of HA increased with Zn ≥ 2.5% as shown in Fig. 4.4a.It can be seen from Fig. 4.4b that Ag ≥ 2.5% has no effect on the crystallinity at all concentrations of Sr. Therefore, nominal crystallinity of HA can be achieved with Ag concentration ≥ 2.5% when doped along with Sr upto 5%. However, when the Ag is < 2.5% the crystallinity of HA can be increased with 5% Sr. The interaction between Sr and F co-doping in changing the crystallinity, Fig. 4.4c, is similar to Sr-Ag doping, except that the former co-doping exhibited interaction when F > 2.5% and in the latter the interaction exists when Ag < 2.5%. Therefore, HA with F > 2.5% and up to 5% Sr can provide minimum changes in the HA crystallinity. Fig. 4.4d shows that the individual effect of Zn on crystallinity dominates in the presence of Ag < 2.5%. However, the negative influence of Zn on decreasing the crystallinity can be compensated by co-doping with Ag ≥ 2.5%, i.e., interaction between Zn and Ag exists when Ag ≥ 2.5%. This is attributed to the individual effect of Ag in increasing the crystallinity when its concentration is ≥ 2.5%, as shown in Fig. 4.3a. The parallel lines of Ag with 2.5% and 5%, up to 2.5% Zn indicates no interaction. However, further increasing of Zn content results in increase of crystallinity at 5% Ag while a decrease of crystallinity at 2.5% Ag. Strong interaction in Zn-F and Ag-F co-doping was observed as shown in Figs. 4.4e and f, respectively. Nominal crystallinity appears to form in 2.5Zn-2.5F and 2.5Ag-2.5F compositions.

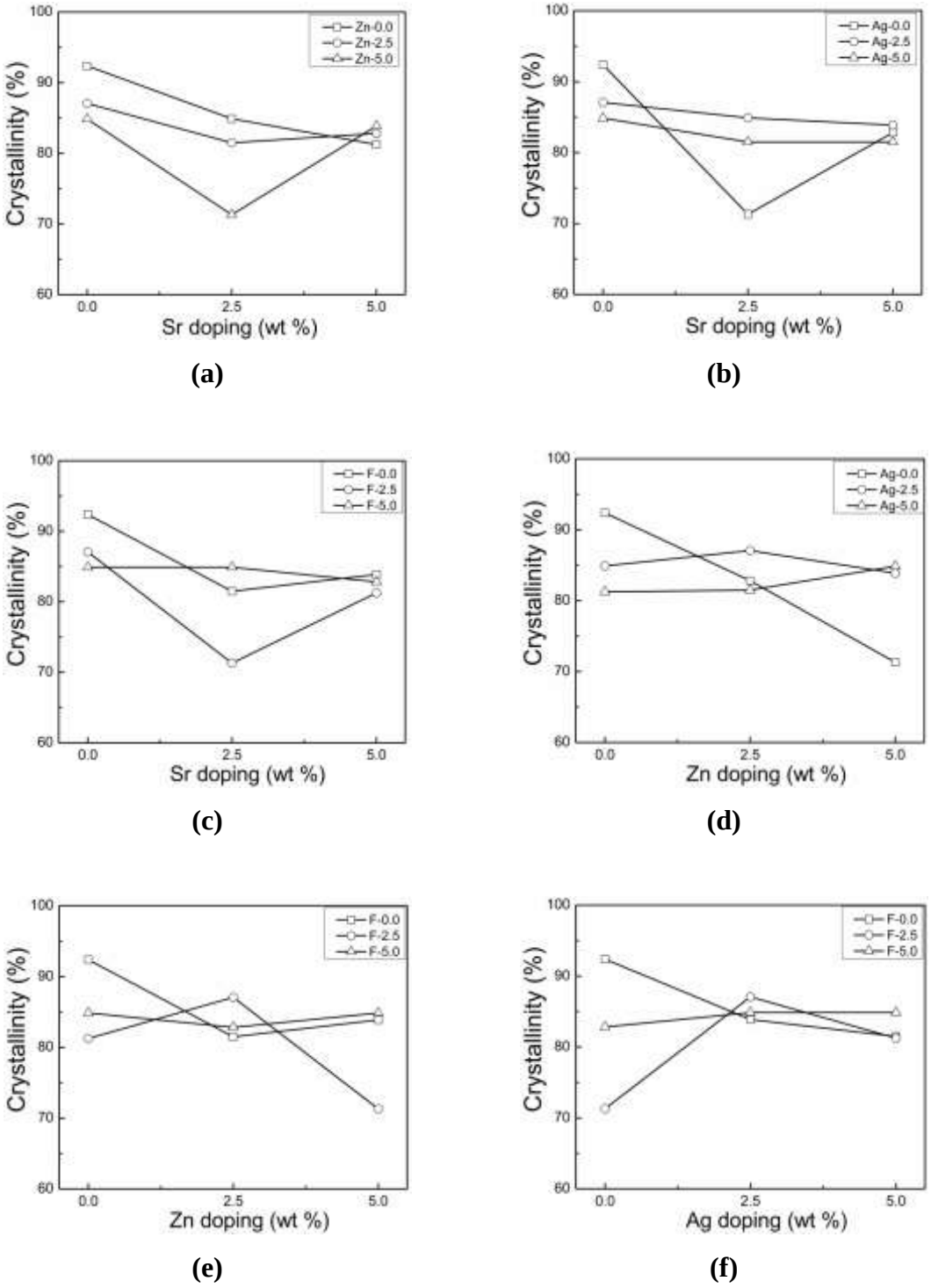

Fig. 4.4 Influence of binary ion doping on crystallinity of HA after doping with (a) Zn-Sr, (b) Ag-Sr, (c) F-Sr, (d) Ag-Zn, (e) F-Zn, (f) F-Ag.

However, HA crystallinity can be increased with increasing concentration of Ag at 5%F. For the F < 2.5%, the crystallinity continuously decreases with increasing Ag concentration. In summary, from these binary interactions it can be seen that maximum crystallinity in doped HA can be achieved if the binary dopant concentrations is < 2.5%. However, the lowest crystallinity of HA was found to depend on binary ion doping combination. For example, minimum crystallinity of Sr doped HA was observed with 2.5Sr+5Zn or 2.5 F or <2.5Ag and Zn doped HA showed minimum crystallinity at 5Zn+<2.5Ag or 2.5F. For relatively high dissolution rate one can use HA doped with 2.5F+ <2.5Ag.

4.1.4 Ternary and quaternary ion doping affect crystallinity of HA

Assessing the effect of multiple ion doping (ternary and quaternary) on crystallinity and crystallite size of HA is highly complex. There is no method to identify the same using standard DOE analysis. Therefore, we have considered the binary doping effect to identify HA compositions containing Sr and Zn that can provide nominal and lowest crystallinity in doped HA. Then, these binary compositions were used to assess the effect of other two dopants namely F and Ag on crystallinity. Binary compositions of HA thus identified were 2.5Sr-2.5Zn, 2.5Sr-5.0Zn, 5.0Sr-2.5Zn and 5.0Sr-5.0Zn (Fig. 4.4a). The effect of F and Ag addition on crystallinity of these Sr-Zn doped HA is presented in Fig. 4.5a and b, respectively. Interestingly, the ternary interaction plots were found to be parallel, which indicates the absence of interaction between third dopant (F or Ag) and Sr-Zn binary doping on the crystallinity of HA. Further, the influence of F and Ag as ternary dopant to HA is very similar to their respective individual effects on crystallinity (as shown in Fig. 4.3a). For example, the crystallinity was lowest at 2.5%F whether it is added to HA as individual or ternary dopant. To achieve nominal crystallinity in Sr-Zn-F doped HA, Fig. 4.5a, the composition would be 5.0 Sr-2.5Zn with 5.0F or <2.5F.To achieve relatively more degradability, with lowest crystallinity, a composition with 2.5Sr-5.0Zn-2.5F can be used. From Fig. 4.5b, ternary composition (i.e., 5.0Sr-2.5Zn-2.5Ag) is expected to exhibit antibacterial properties to HA. For other binary compositions of Sr-Zn, the crystallinity close to nominal was observed at 2.5% Ag. The influence of F and Ag doping on the crystallinity of ternary ion doped HA (Sr-Zn-Ag and Sr-Zn-F) is presented in Figs. 4.5c and d, respectively. As with ternary interactions, no interaction between Sr-Zn-Ag and Sr-Zn-F doped HA and

quaternary ion doping of F and Ag, respectively, was observed. From the quaternary interactions it was noted that HA with 5.0Sr-2.5Zn-2.5Ag-5.0F or <2.5F provides nominal crystallinity.

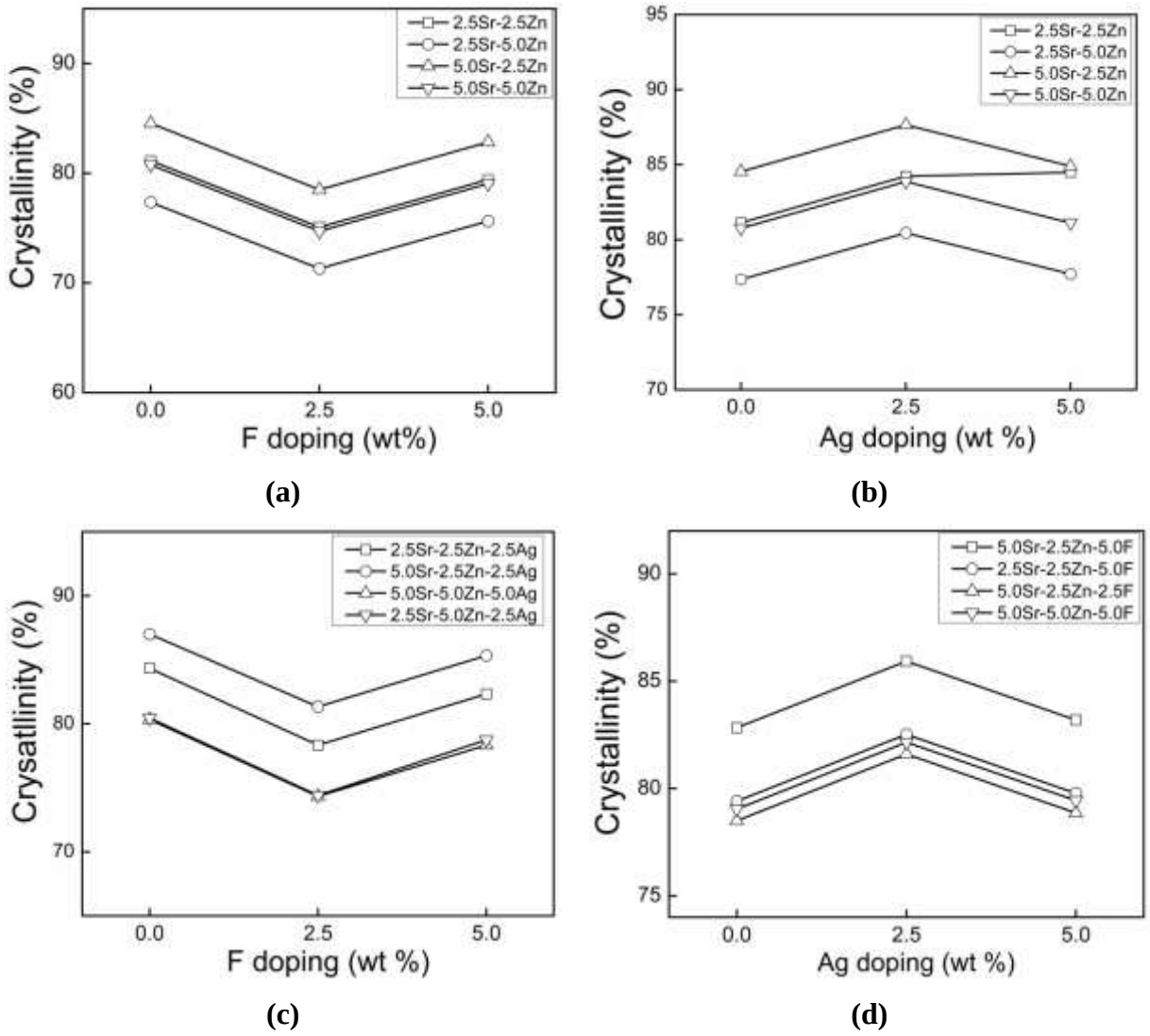

Fig. 4.5 Influence of ternary ion on crystallinity of binary ion doped HA; (a) F + Sr-Zn, and (b) Ag + Sr-Zn. Effect of quaternary ion on crystallinity of ternary ion doped HA; (c) F + Sr-Zn-Ag, and (d) Ag + Sr-Zn-F.

General analysis of individual, binary, ternary and quaternary ion doping of HA with Sr^{+2}, Zn^{+2}, Ag^{+} and F^{-} showed that the crystallinity decreases from 92% to 80-89% with individual doping. It is further decreased to 72-92%,72-88%, and 74-87% for binary doping,

ternary and quaternary doping system, respectively. Since the contribution of Ag towards crystallinity is minimum (Table 3), hence its addition as ternary or quaternary dopant provides more flexibility to tailor the composition without significantly affecting the crystallinity. Similar flexibility can be achieved with the addition of F although its effect is lesser than that of Ag.

4.2 Effect of multi-ion doping on crystallite size

4.2.1 Binary ion doping

Following the methodology used to analyze the effect of binary ion doping on crystallinity, the changes in the crystallite size of HA as a function of binary dopant concentration is also assessed and reported in this section. The binary interaction plots of crystallite size, presented in Fig. 4.6, clearly demonstrate strong interaction between different 5F-<2.5Zn, 5Ag-2.5F and 2.5F-<2.5Ag. binary dopants and their concentration. Compared to crystallinity, the binary interaction appears to be relatively strong in crystallite size. Table 4.1 shows that the crystallite size of undoped HA powder (L1) is 44 nm. The main effects of dopants on crystallite size, Fig. 4.3b, indicate that the crystallite size can vary between 39 nm and 54 nm depending on the dopant and its concentration. However, with binary doping it was observed, Fig. 4.6, that a minimum crystallite size of 31 nm can be achieved with some binary compositions and other combinations resulted in crystallite sizes up to 59 nm.

The interaction between Sr and Zn on crystallite size is shown in Fig. 4.6a. A gradual decrease in the crystallite size was observed with increase in Sr concentration at 2.5Zn. This clearly shows a maximum crystallite size when added to HA as single dopant (Fig. 4.3b). Similar effect of Sr can be seen in the presence of 2.5Ag/5Ag and 5F, respectively, as shown in Fig. 4.6b and c. These observations clearly demonstrate positive influence of Sr co-doping with Zn, Ag, F etc. in achieving finer crystallite size in binary doped HA. The binary doping concentrations, involving Sr, Zn, Ag and F, that can achieve crystallite size (32-34 nm) smaller than pure HA (44 nm) include 2.5Sr-5.0Zn, 5.0Sr-<2.5Zn, 2.5Sr-<2.5Ag, 5.0Sr-5.0Ag, 2.5Sr-2.5F and 5.0Sr-2.5F.The interaction between Zn and Ag co-doping on crystallite size, Fig. 4.6d, appears to be minimum when the concentration of Ag is ≤ 2.5, where lowest crystallite size was observed at 5.0Zn.

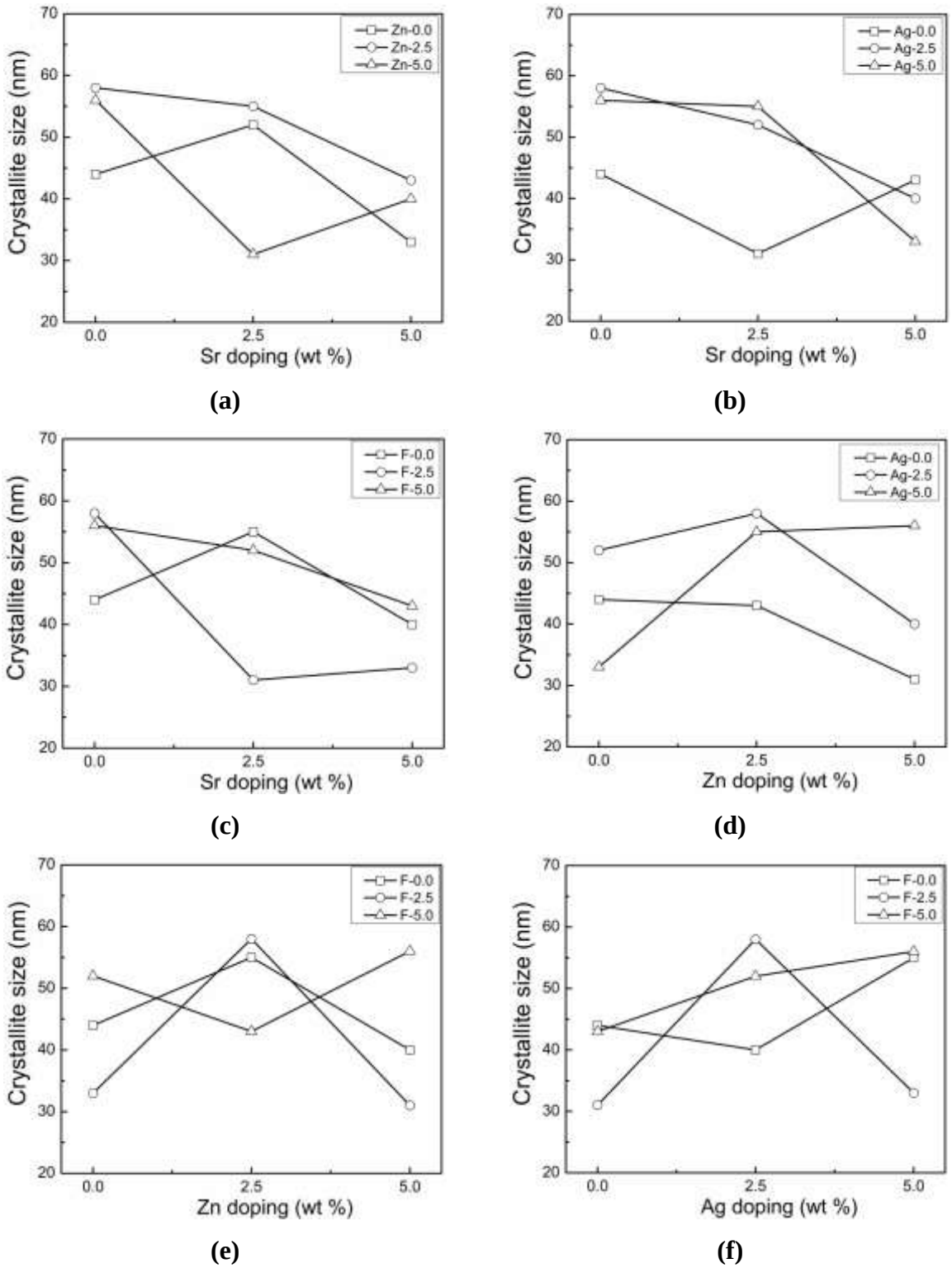

Fig. 4.6 Effect of binary ion doping on crystallite size of HA doped with (a) Zn-Sr, (b) Ag-Sr, (c) F-Sr, (d) Ag-Zn, (e) F-Zn, and (f) F-Ag.

However, at 5.0Ag increasing the Zn concentration increased the crystallite size to 58 nm. Crystallite size comparable to that of pure HA can be achieved with binary doping of 2.5Ag and 5 Zn. Similarly, the effect of Zn and Ag concentration on crystallite size was found to be strongly dependent on F concentration as shown in Fig. 4.6e and f, respectively. Lowest crystallite size of 31 nm was observed with 2.5F-5Zn and comparable crystallite size of 33 nm can also be achieved with 2.5F-5Ag (Fig. 4.6f). Significant increase in the crystallite size was observed with Ag concentration when doped with 5% and < 2.5% F (Fig. 4.6f). In other words, finer crystallite size (i.e., 31-34 nm) can be achieved for the compositions named as 5Ag-<2.5Zn, 5Zn-<2.5Ag, 2.5F-5Zn, 2.

4.2.2 Ternary and quaternary ion doping

Figure 4.7a and b show the effect of Ag and F on the Sr-Zn binary ion doped HA compositions. Binary compositions of HA identified are 2.5Sr-2.5Zn, 2.5Sr-5.0Zn, 5.0Sr-2.5Zn and 5.0Sr-5.0Zn. The ternary doping of Ag at concentration ≤ 2.5% resulted in small crystallite size in Sr-Zn doped HA (Fig. 4.7a). Binary doping of HA with 5.0Sr-5.0Zn is found to provide crystallite size smaller than pure HA irrespective of Ag concentration. However, other binary compositions of Sr and Zn can achieve smallest crystallite size with Ag < 2.5%.Therefore, it can be said that fine crystallite size along with antibacterial properties can be achieved in 5.0Sr-5.0Zn HA co-doped with ≤ 2.5% Ag. On the other hand, Fig. 4.7b shows that the ternary doping of F at concentrations (up to 5 %) in Sr-Zn doped HA results in crystallite size less than pure HA, however, there is an exceptional case of 2.5Sr-2.5Zn.

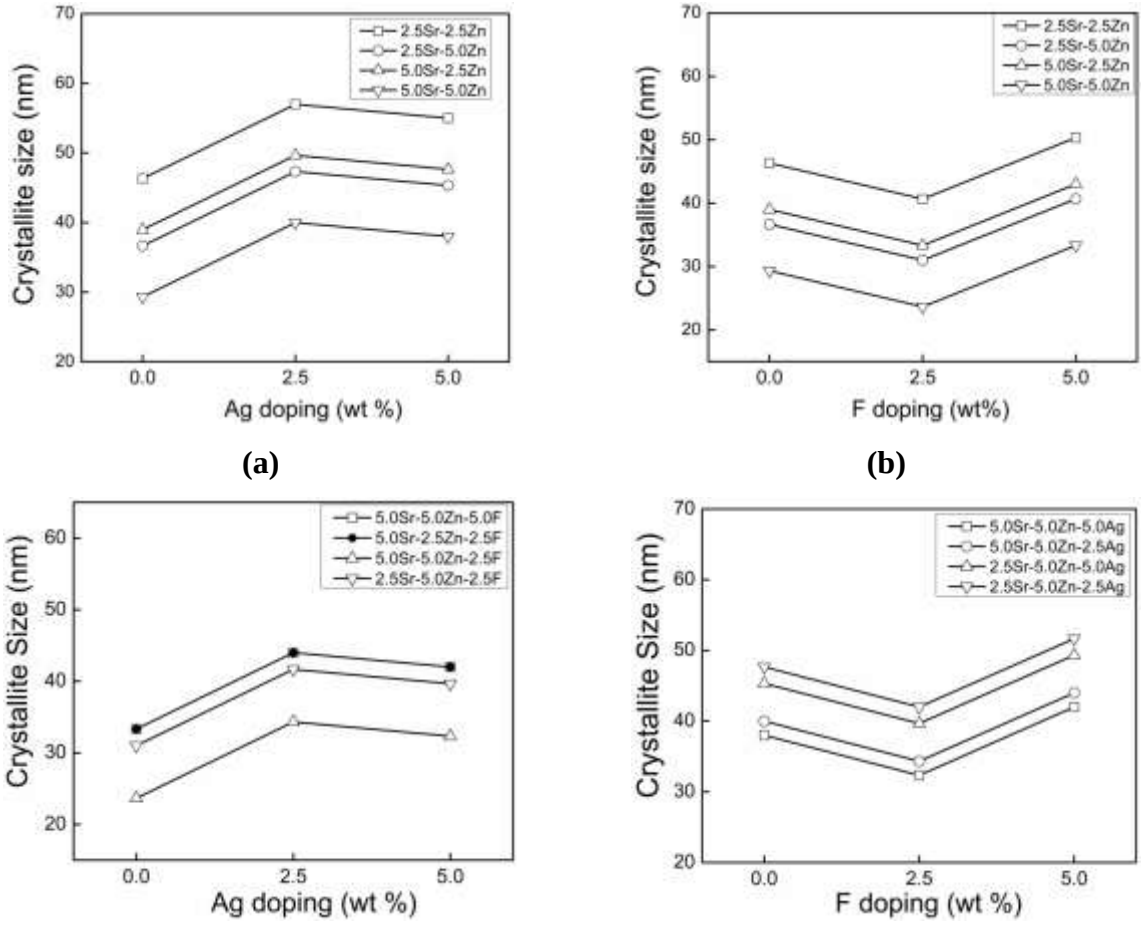

Fig. 4.7 Influence of ternary ion on crystallite size of binary ion doped HA; (a) Ag + Sr-Zn, and (b) F + Sr-Zn. Effect of quaternary ion on crystallite size of ternary ion doped HA; (c) Ag + Sr-Zn-F, and (d) F + Sr-Zn-Ag.

The quaternary doping effect of Ag and F on the crystallite size of Sr-Zn-F and Sr-Zn-Ag doped HA is shown in Figs. 4.7c and d, respectively. This also indicates trend similar to those of ternary doping. From the quaternary interactions it was noted that HA doping with 5.0Sr-5.0Zn-2.5F-≤2.5Ag (Fig. 4.7c) or 5.0Sr-5.0Zn-5.0Ag-2.5F (Fig. 4.7d) provides smaller crystallite size.

4.3 Chemical composition by X-Ray fluorescence (XRF)

XRF provides the quantitative composition of the undoped and doped HA samples. The compositions of the undoped and doped HA samples examined by XRF are summarized in Table 4.3 which shows the presence of all doping elements in their respective oxide form except F that

obtained in the elemental. The XRF data clearly reveals and confirm that doping of all four elements was successfully done using high energy planetary ball milling.

Table 4.3 Chemical composition in wt% (XRF) of undoped and doped HA samples

	CaO	**P_2O_5**	**SrO**	**ZnO**	**Ag_2O**	**F**	**SiO_2**	**MgO**
L1	58.73	40.55	0.02	0.00	0.00	0.00	0.60	0.03
L2	57.31	34.67	0.02	2.43	2.48	2.08	0.50	0.47
L3	53.63	32.07	0.03	4.57	4.63	3.39	0.87	0.70
L4	56.25	32.92	2.33	0.00	2.38	4.53	0.40	0.54
L5	55.70	33.11	2.47	2.42	4.88	0.00	1.01	0.42
L6	57.12	32.24	2.48	4.54	0.00	2.40	0.39	0.39
L7	54.67	32.39	4.91	0.00	4.94	2.22	0.35	0.45
L8	55.78	31.64	4.89	2.41	0.00	4.19	0.35	0.35
L9	56.12	31.13	4.94	4.79	2.20	0.00	0.47	0.37

4.4 FTIR analysis of undoped and doped HA compositions

The FTIR spectra of sintered pure (L1) and doped HA compositions (L2-L9) are compared in Fig. 4.8. Only functional groups with lowest and highest percentage transmittances are shown in the plots. It is well known that IR spectra of chemical compounds originate due to different modes of vibration and rotation of characteristics functional group. Fig. 4.8shows characteristics bands of water (OH^-), phosphate and carbonate species that corresponds to the HA structure. For better understanding and clarification, the summary of FTIR spectra with respective functional group present in pure HA and doped HA compositions are shown in Table 4.4.

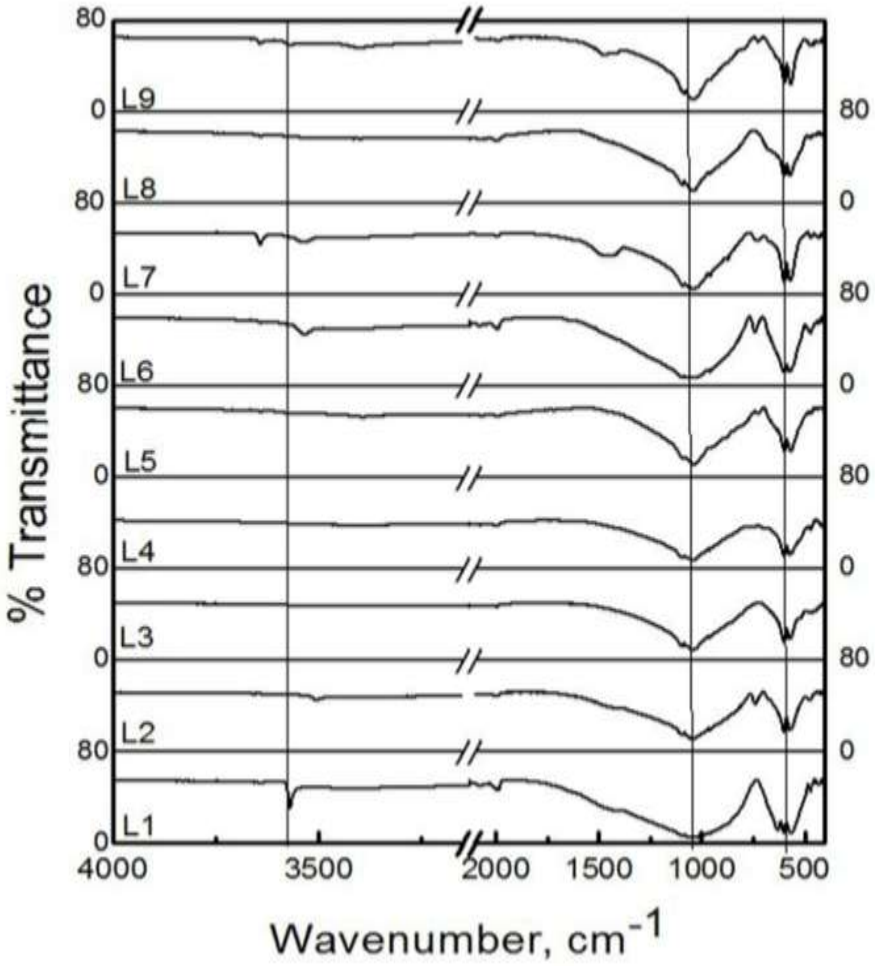

Fig. 4.8 FTIR spectra of undoped and doped HA samples.

From Fig. 4.8, it is seen that the pure HA exhibits librational (ν1) modes of hydroxyl (OH^-) group in the wavelength region of 625-635 cm^{-1}. Further the stretching (vibration) modes (ν5) of the same hydroxyl group were also observed in the broad wavelength region of 3400-3800 cm^{-1}. It also exhibits a transmittance peak of hydroxyl group at 3571 cm^{-1} which confirms the crystalline nature of synthesized HA. In case of phosphate species, the major characteristics band of PO_4^{3-} functional groups are in the regions of 595-605(ν4), 565-575 (ν4), 955-965 (ν1), 1020-1040 (ν3) and 1080-1100 (ν3) cm^{-1} with vibration modes in almost all pure and doped HA compositions.

The presence of PO_4^{3-} bands demonstrates that doping ions did not alter the basic structure of HA and confirm the purity of HA. Small hump or band at 1510-1380 cm^{-1} and 880-890 cm^{-1} region represents asymmetric stretching (ν3) of the C-O of carbonate group, which

revealed some level of carbonate substitution. Presence of CO_3^{2-} in doped HA samples is primarily due to $SrCO_3$ which was used as precursor material. Further, L2 (2.5Zn-2.5Ag-2.5F) and L6 (2.5Sr-5.0Zn-2.5F) samples showed OH^- structural group (3571 cm^{-1}) shifting towards lower wavenumbers and L7 (5.0Sr-5.0Ag-2.5F) and L9 (5.0Sr-5.0Zn-2.5Ag) samples exhibited shifting towards higher wavenumbers compared to pure HA (L1). These shifting could be attributable to the doping of different ions (Sr^{+2}, Zn^{+2}, Ag^+ and F^-) with varying ionic radii. Further, L3 (5.0Zn-5.0Ag-5F), L4 (2.5Sr-2.5Ag-5F), and L8 (5.0Sr-2.5Zn-5F) samples exhibited no peaks or peaks with negligible intensity of OH^- ion structural group, this can be correlated with substitution of OH^- ion [20, 22, 25]. IR spectra attributed to phosphate group of L1 was found at 1021 and 1044 cm^{-1}, but doped HA (L2-L9) compositions showed this PO_4^{3-} group at higher wavenumbers, i.e., 1044-1080 cm^{-1} due to addition of dopants. Overall shifting of characteristic bands position and decreased peak intensities can be expected due to combined effect of doping of elements into HA. Further, L6 and L7 compositions showed strong band at around 3420-3450 cm^{-1} which can be assigned to metal-OH stretching mode. Formation of metal-OH may be responsible for observed changes in the crystallinity and can affect the dissolution behavior for HA.

Table 4.4 Summary of FTIR spectra of undoped (L1) and doped (L2-L9) HA samples.

	PO_4^{3-} band (v4)	**PO_4^{3-} band (v4)**	**OH^- Structural**	**CO_3^{2-} group**	**PO_4^{3-} stretch (v1)**	**PO_4^{3-} band (v3)**	**PO_4^{3-} band (v3)**	**CO_3^{2-} groups (v3)**	**OH- Structural**
L1	563	605	631	880	960	1021	1044	1416	3571
L2	565	603	NA [#]	NA	962	1044	1070	1454	NA
L3	571	601	NA	NA	964	1046	1072	NA	NA
L4	572	601	NA	NA	962	1048	1080	NA	NA
L5	565	598	624	886	963	1046	1074	NA	NA
L6	570	600	626	NA	966	1052	1076	NA	NA
L7	568	599	NA	884	960	1049	1075	1455	3624
L8	568	599	NA	NA	962	1048	1073	1461	3754
L9	563	598	628	881	959	1047	1078	1456	3680

[#] NA: Not applicable

4.5 Effect of dopants on hardness of HA and doped HA

4.5.1 Main effect of dopants on hardness

The hardness is one of the important characteristic of HA that control its mechanical stability for various bone replacement applications. Therefore, this has been considered as response parameter to assess the influence of different dopants on the hardness of HA. An "analysis of means" (ANOM) or main effect plot was used to determine the effect of individual dopant on mean response in terms of hardness of HA. During ANOM the main effects of dopants on microhardness (GPa) of HA were determined using *'nominal is best'* condition. The criterion of selecting 'nominal is best' for the microhardness is based on previous findings, i.e., too high hardness can increase brittleness tendency or indirectly increase tendency of catastrophic failure with surrounding bone while too low hardness of HA can lose its mechanical stability and thus may not sustain load bearing capacity.

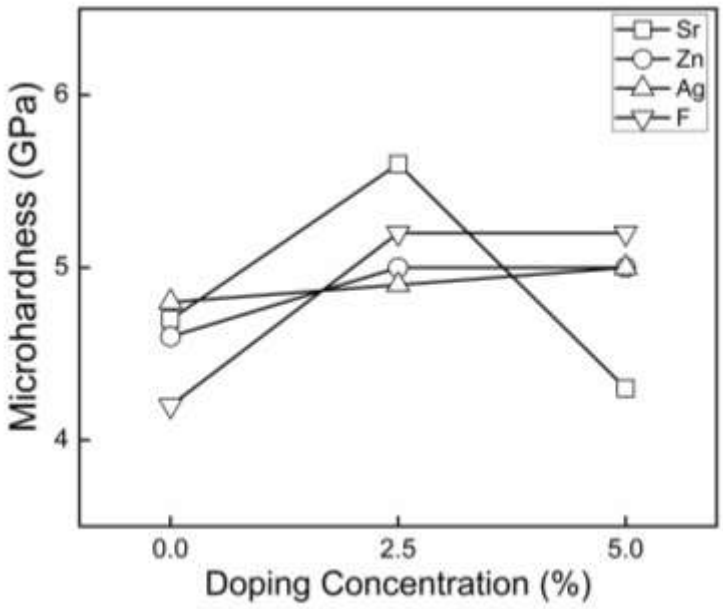

Fig. 4.9 Main effect on different dopants and their concentration on microhardness

Although, HA is hard but because of its brittleness, its applications are restricted to non-load bearing application. From the point of view of its applications in bioactive coatings, bone cementing, target drug devilry etc. the effect of dopants on the hardness of HA has been investigation and displayed in Fig. 4.9. It can be seen that the addition of Sr^{2+}upto 2.5% increased the microhardness significantly. Thereafter further addition of Sr^{2+} drastically reduces the microhardness. In contrast to this, other three doping elements (Zn, Ag, F) increased the microhardness for concentration up to 5%. At 2.5 % concentration, all doping elements showed relatively higher (that falls under nominal is best range) hardness than undoped HA. The addition of 5 % F^- ion into HA structure increased the micro hardness to about 5.26 GPa which is maximum compared to other doped HA samples [20, 22]. This is due to fact that F^- ions replaced OH^- into HA structure owing to high affinity which ultimately leads to decrease in porosity in the HA samples. The effect of doping of Zn and Ag ions on microhardness of HA is lower than those of Sr^{2+} and F^-ions [195].

4.5.2 Binary ion doping

The effect of binary dopants on micro hardness of HA is shown in Fig. 4.10. It can be seen that most of the lines are not parallel to each other confirming the clear interaction between doping ions. The interactive effect between Zn and Sr doping (Fig. 4.10a) indicates that the

highest microhardness (6.04 GPa) is obtained by the addition of Sr 2.5 % and Zn 5.0% (2.5Sr-5.0Zn-HA) into HA. The second highest microhardness (5.7 GPa) is obtained by the addition of Sr2.5 % into HA structure which is clearly confirming the finding from individual/main effect plot shown in Fig. 4.9. Further the lowest microhardness (3.80 GPa) but slightly higher than pure HA (3.70 GPa) is obtained when both the ions are doped at higher concentration of 5 % into HA. However, to achieve nominal microhardness both ions should be doped at 2.5 % (each) into HA structure. So it is clear from the Fig. 10a that higher concentration of the ions together (Sr^{2+}, Zn^{2+}) is not desirable to get nominal hardness for various biomedical applications. Figure 4.10bshows that $Ag^{+}\geq$ 2.5% decreases microhardness when $Sr^{2+}\geq$ 2.5% is also added into HA structure. However, the highest hardness is obtained when only Sr content in HA is 2.5%. The positive influence of Sr^{2+}upto 2.5% maintains the nominal hardness of HA with irrespective of Ag concentrations. The interaction effect between Sr^{2+} and F^{-} on hardness of HA is shown in Fig. 4.10c. It indicates that Sr^{2+} ion with 2.5 % has positive influence when doped with $F^{-}\geq$ 2.5% into HA structure. Hence, the nominal microhardness can be achieved by the addition of $F^{-}\geq$ 2.5% into HA structure. The highest microhardness (6.04 GPa) is obtained when both the ions have concentration of about 2.5%. The second highest microhardness (5.7 GPa) is obtained when $Sr^{2+}$and F^{-} concentrations are 2.5 % and 5.0 %, respectively. The lowest hardness (3.8 GPa) is obtained when $Sr^{2+}$is 5.0% in absence of F^{-} ions. It is clearly investigated that higher concentration of Sr^{2+} (> 2.5%) has negative influence on microhardness of the HA when co-doped with F^{-}. In contrast, the higher concentration of F^{-}as individual dopant is favorable (Fig. 4. 9) to provide mechanical stability of HA products without affecting biological response.

Fig. 4.10d shows the binary interaction effect between Ag^{2+} and Zn^{2+} on microhardness of HA. It can be seen that Ag-0 line shows purely increasing trend in microhardness when Zn^{2+} ion concentration is increased from 0 to 5 %. Similarly, Ag-5.0 (5 % Ag^{2+} ion doped HA) line show increasing trend with increasing Zn^{2+} concentration. In contrast, Ag-2.5 line shows a continuous decreasing trend in microhardness when Zn^{2+} concentration increased from 0 to 5%. So from this binary plot it can be seen that both at higher concentration increases the microhardness. The nominal microhardness scan be obtained by adding 2.5% concentration of each (Ag^{2+} and Zn^{2+}) ions.

The binary interaction effect between Zn^{2+} and F^{-} on microhardness of HA is shown in Fig. 4.10e. It can be clearly seen that F-2.5 and Zn-2.5 shows nominal range of microhardness.

On further increasing (i.e., > 2.5%) concentration of $F^-$with 2.5 % Zn^{2+} (F-2.5 line), there is an increasing trend in microhardness. F-5.0 line shows an initial decrement in microhardness upto 2.5% of Zn and thereafter, there is increasing trend. F-0.0 line in combination with Zn-0.0 % or 5.0% shows the lowest microhardness (3.8 GPa) indicating that the nominal microhardness can be achieved for 2.5 % Zn^{2+}doped HA. Further F-2.5 and F-5.0 lines with Zn ≥ 2.5% show an increasing trend. For nominal microhardness, the concentration of $F^-$and Zn^{2+}ions should be 2.5 % each. If F^- concentration increased to ≥ 2.5% then the combined or binary effect on other properties such as crystallinity, dissolution and other biological response may play key roles.

From Fig. 4.10f, it can be seen that F-2.5 line with 0 % Ag shows the highest microhardness (6.04 GPa) which is approximately doubled than the undoped HA. On increasing concentration from 0 to 5 % Ag^+ ion along with F^- (at 2.5 %), there is a gradual decreasing trend in microhardness. The second highest microhardness (5.7 GPa) is achieved at 5 % F^-in combination of 2.5% Ag^+ ion. The lowest hardness is obtained when Ag^+ ion is either 0% or 2.5% without F^-HA. For a nominal hardness, both the ions can be doped with 2.5 % each into HA.

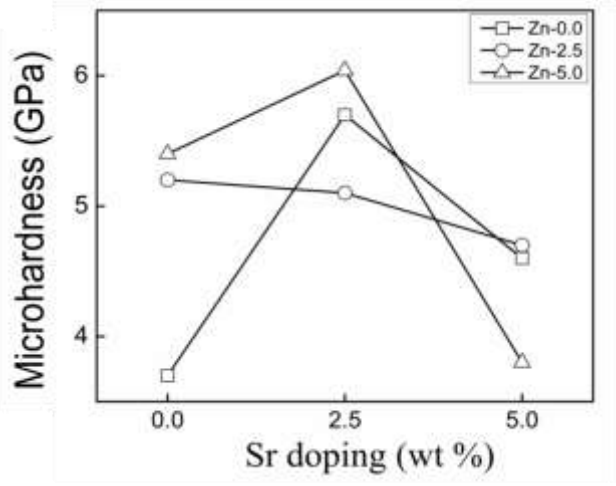
Zn-0.0
Zn-2.5
Zn-5.0
Microhardness (GPa)
Sr doping (wt %)

(a)

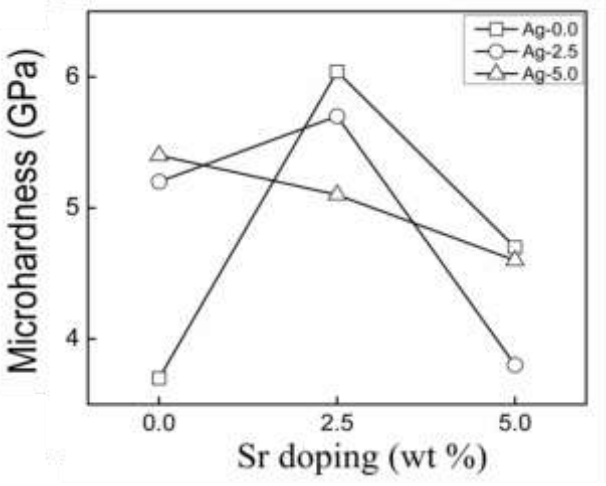
Ag-0.0
Ag-2.5
Ag-5.0
Microhardness (GPa)
Sr doping (wt %)

(b)

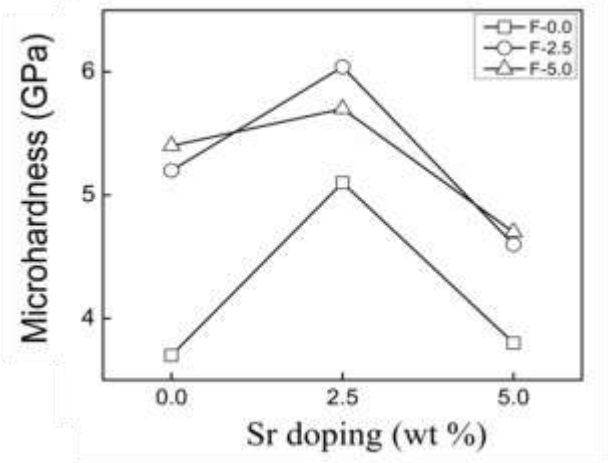
F-0.0
F-2.5
F-5.0
Microhardness (GPa)
Sr doping (wt %)

(c)

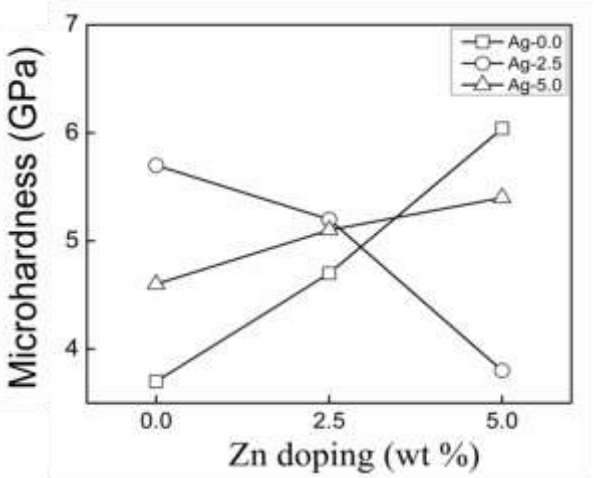
Ag-0.0
Ag-2.5
Ag-5.0
Microhardness (GPa)
Zn doping (wt %)

(d)

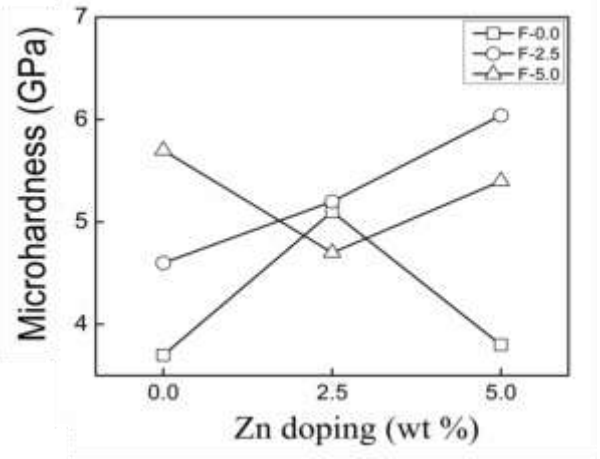
F-0.0
F-2.5
F-5.0
Microhardness (GPa)
Zn doping (wt %)

(e)

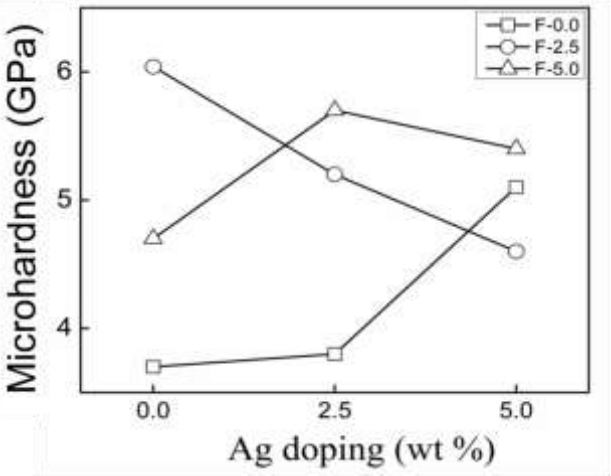
F-0.0
F-2.5
F-5.0
Microhardness (GPa)
Ag doping (wt %)

(f)

Fig. 4.10 Influence of binary ion doping on microhardness of HA (a) Zn-Sr, (b) Ag-Sr, (c) F-Sr, (d) Ag-Zn, (e) F-Zn, (f) F-Ag.

4.5.3 Ternary and quaternary ion doping

Assessing the effect of multiple ion doping (ternary and quaternary) on microhardness of HA is quite tedious. In this section, we have considered the effect of F^- and Ag^+ ions as ternary and quaternary on the microhardness of the HA doped with Sr(2.5% and 5%) and Zn (2.5% and 5%) using standard DOE method.

The effect of F and Ag addition on microhardness of the Sr-Zn doped HA is shown in Fig. 4.11a and b, respectively. It is interesting to see that all the lines are almost parallel, which indicates no interaction between third dopant (F^- or Ag^+) and Sr-Zn binary system on the microhardness of HA. This effect is similar to those of individual effect of either F^-or Ag^+ (Fig. 4.9). The F^- as ternary ion into Sr-Zn doped HA increases microhardness when added up to 2.5% and thereafter the effect is negligible (Fig 11a). In contrast, the addition of Ag^+ as ternary has no influence on microhardness of Sr-Zn doped HA. Similar trends can be seen in quaternary ion doped HA as shown in Fig 11c and d. The best ternary and quarternary compositions of HA for high hardness would be 2.5Sr-5.0Zn-2.5F or 2.5Ag and 2.5Sr-5.0Zn-2.5Ag-2.5F, respectively. Interestingly, the concentration of Zn, Ag and F in these compositions can also ensure smaller crystallite size.

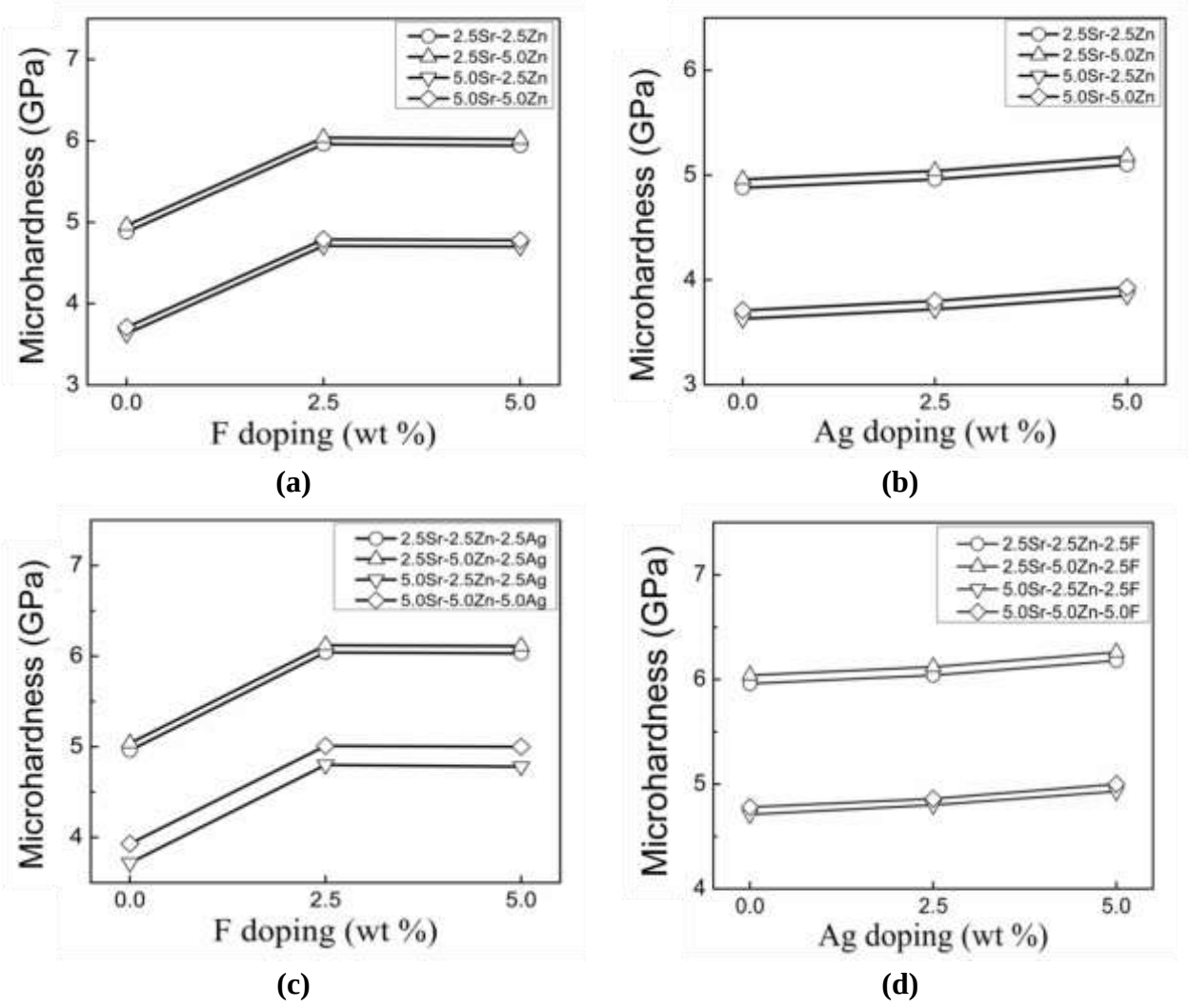

Fig. 4.11 (a-b) Influence of ternary ion on microhardness of binary ion doped HA (a) F+ Sr-Zn, (b) Ag + Sr-Zn, (c-d) Effect of quaternary ion on crystallinity of ternary ion doped HA (c) F + Sr-Zn-Ag, (d) Ag + Sr-Zn-F.

4.6 *In vitro* cell proliferation

The viability of NIH3T3 cells (normalized with respect to pure HA, i.e., L1) on pure HA (L1) and doped HA (L2-L9) after 3, 5 and 7daysof culture is shown in Fig. 4.12. The data revealed clear influence of different dopants and their concentration on cell proliferation. All compositions showed increase in proliferation up to 5 days of culture (except L7) by the end of day 7 considerable decrease in the proliferation was observed in all samples except L3 and L4. As shown in Table 4.5, the proliferation on L3 (5.0Zn-5.0Ag-5.0F), although gradually increased from 38% to 70% with culture duration, is lowest amongst the samples. This could be due to potential toxic effects of Ag^{+} and F^{-}at high concentration (5 wt. %). However, the negative effect of Ag^{+} decreased when its concentration was reduced to 2.5% in L4 (2.5Sr-2.5Ag-5F). Moreover, the proliferation reached close to pure HA (L1) at day 5 and increased to 142% at day 7 due to positive influence of Sr on cell proliferation [51, 57, 58]. Among the compositions, samples with 5.0Sr-5.0Ag-2.5F (L7) showed drastic decrease in the cell proliferation from 205% at 3 day to 76% at 7 day. This could be due to long-term toxic effect of Ag [59-61], which could not be compensated with Sr. Almost 2-fold increase in the early-stage proliferation was recorded with L2 (2.5Zn-2.5Ag.-2.5F), L6 (2.5Sr-5.0Zn-2.5F), L7 (5.0Sr-5.0Ag-2.5F) and L9 (5.0Sr-5.0Zn-2.5Ag) after 3 days of culture duration. All compositions continued to show and an increase in the cell proliferation up to 5 days (except L7 which showed cell inhibition). However, after 7 days the cell proliferation on L2, L5, L6, L8 and L9 samples decreased and reached close to that of pure HA (L1). The potential reason for this decreased proliferation, particularly after 7 days, is believed to be continued high growth rate of cells on these samples with limited surface area that can support these highly proliferating cells. It is very interesting to note that the cell proliferation on these samples was never below that of L1 (pure HA), which demonstrate non-toxicity of these HA compositions. Present results suggest that HA compositions with up to 5.0%Sr, 2.5-5.0%Zn, up to 2.5% Ag and F can aid in enhanced cell proliferation compared to pure HA.

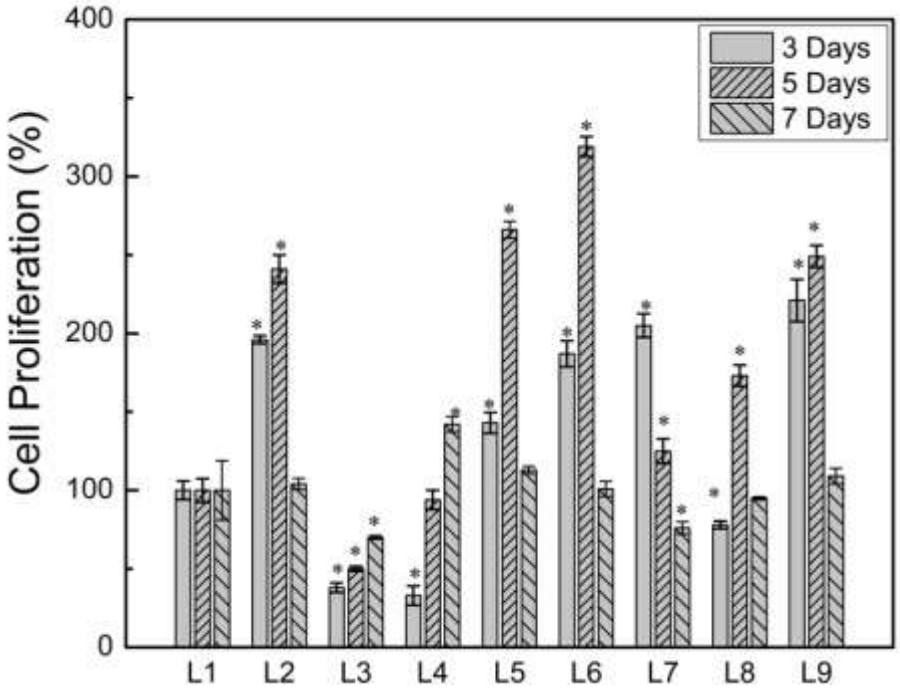

Fig. 4.12 The influence of HA composition on NIH3T3 cell proliferation * $p < 0.05$ with respect to pure HA (L1).

Table 4.5 Normalized NIH3T3 cell proliferations (%) on different HA compositions.

Composition	3 days	5 days	7 days
L1	100 ± 5.9	100 ± 7.5	100 ± 18.9
L2	196 ± 2.5	241 ± 8.9	104 ± 3.6
L3	38 ± 3.0	50 ± 1.6	70 ± 1.2
L4	33 ± 6.2	94 ± 6.1	142 ± 4.8
L5	143 ± 6.7	266 ± 5.4	113 ± 2.4
L6	187 ± 8.3	319 ± 6.3	101 ± 4.8
L7	205 ± 7.5	125 ± 7.8	76 ± 3.9
L8	78 ± 2.5	173 ± 6.8	95 ± 1.0
L9	221 ± 3.6	249 ± 8.34	95 ± 2.8

4.6.1 Main effects of dopants on cell proliferation

To optimize the concentration of doping elements that can enhance the cytocompatibility of HA, we have used "analysis of means" (ANOM). During this analysis the main effect of

dopants on cell proliferation was estimated using '*higher is best*' condition. The influence of dopant concentration on mean cell proliferation (%) is presented in Fig. 4.13. It can be seen from Fig. 4.14 that addition of Sr (up to 5%) increases the cell proliferation during early 3 days (Fig 4.13a). However, for long-term *in vitro* cytocompatibility, its concentration should be restricted to 2.5%, although the proliferation is similar to that of pure HA at 5%. Similar effect was observed with Zn addition and its concentration above 2.5 % appears to decrease cell proliferation after 7 days of culture (Fig. 4.13c). As shown in Fig. 4.13a, during initial 3 days F^- is found to have maximum inhibitory effect on cell proliferation at 5 %, which gradually decreased with culture duration, while the effect of Ag appears to minimum when its concentration is limited to 2.5 %.

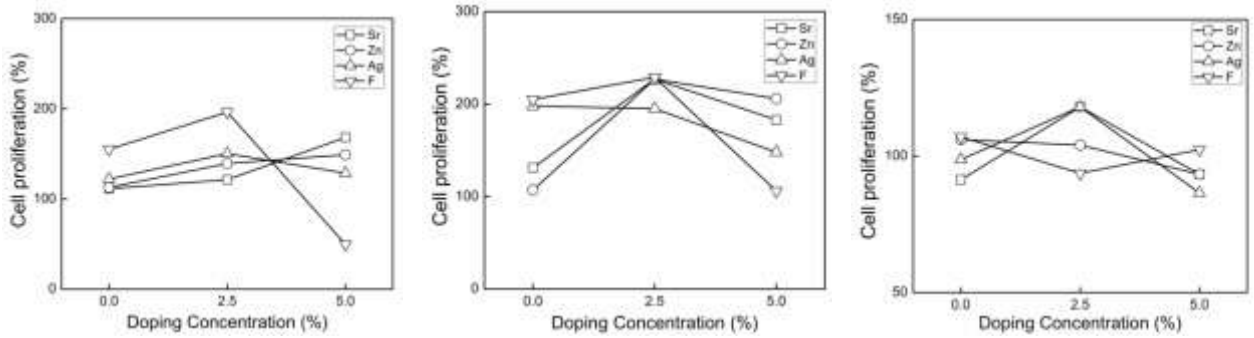

(a) (b) (c)

Fig. 4.13 Main effects of different dopants and their concentration on cell proliferation (%) (a) 3 days (b) 5 days (c) 7 days.

The percent contribution of each dopant toward in-vitro cell proliferation on different HA samples is shown in Table 4.6. It is interesting to note the contribution of each dopant changed with culture duration. For example, the contribution of Sr and Ag gradually increased with culture duration. While the contribution of F decreasing from 79% to 8% with culture duration. Mixed trend can be seen with Zn, which showed maximum contribution at day 5. During initial culture period of 3 days F had highest influence of 79.32% followed by Sr with 12.81% and other two elements had minimal effect. However, at the end of 7 day culture the influence of Ag (44.39%) marginally dominated that of Sr (39.56%) and the effect of Zn (7.90%) and F (8.15%) was very close. To rank the present doping elements in terms of their overall influence on NIH3T3 cell proliferation we have considered their cumulative effect (Table 4.3), and the

ranking was F>Sr>Ag>Zn. Based on these individual effects of dopants, high 3-days cell proliferation can be achieved with high concentration of Sr and Zn with intermediate concentration of Ag and F. However, for 7-days cytocompatibility the concentration of Sr and Ag can be fixed at 2.5 %, and Zn and F must be ≤ 2.5 %.

Table 4.6 Percent contribution of doping elements in changing the proliferation of NIH3T3 cells *in vitro*.

Doping element	3 days	5 days	7 days	Cumulative
Sr	12.81	20.09	39.56	72.46
Zn	4.84	36.02	7.90	48.76
Ag	3.09	6.98	44.39	54.46
F	79.32	36.91	8.15	124.38

4.6.2 Influence of multi-ion doping on early-stage cell proliferation

From the main doping effects, it is difficult to assess the influence of binary, ternary and quaternary ion doping on cell proliferation. For example, after 3 days the cell proliferation was lowest on HA with 5 % F (Fig. 4.13a), but this cellular inhibition can be reduced if other dopants with positive influence are added to HA. Therefore, interactions between different dopants in changing the cell proliferation are extremely useful. For this purpose, we have considered early-stage (3 days), provide an idea on rapid tissue integration with artificial implants) and later-stage (7 days), provide long term stability and toxic effects of ion doping) cell proliferation to understand the effect of binary, ternary and quaternary ion doping.

The influence of binary ion doping on cell proliferation of NIH3T3 on HA is shown in Fig. 4.14. The binary ion doping involving Sr, Zn and Ag found to have strong interaction (non-parallel lines in Fig. 4.14a, b and d) suggesting individual effect of one of these dopants on cell proliferation depends on the concentration of one of the other two dopants. Conversely, significantly less interaction can be seen between anionic dopant, F, and cationic dopants (Sr, Zn and Ag) as shown in Fig. 4.14c, e and f. However, some interaction appeared when the concentration of F ≤ 2.5 %. This trend is expected as up to 2.5% F addition increased the cell proliferation during initial 3 days and at 5 % significant cell inhibition was observed (Fig. 4.13a). However, relatively high influence of Sr, Zn and Ag, in enhancing the cell proliferation (Fig.

4.13a) resulted in improved cell proliferation on F-Sr doped HA when the Srwas 5 % in the presence of 5 % F (Fig. 4.14c). Similarly, the inhibitory effect of Zn and Ag at high concentration (5 %) resulted in low cell viability on F-Zn and F-Ag co-doped HA samples, as shown in Figs. 4.14e and f. Therefore, for enhanced early-stage cell proliferation F must be ≤ 2.5 % in F-5Sr, F-5Zn and F-2.5Ag binary doped HA. From binary interaction of Zn-Sr, Fig. 4.14a, it can be seen that maximum cell viability can be achieved with 5Zn-5Sr (~ 221%) and 2.5Zn-≤2.5Sr (~ 200%). While the toxic effect of high Ag concentration appears to be compensated by co-doping with 5 %Sr, Fig. 4.14b. For potentially good anti-bacterial properties along with cell viability HA with 2.5-5.0 % Ag and 2.5 % Zn appears to be optimal. From the binary interactions, it can be said that early-stage cell proliferation better than pure HA can be achieved with ≤ 2.5 % F, ≤ 2.5 % Ag, 2.5-5 % Sr and Zn. Furthermore, inhibitory effect of one dopant can be easily compensated by adding appropriate concentration of dopant with high cell viability. For example, the cell viability of HA with 5 % Ag (~ 120%, Fig. 4.13a) can be further enhanced to ~ 200 % by co-doping with 5 % Sr, as shown in Fig. 4.14b.

It is not possible to examine the influence of ternary and quaternary doping on cell proliferation using standard DOE method. Therefore, HA compositions co-doped with Sr and Zn exhibiting high early-stage cell proliferation were selected. Then the effect of ternary doping of either F or Ag on the cell proliferation of Sr-Zn co-doped HA was examined. The effect of F and Ag addition as ternary dopants on cell proliferation of different Sr-Zn co-doped HA samples (with high proliferation, 4.14a) is shown in Fig. 4.15a and b, respectively. No interaction between Sr-Zn binary doping with ternary doping of F or Ag could be seen (parallel lines).The proliferation of NIH3T3 cells was lowest when the concentration of F was 5 % (Fig. 4.15a) and it was maximum when Ag was 2.5 % (Fig. 4.15b) whether they were added as individual or ternary doping element. Similarly, the positive influence of 2.5F as ternary doping in Sr-Zn co-doped HA enhanced the proliferation, Fig. 4.15a, and is higher than that of Sr-Zn binary doped HA, Fig. 4.14a. However, addition of Ag to these binary doped HA did not show significant increase in the cell proliferation presumably due to its relatively less positive influence than F (Fig. 4.12a). Nonetheless, as shown in Fig. 4.14b, ternary addition of Ag up to 5 % appears to be non-toxic as the proliferation of all compositions was always higher than that of pure HA. Therefore, to achieve high early-stage cell proliferation in ternary ion doped HA the compositions would be 5Sr-5Zn-2.5Ag and 5Sr-2.5Zn-2.5Ag. Similarly, the concentration of F

would be 2.5 % in these Sr-Zn doped HA for best early-state proliferation. Fig. 4.14c and d show the effect of F and Ag doping on the cell viability of Sr-Zn-Ag and Sr-Zn-F doped HA, respectively. Here again no interaction between ternary doped HA and quaternary ion doping was observed. The analysis of Sr^{+2}, Zn^{+2},Ag^{+} and F^{-} ions doping in HA shows that the early-stage cell proliferation was always higher than pure HA, except at 5 % F^{-}. With individual doping, the proliferation increased to 110-190% and varied between 40-220% with binary doping. When the HA was doped with ternary and quaternary doping the cell proliferation was between 40 and 240%. From these effects it can be said that HA with 5.0Sr-2.5Zn-2.5Ag-2.5F provides excellent *in vitro* cell-materials interaction.

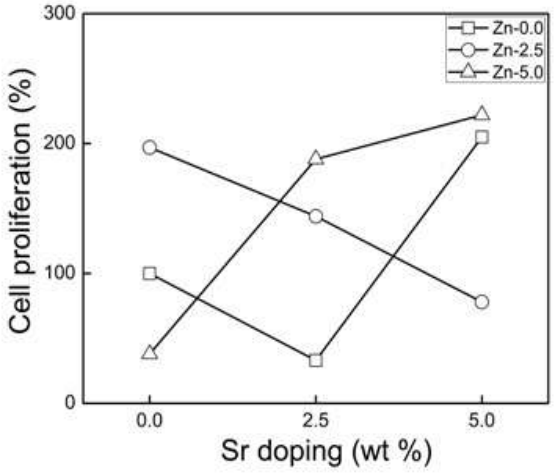
Zn-0.0
Zn-2.5
Zn-5.0
Cell proliferation (%)
Sr doping (wt %)
0
100
200
300
0.0
2.5
5.0

(a)

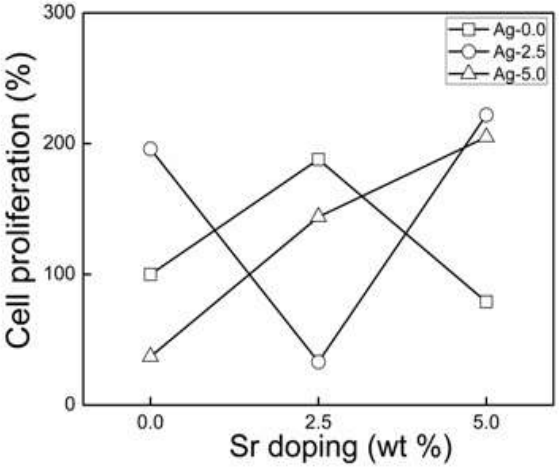
Ag-0.0
Ag-2.5
Ag-5.0
Cell proliferation (%)
Sr doping (wt %)
0
100
200
300
0.0
2.5
5.0

(b)

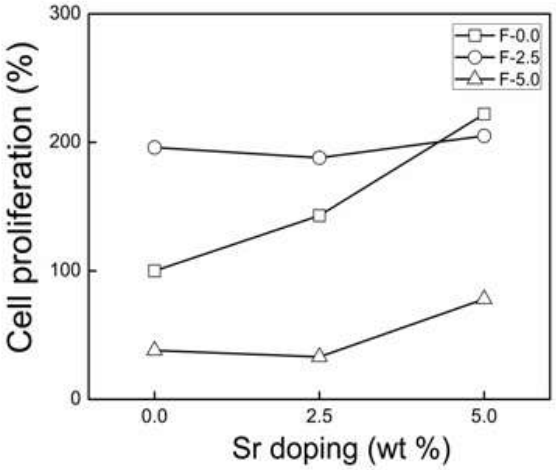
F-0.0
F-2.5
F-5.0
Cell proliferation (%)
Sr doping (wt %)
0
100
200
300
0.0
2.5
5.0

(c)

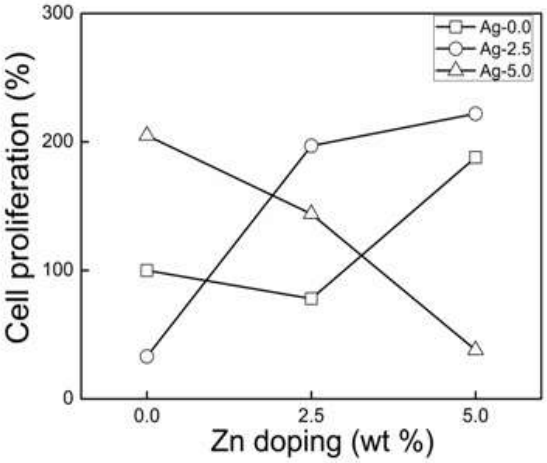
Ag-0.0
Ag-2.5
Ag-5.0
Cell proliferation (%)
Zn doping (wt %)
0
100
200
300
0.0
2.5
5.0

(d)

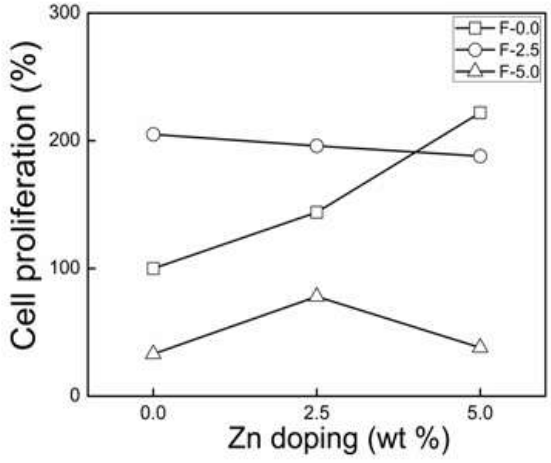
F-0.0
F-2.5
F-5.0
Cell proliferation (%)
Zn doping (wt %)
0
100
200
300
0.0
2.5
5.0

(e)

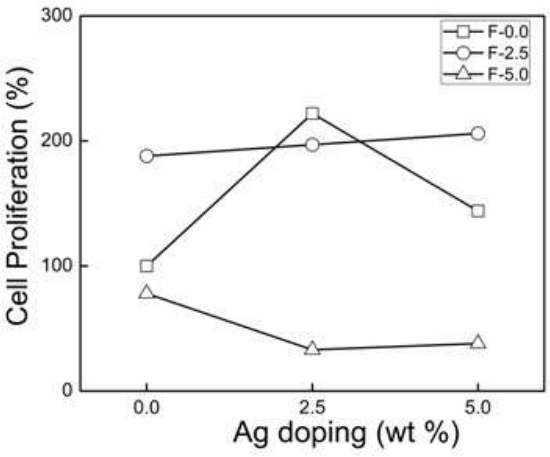
F-0.0
F-2.5
F-5.0
Cell Proliferation (%)
Ag doping (wt %)
0
100
200
300
0.0
2.5
5.0

(f)

Fig. 4.14 The effect of binary ion doping and their concentration on early-stage (3 days) NIH3T3 cell proliferation (%) on HA (a) Zn-Sr (b) Ag-Sr (c) F-Sr (d) Ag-Zn (e) F-Zn (f) F-Ag.

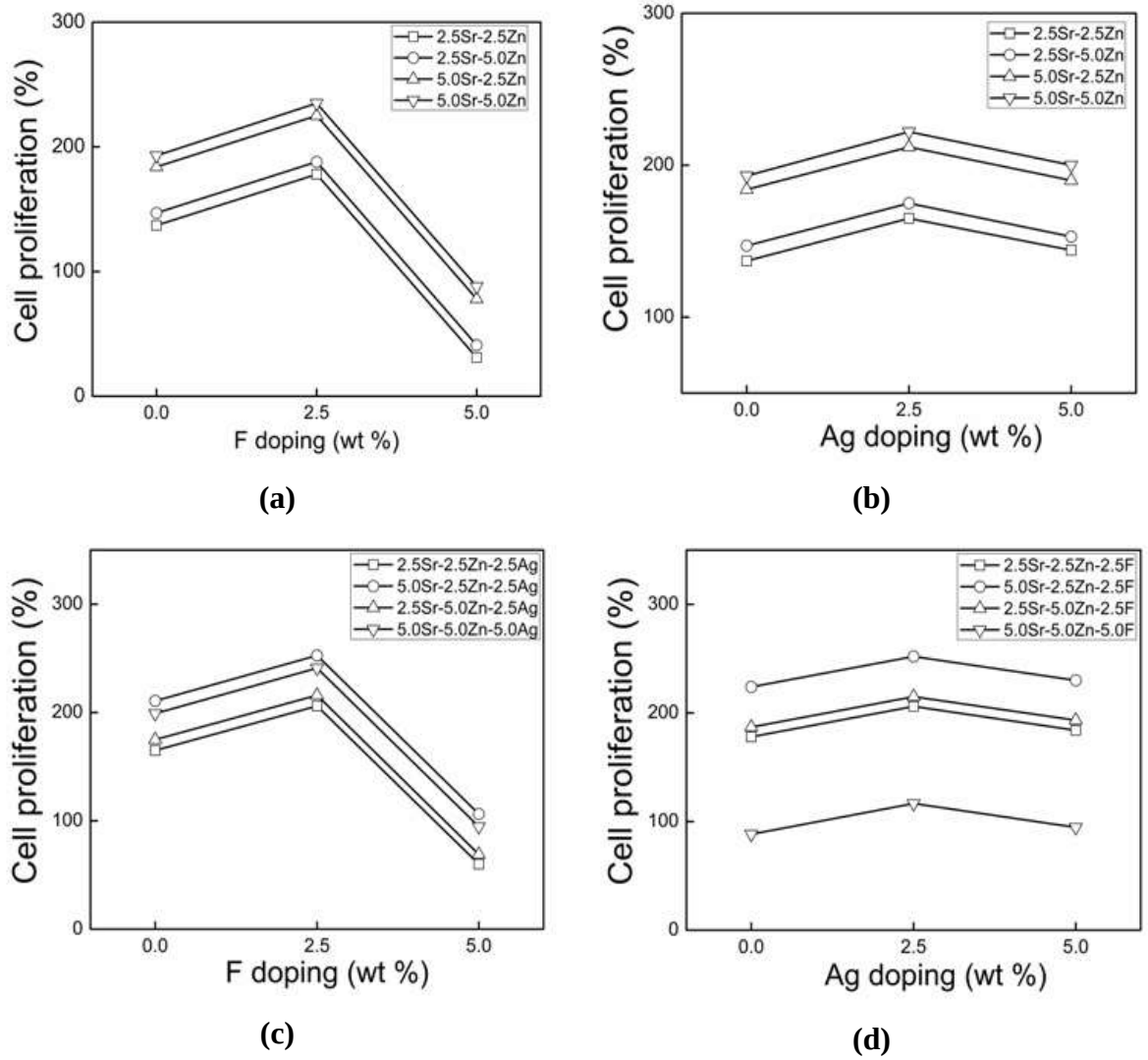

Fig. 4.15 (a,b) Influence of ternary ion on early-stage NIH3T3 cell proliferation (3 days) on binary ion doped HA (a)F+Sr-Zn, (b) Ag+Sr-Zn, (c,d) Effect of quaternary ion on 3 day cell proliferation of ternary ion doped HA (c) F+Sr-Zn-Ag, (d) Ag+Sr-Zn-F.

4.6.3 Influence of multi-ion doping on later-stage cell proliferation

The later-stage cell proliferation (7 days) on binary ion doped HA is presented in Fig. 4.16. The binary composition which exhibits high cell proliferation appears to be different for early-stage and later-stage proliferation suggesting long-term effects of different dopants and their concentration. For example, during early-stage cell proliferation the cells proliferated

rapidly on majority of HA compositions with 5 % Sr. However, when the culture duration was increased to 7 days, Fig. 4.16a-c, the proliferation was high on HA samples with 2.5 wt.% Sr. Therefore, high concentration of Sr have some inhibitory effect on long-term cell proliferation, especially in the presence of secondary ions (Zn, Ag and F). Zn doping found to have relatively stable effect during entire culture period i.e. Zn ≤ 2.5 % found to be optimal to achieve better early-stage as well as later-stage (Fig. 4.16a, d and e) proliferation than pure HA. These observations are in line with individual effects of dopants on cell proliferation at day 7. For better and stable later-stage cell proliferation the binary compositions of HA must restrict the concentration of each dopants to ≤ 2.5 %.

The influence of ternary additions of F and Ag on later-stage cell proliferation on Sr-Zn-HA is shown in Fig. 4.17a and b, respectively. The individual effect of F and Ag on later-stage proliferation, Fig. 2c, is clearly reflected in ternary interactions as well. Similarly, the influence of F on Sr-Zn-HA compositions is relatively less compared to Ag and in both cases 2.5Sr-2.5Zn-HA and 2.5Sr-5Zn-HA exhibited better later-stage cell proliferation compared to pure HA. However, the inhibitory effect of 2.5 % F (Fig. 2c) on proliferation has been nullified in these compositions with same concentration of F, i.e., the proliferation is more than pure HA. Similar beneficial effect of ternary doping of Ag into above HA compositions can be seen from Fig. 4.17a and b. Regardless of Zn, Ag and F concentration, high concentration of Sr (5 %) in Sr-Zn-Ag/F-HA appears to have some inhibitory effect on later-stage cell proliferation. Therefore, for high and stable later-stage cytocompatibility the ternary composition of HA would be 2.5Sr-2.5Zn or 2.5Sr-5Zn with up to 5 % F or Ag. The cell proliferation on quaternary ion doped HA sample is presented in Fig. 4.17c and d. One important observation is that the presence of 2.5 % Ag in Sr-Zn-HA enhanced the cell proliferation at all concentrations of F, Fig. 4.17c. For example, the proliferation of 2.5Sr-2.5Zn-2.5F increased from 120% (Fig. 4.17a) to 140% in the presence of 2.5 % Ag (Fig. 4.17c). The analysis of later-stage cell proliferation on multi-ion HA suggests that for enhanced long-term cytocompatibility the compositions of HA would contain up to 5 % F in 2.5Sr-2.5Zn-2.5Ag, 2.5Sr-5Zn-2.5Ag and 5Sr-2.5Zn-2.5Ag.

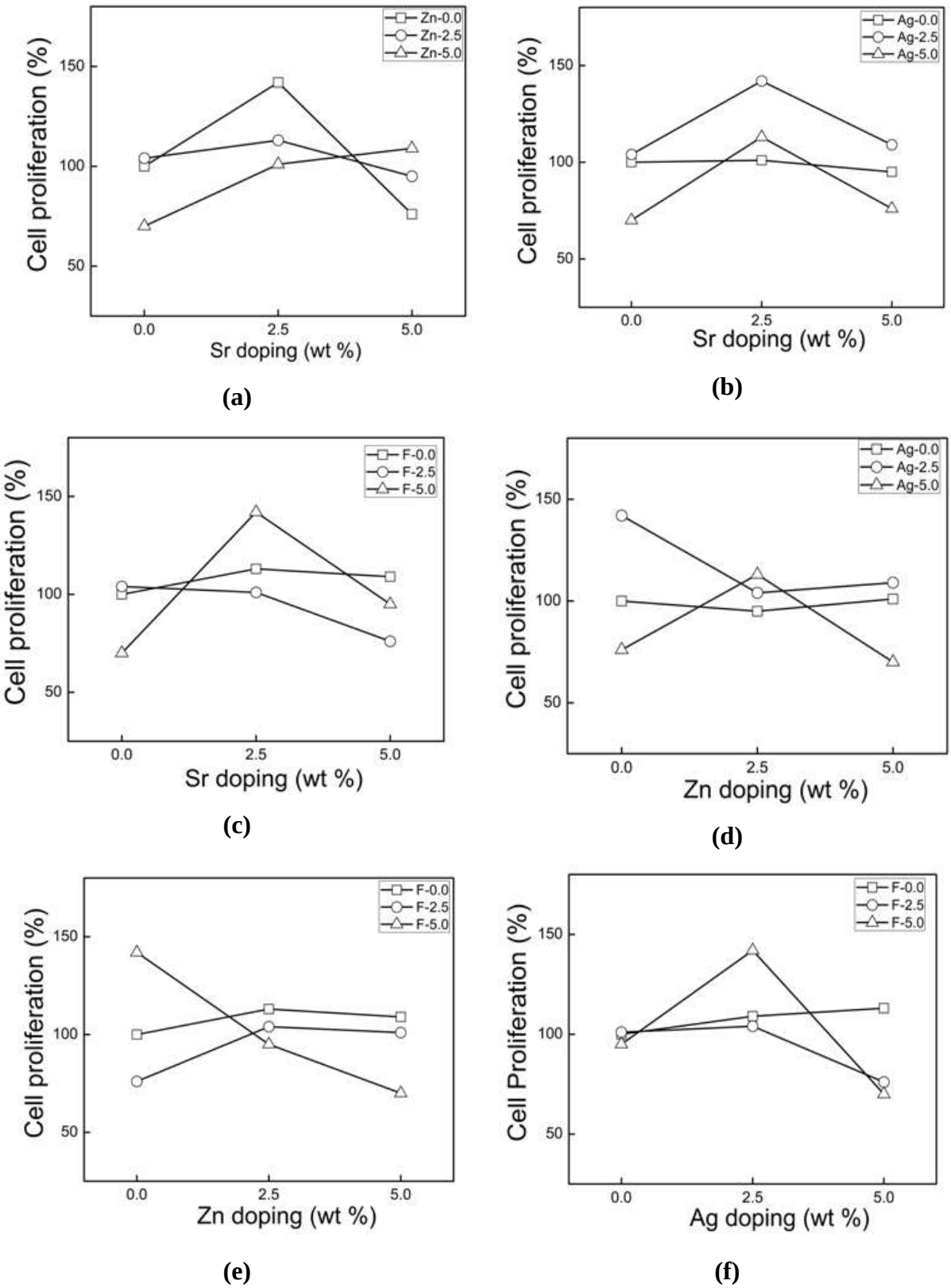

Fig. 4.16 Variations in later-stage (7 days) proliferation (%) of NIH3T3 cells on HA due to binary ion doping (a) Zn-Sr (b) Ag-Sr (c) F-Sr (d) Ag-Zn (e) F-Zn (f) F-Ag.

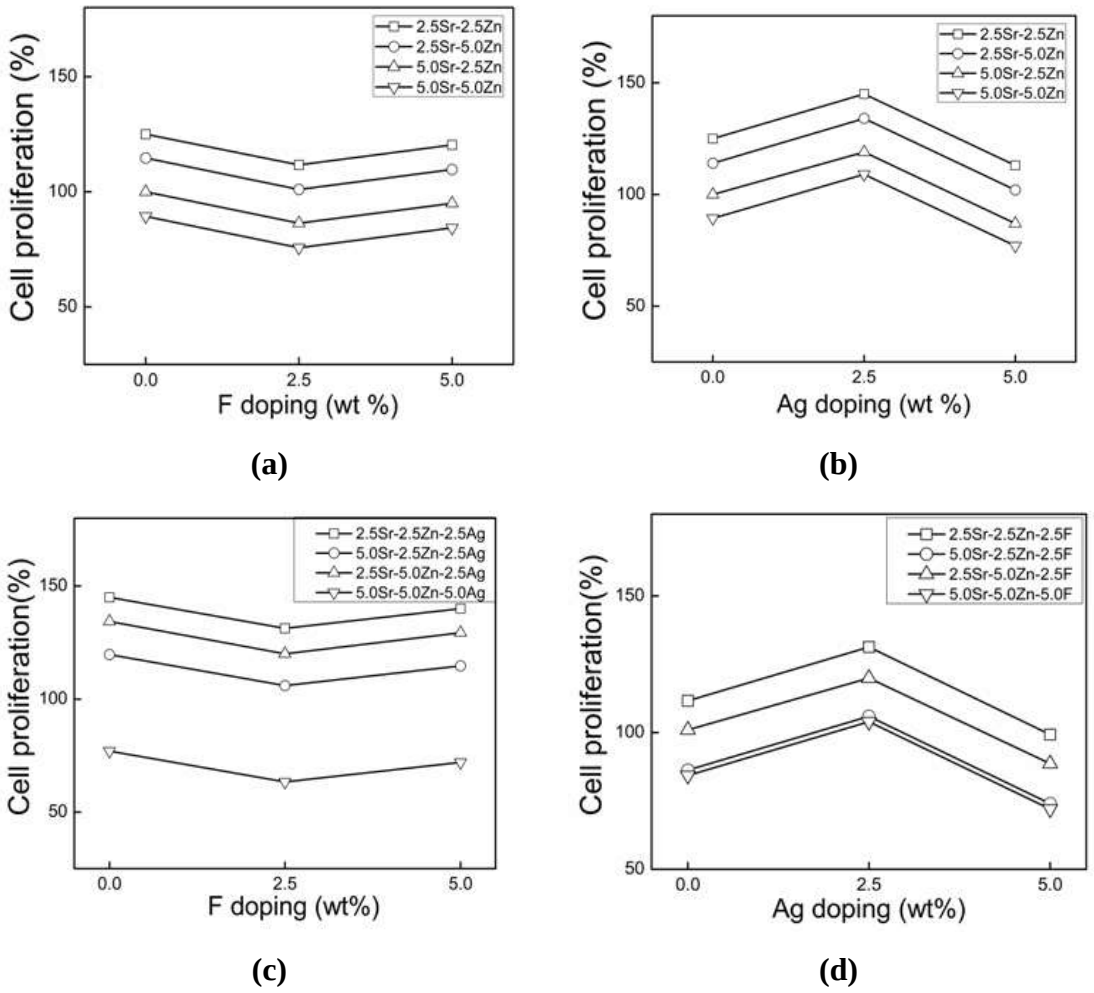

Fig. 4.17 (a,b) Influence of ternary ion doping on later-stage (7 days) proliferation of NIH3T3 cells on HA (a)F+Sr-Zn, (b) Ag+Sr-Zn, (c-d) Variation in 7 days cell proliferation on quaternary ion doped HA (c) F+Sr-Zn-Ag, (d) Ag+Sr-Zn-F.

4.6.4 Cell adhesion (morphology) study

The multi-ion substitution binary, ternary and quaternary or in combination of naturally occurring ionic species into HA not only alters the structural, mechanical, thermal properties but also plays significant role in the biological responses of osteoblasts [138]. The spreading that follows attachment is critical for the consequent behavior of bone cells that are in contact with the implant [196]. NIH3T3 fibroblast mouse cell culture study on selected samples namely L1, L6 and L9 was carried out by incubating the samples for 03, 05, 07 days and the morphologies developed are represented in Fig. 4.18. These images indicate that seeded cells were adherent

and well spreaded on to the surfaces of the samples and exhibited active cytoskeleton extension, which is comparable with the cell morphology. It can be seen that the growth of the cells increased from 3 day to 7 days of incubation on undoped HA (L1). The fibroblast (NIH3T3) cells on the L1 sample are clearly visible as dark region (Fig.4.18). The cells attachment can clearly be seen to be increasing with incubation period. In contrast to sample L1, the cell growth has been found increasing after incubation of 3 and 5 days thereafter with increase of incubation period of 7 days, the cell growth marginally reduced in sample L6 and L9. It appears that the osteoblast activities is effective upto the incubation period and thereafter with further increase of incubation upto seven 7 resulted in inhibition of growth. However, sample L6 (2.5Sr-5.0Zn-2.5F) exhibited results similar to that of L1 sample upto 3 days. After 5 days the multi-ion doped L6 sample exhibited higher cell growth than undoped HA samples. The SEM images are manifesting the differentiations in cell morphology and typically dense surface on both undoped and doped HA samples. NIH3T3 cells demonstrated a typical osteoblast phenotype, which appeared three dimensional and flattened with numerous filopodia and lamellipodia. These results demonstrated that the multi-ion substitution in various combinations into HA may support the cell growth.

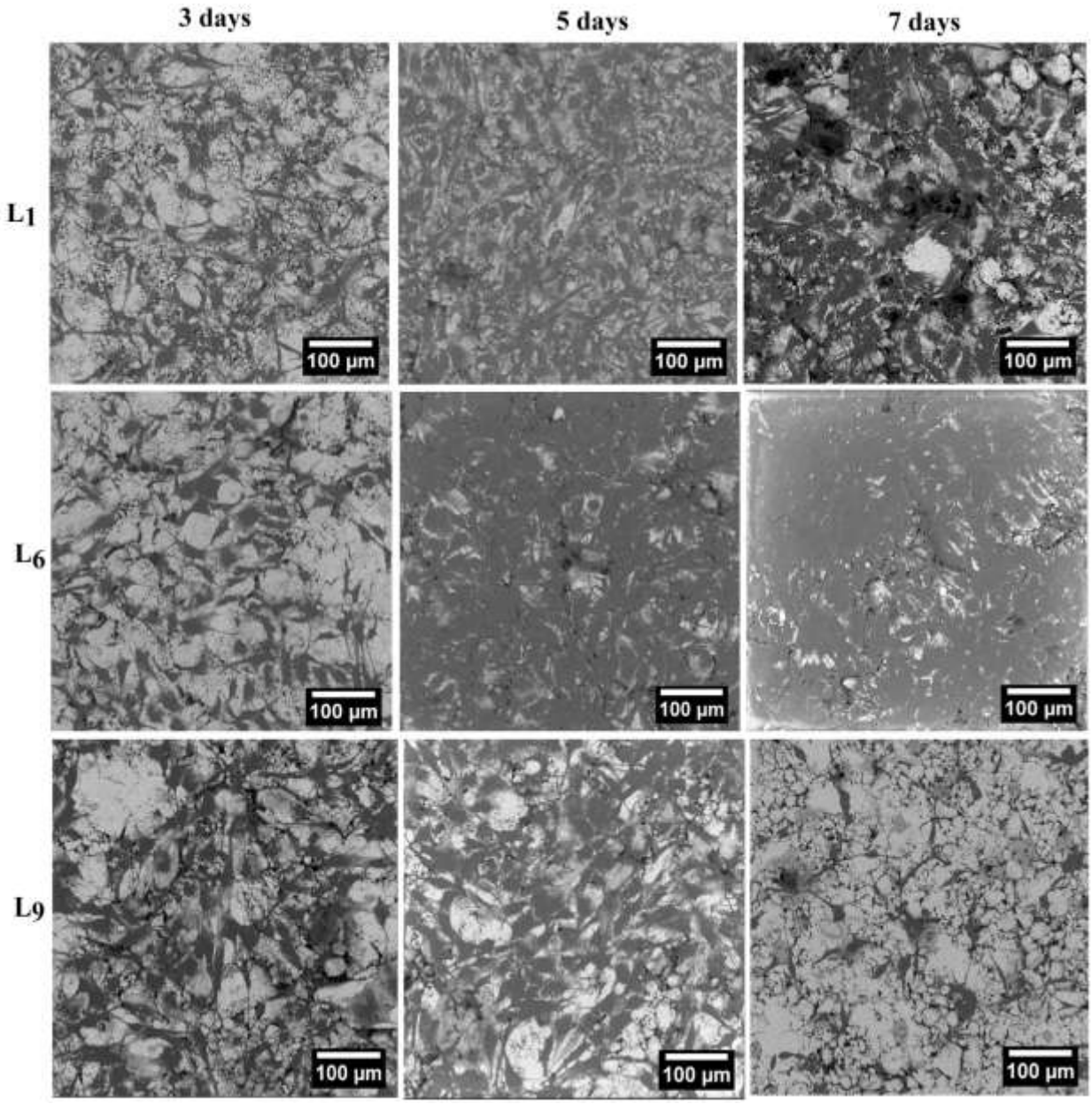

Fig. 4.18 Typical SEM images showing cell morphologies developed on L1, L6 and L9 samples after 3, 5, 7 days of incubation

4.7 *In vitro* ion release and bioactivity

The concentration of different ions released from pure and doped HA is shown in Fig. 4.19. As expected, the concentration of Ca^{+2} was maximum (up to 120 ppm, Fig. 4.19a) followed by P^{+5} which showed concentrations between 2 ppm and 7 ppm, Fig. 4.19b. Compared to pure HA (L1 in Fig. 4.19a) the doped HA samples, except few, showed relatively high concentration

of Ca^{+2} and P^{+5}. The potential reasons for relatively high ion release due to doping would be (i) changes in the crystallinity and crystallite size [197] and (ii) lattice strain or distortion [197] that occurs due to replacement of these cations with dopants namely Sr^{+2}, Zn^{+2} and Ag^{+}. The changes in the crystallinity and crystallite size of present compositions have been reported in our earlier study [198]. Further the extent of lattice strain depends on the ionic radii difference between Ca^{+2} and dopants. The calculated difference was +18%, –26% and +15% for Sr^{+2}, Zn^{+2} and Ag^{+} ions, respectively. The release of Ag^{+} appears to be independent of its concentration, Fig. 4.19e, due to its small difference in ion radii compared to Ca^{+2}. The large ionic radii difference of Zn^{+2} clearly showed concentration dependent release i.e. high concentration resulted in more release, as shown in Fig. 4.19d. However, in spite of small ion radii difference of +18%, the Sr doped HA samples showed high amount of ion release when its concentration was 5 wt.% compared to other samples with 2.5 wt.%, except L4 samples. This suggests the presence of some interaction effect of other dopants on the release of Sr^{+2}.Typically the base concentration (0 day) of Ca^{+2} and P^{+5} ions in SBF is 100 ppm and 31 ppm, respectively. Lower concentration of these ions in the SBF after immersion for 7 and 14 days indicates formation of apatite like precipitates on different HA samples. After immersion, all samples showed a weight gain of approximately 1 to 2.5% (data not shown here) indicating some bone-like apatite precipitation. Overall, the observed ion release from present doped HA expected to have known effects on biomineralization of HA.

It is well-known that the ions released from doped HA samples have direct influence on cell viability due to their action on various cellular activities. Therefore, it is important to correlate the concentration of ions released from different samples on cell viability. The maximum concentration of Zn^{+2} ion released by present multi-ion doped HA samples was ~ 2.4 ppm and at this concentration no cytotoxicity on NIH3T3 cells can be seen. This understandable as the Zn^{+2} ion concentration up to 8 ppm do not induced any cell death [199] and presence of Ca^{+2} in the culture media can up regulate the cell cycle function leading to significant decrease in the inhibitory effect of Zn^{+2} if any [200]. Zinc ions also found to protect the mouse fibroblast cells from toxicity of other ions such as Co^{+2} [201]. Although Sr^{+2} ions promote cell proliferation and stimulate bone formation [202], burst release of high concentration of Sr^{+2} (1.3 ppm) from L4 samples resulted in relatively less cell proliferation compared to other samples containing Sr. Further, the positive influence of Zn^{+2} and F^{-}in L5-L9 compositions would have facilitated slow release of Sr^{+2} and enhanced the cell proliferation [203,204] on these sample. The concentration

of Ag^{+} released from different samples, ~ 0.12 to 0.18 ppm, is less than the toxic limit for different cells (3-10 ppm) [205,206]. However, samples with high concentration of Ag showed some cellular inhibition, for example L3 and L4, which is presumably due to either absence or high concentration of other dopants.

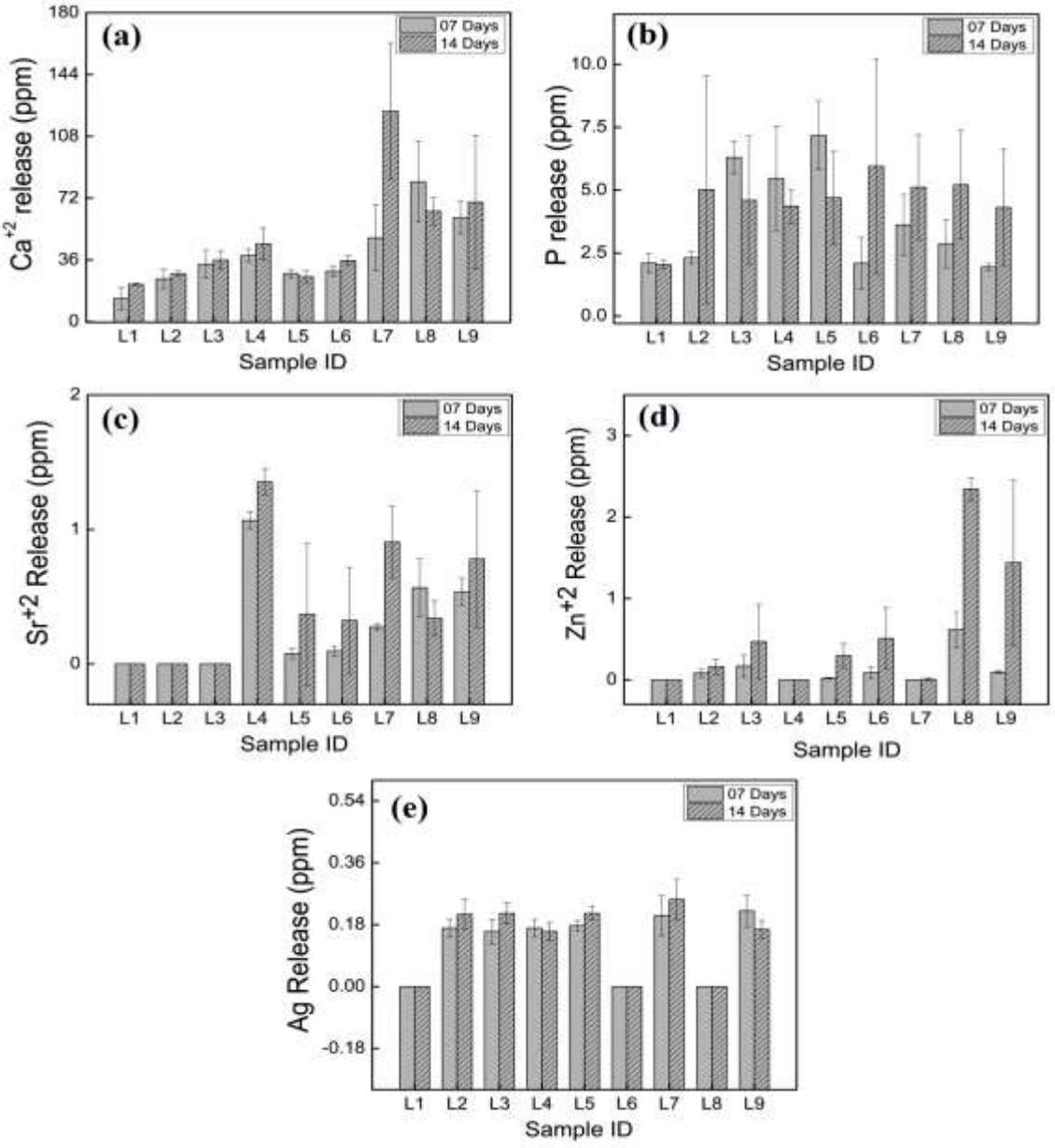

Fig. 4.19 *In vitro* release of different ions from different HA samples after 7 and 14 days of immersion in SBF(a) Ca^{+2} ion (b) P^{+5} ion (c) Sr^{+2} ion (d) Zn^{+2} ion (e) Ag^{+} ion

The formation of apatite precipitation on these samples was examined to qualitatively assess the influence of different ion doping on bioactivity. Fig. 4.20 shows the surface morphology and apatite precipitation on pure and selected doped HA samples after 7 and 14 days of immersion in SBF. Irrespective of HA composition no significant amount of precipitation was observed during initial 7 days of immersion. However, the precipitation increased with immersion time and distinguishable precipitates could be seen on the samples immersed for 14 days. Among the doped HA samples, no visible precipitation was observed on L3 sample (5Zn-5Ag-5F-HA) which also exhibited lowest cell proliferation (Table 4.5). Similarly, the L4 samples (2.5Sr-2.5Ag-5F-HA) showed some isolated and small agglomerates of apatite precipitates, which can be seen in the inset. Therefore it appears that high concentration of F is not favorable for apatite precipitation. More dense and characteristic apatite precipitates were observed on the surface of L6 samples (2.5Sr-5.0Zn-2.5F) both at 7 and 14 days of immersion. Typical flower like nano crystals of apatite were formed on these samples. High magnification micrographs (inset) clearly shows that the apatite formation is improved due to doping of Sr, Zn and F into HA compared to that of pure HA (L1). In fact, this sample (L6) also showed excellent cell proliferation compared to pure HA. Small variations in the morphology of apatite precipitates on the present samples could be due to changes in the ion concentration and pH of SBF as a function of immersion duration. However, the Ca/P molar ratio of the apatite precipitates, determined using EDX, was in the range of 1.6 to 1.9, which is close to HA (1.67).

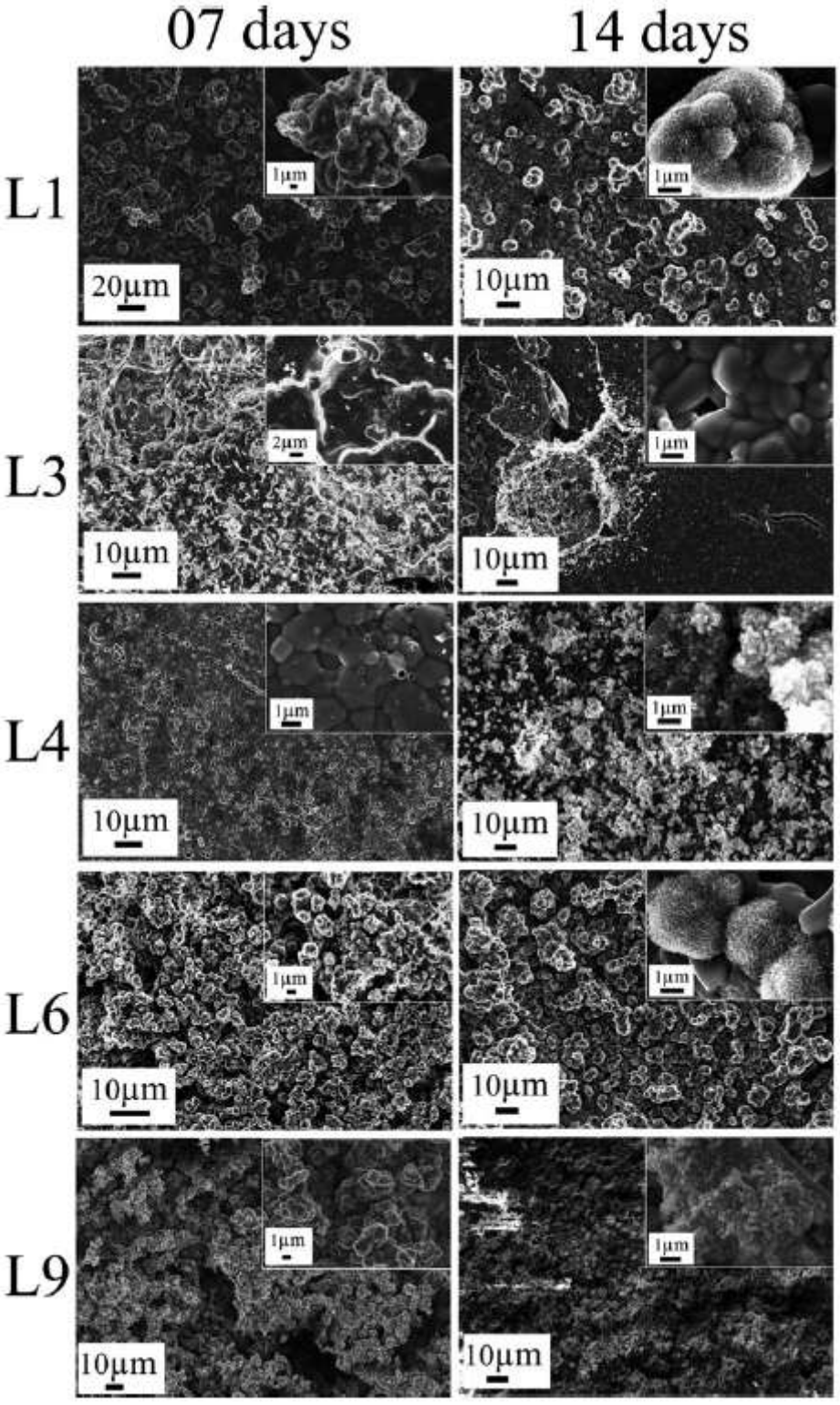

Fig. 4.20 FESEM micrographs showing typical surface morphology and apatite precipitation on pure and doped HA samples after 7 and 14 days of immersion in SBF.

4.8 Effect of dopants on microstructure

4.8.1 Morphology of synthesized HA powders

TEM analysis of undoped and doped HA (L1-L9) samples has been carried out to examine the size, morphology and crystallite or particle size of HA (Figure 4.21). It has been observed that most of the particles appear as irregular plate like particles. The particles size of both undoped and doped HA powders have been found to vary from 20 nm to 600 nm. Additionally, few particles with size of 1.2 μm were also observed. Majority of particles of doped HA have sizes finer than 500 nm (Figures 4.21a-c). Rod like morphology has also been noticed in sample L9 (Figure 4.21c). Due to high surface area to volume ratio, aggregates of nanoparticles have been observed. Some nanoparticles have been observed to be single crystallite while the others with sub-grains having crystallite size as small as 8-10 nm as revealed by HRTEM. Typical HRTEM images obtained from single particles of undoped and doped HA powder sample are shown in Fig. 4.21. It can be seen that each single particle consists of multiple crystallites which are oriented in different directions. These HRTEM images also show characteristic lattice fringes of polycrystalline HA with d spacing corresponding to characteristics atomic planes of HA (JCPDS file No. 00-009-432). The observed values of d-spacing of doped HA crystallites are found to be slightly different than those of pure HA or standard values (Table 4.7) which may be attributed to the presence of dopants in the HA lattice. Figure 4.21c shows the presence of ZnO phase which has also been identified in XRD analysis. The crystallite size of undoped and doped HA revealed by TEM is much smaller than those analyzed by XRD.

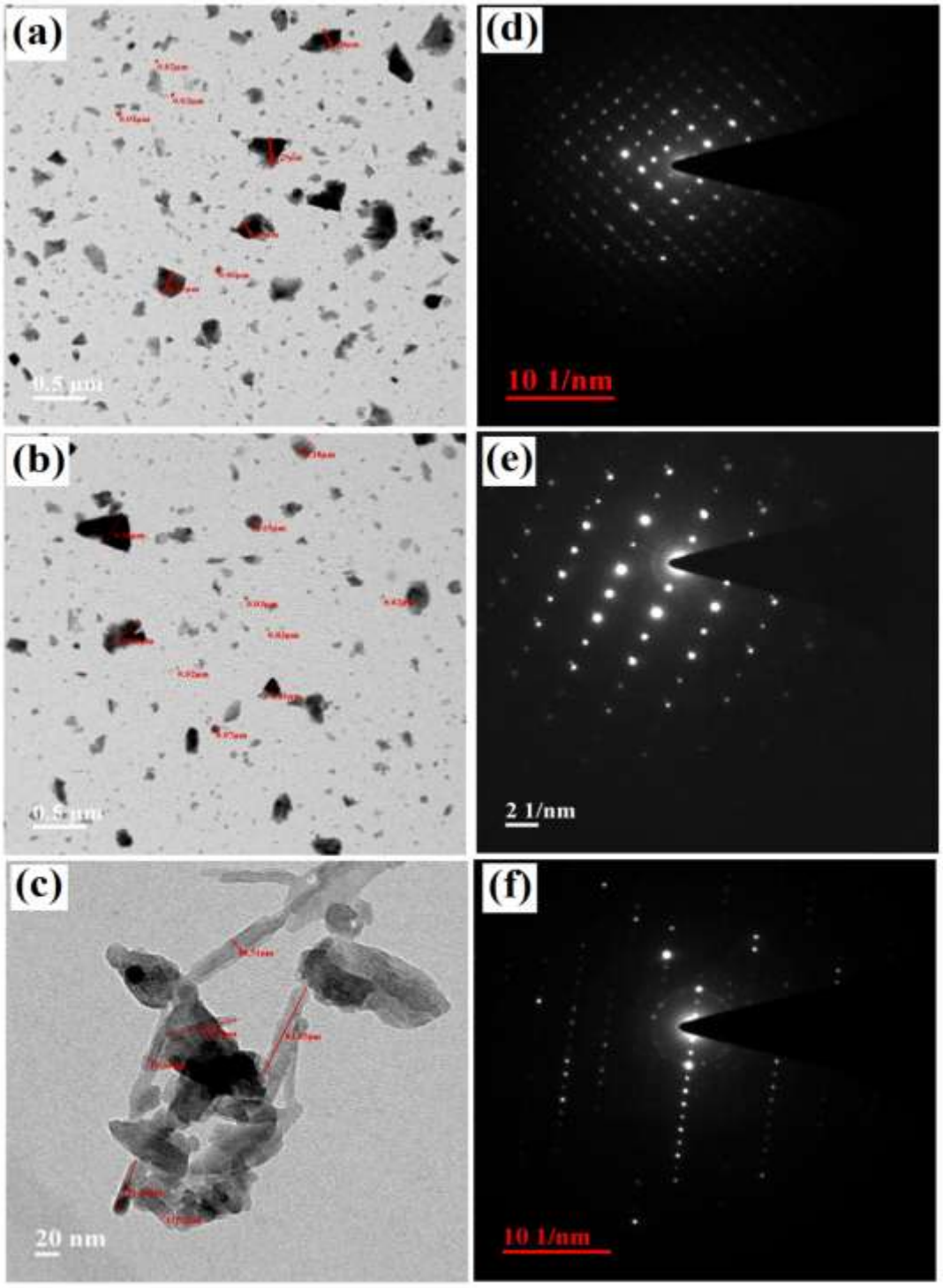

Figure 4.21 TEM micrographs of (a), (b) and (c) showing the powder morphology of L1, L6 and L9 samples and (d) (e) and (f) showing respective SAED pattern of corresponding of (a), (b) and (c) images

The discrepancy in size difference obtained by TEM and XRD may be attributed to; (i) sampling (in TEM, suspended solution of ppm level concentration is taken which may not be true representation of bulk powder sample) and (ii) broadening due to instrumental error (actual peak broadening is due smaller crystallite size, instrumental error and stresses or strain). The presence of stresses or strain in the sintered powder can be neglected because sintered powder was used. As shown in Fig. 4.21d-f, selected area electron diffraction (SAED) patterns of the powder samples of undoped and doped confirm high degree of crystallinity of HA powders. These findings are in support with XRD results. Energy dispersive spectroscopy (EDS) confirms (Fig. 4.23) the presence of doping ions in the HA structure.

Table 4.7 The observed and standard d-spacing of HA

Compositions	**Observed d-value (nm)**	**Standard d-value (nm)**
L1	0.344	0.344 (002)
L6 (2.5Sr-5Zn-2.5F)	0.333	0.344 (002)
L8 (5Sr-2.5Zn-5F)	0.244 (ZnO) 0.250 0.267	0.248 (101) 0.253 (301) 0.263(202)
L9 (5Sr-5Zn-2.5Ag)	0.250 0.300 0.300	0.253 (301) 0.308 (210) 0.308 (----)

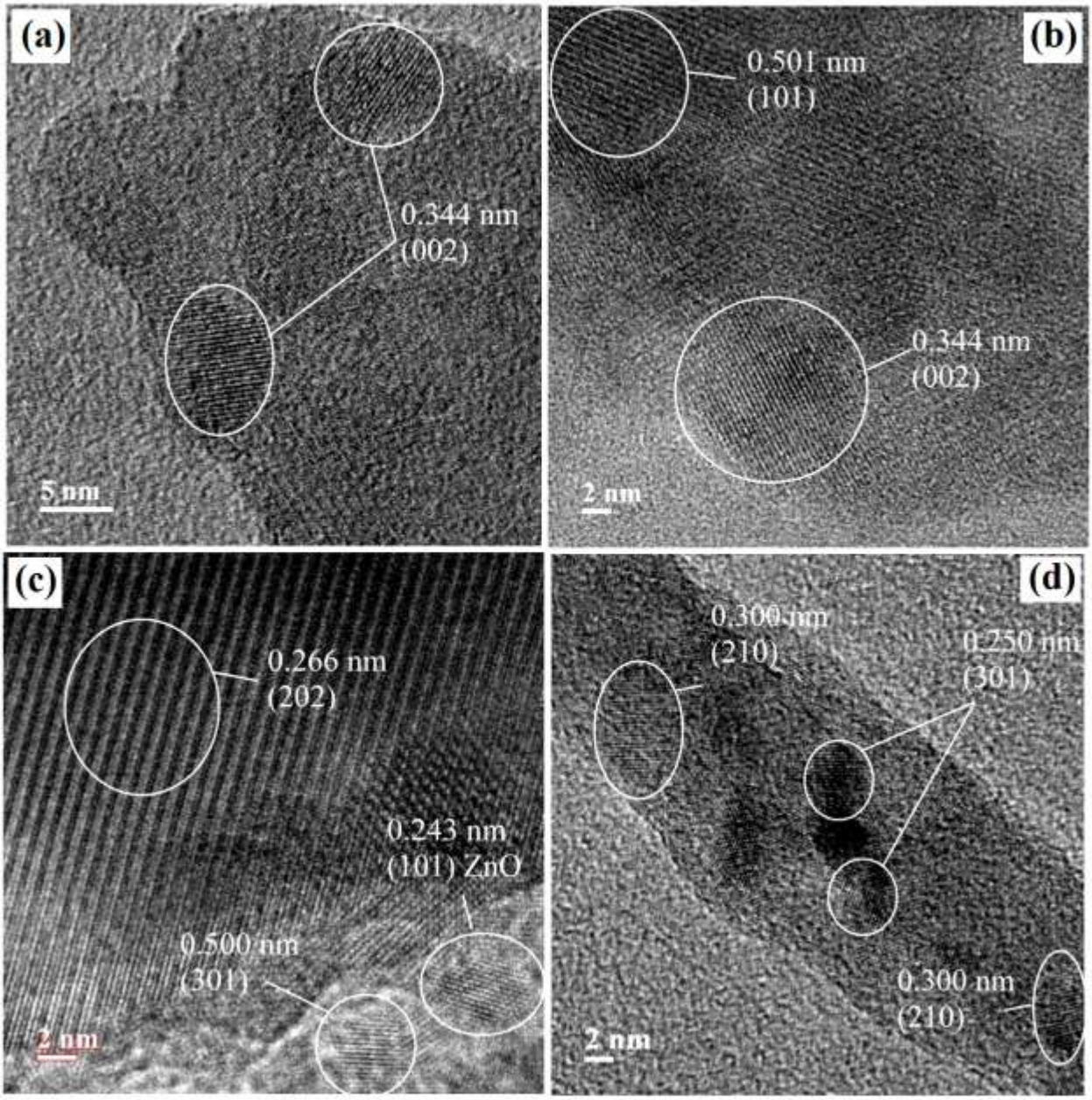

Fig. 4.22 HRTEM images showing the effect of doping on interplanar spacing of selected HA samples; (a) pure HA (L1), (b) 2.5Sr-5Zn-2.5F HA (L6), (c) 5Sr-2.5Zn-5F HA (L8) and (d) 5Sr-5Zn-2.5Ag HA (L9)

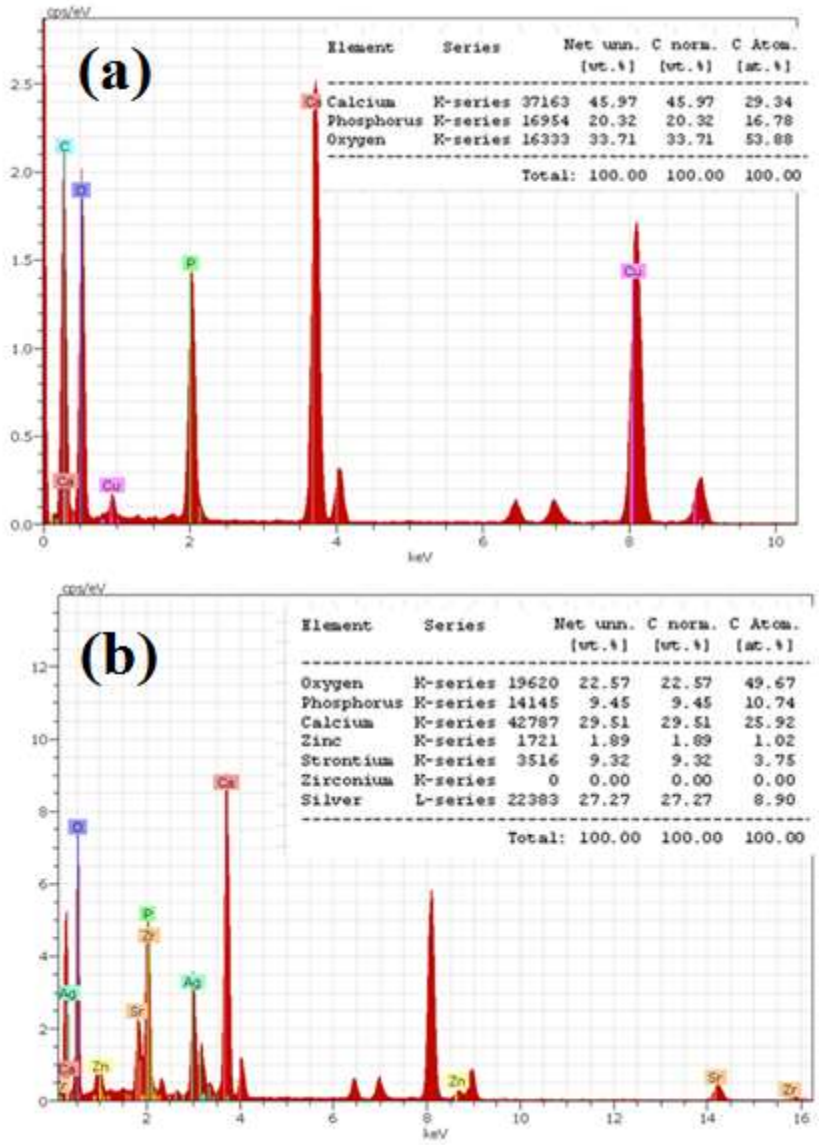

Figure 4.23 EDS pattern of (a) L-1 and (b) L-9 samples

4.8.3 Morphology of HA pellets after *in-vitro* study

The density and porosity of sintered HA samples with different dopants is presented in Table 4.8. The data showed that multi-ion doping do not have deleterious effect on sintered density of HA. The density of pure HA (L1) increased from 2.99 g/cc (95%) to a range between 3.01 and 3.11g/cc (99%) due to multi-ion doping. It can be seen that Sr and F doping have relatively more influence on the density of sintered HA compared to other dopants. Quantitatively the contribution of F towards changing the sintered density of HA was calculated

to be 69.14% (Table 4.8) followed by Sr with 18.76% contribution. The influence of Ag on sintering is lowest among the dopants. Highest density of ~ 3.1 g/cc (~ 98%) can be achieved with 5%F doping. The high sintered density along with multi-ion doping of HA found to increase the hardness of HA from 3.7GPa to a range between 3.8 and 6.0GPa [198]. Here again Sr and F doping significantly increased the hardness of sintered HA. For the ternary and quaternary ion doped samples, the sintered density of HA is always higher than that of pure HA (L1, 2.99 g/cc) indicating absence of detrimental effects of doping on sintering. The addition of Ag as ternary ion appears to decrease the density of Sr-Zn doped HA marginally. However, this negative effect of Ag can be compensated by adding F ion to Sr-Zn doped HA. The positive influence of F doping on the sintered density of binary and ternary ion doped HA can also be seen in Table 4.8. Typical microstructures of sintered HA with and without doping after *in-vitro* studies are shown in Fig. 4.24. All samples exhibited well-define grain boundaries with some isolated porosity (Figure 4.24). The porosity in these samples ranged between 1.5 to 5.38 % (Table 4.8). Pure HA showed relatively coarse grains compared to doped HA samples, which suggest some grain refinement effect of dopants on HA. The grain size (measured suing linear intercept method) of pure HA (L1) was between 2 and 4 μm, which was decreased to a range of 1.6 to 2.2 μm after multi-ion doping. From this analysis it can be said that high densification is achieved in 2.5Sr-5.0Zn-2.5Ag-2.5 or 5.0F. From cell proliferation point of view also these compositions ensured long-term cytocompatibility as discussed above. Further, the nominal crystallinity and small crystallite size of these HA compositions [198] also would have contributed to their excellent cell proliferation.

Table 4.8 Density (g/cc) and porosity (%) of different HA compositions and contributions (%) of each doping elements towards change in the density.

	L1	**L2**	**L3**	**L4**	**L5**	**L6**	**L7**	**L8**	**L9**
Density	2.99	3.07	3.09	3.10	3.04	3.11	3.03	3.08	3.01
Total porosity	5.38	2.74	2.11	2.00	3.69	1.48	4.11	2.64	4.85
Contribution(%) of doping elements towards change in the density									
			Sr	Zn	Ag	F			
			18.76	11.04	1.06	69.14			

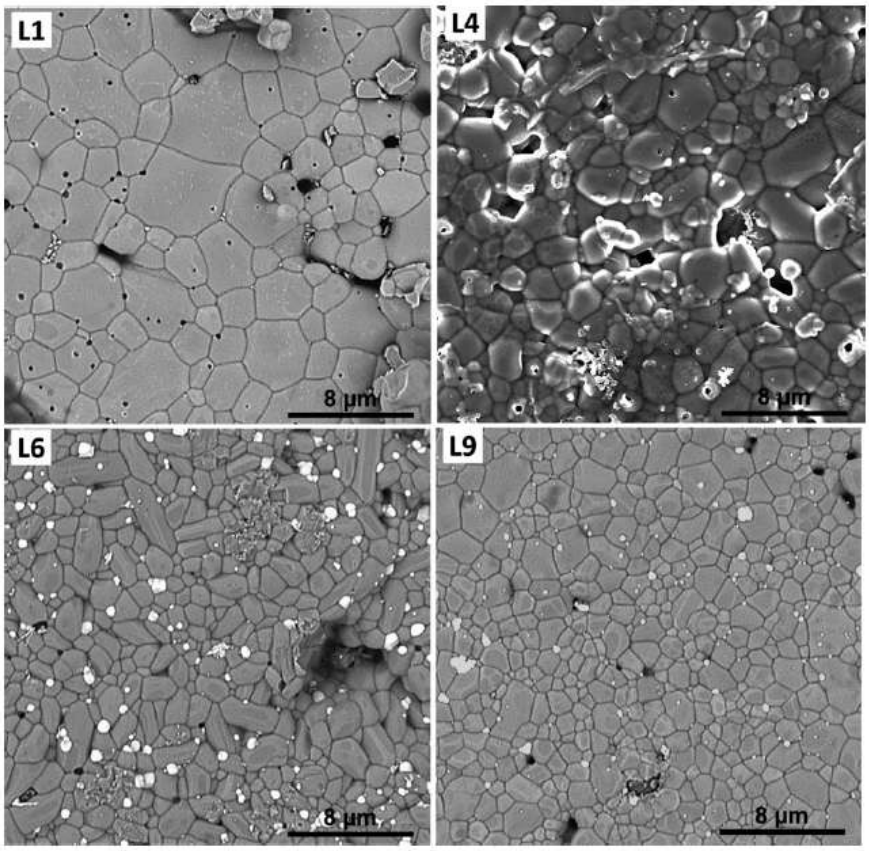

Fig. 4.24 Typical microstructures of pure HA (L1) and multi-ion doped HA samples showing the variations in grain size and porosity.

4.9 Antibacterial study of undoped and doped HA

The results of the antibacterial sensitivity evaluated by the agar disk diffusion method are shown in Fig 4.25.Pure HA and L6 (Sr2.5-2.5Zn-2.5F) samples did not show inhibition zonein presence of *E. Coli* and *S. Aureus* bacteria even after incubation period of 36 h at 37 °C. However, the inhibition zone in the Ag substituted sample (5.0Sr-5.0Zn-2.5Ag-L9) was clearly visible against both the bacteria as shown in Fig. 4.25. Sample L3 (5.0Zn-5.0Ag-5.0F) contains 5 % Ag but did not show any sensitivity towards both the bacteria culture for test durations. Furthermore, the diameters of the inhibition zones of *S. Aureus* were smaller than those of *E. coli* of a given composition of Ag doped HA.

The sample L5 (2.5Sr-2.5Zn-5.0Ag) also exhibits good inhibition zone as compared to other doped and undoped HA sample. The inhibition zone obtained in case of above compositions may be due to combined effect of Ag and Zn ions in doped HA. It is reported earlier that Zn^{+2} block the transport channel by the formation of strong bonds with thiole, imidazole, amino and carboxyl groups of microbe membrane proteins and ultimately leads to bacterial death. Although the diameter of inhibition zone of both *E. Coli*and *S. Aureus*are not found uniformly in circular form. It may be expected that release of metal ions which inhibits bacteria were not uniform. The L9 (5.0Sr-5.0Zn-2.5Ag) sample could be of interest for the various biomedical application where good physico-chemical, in-vitro bioactivity, in-vitro cytotoxicity properties are key requirements.

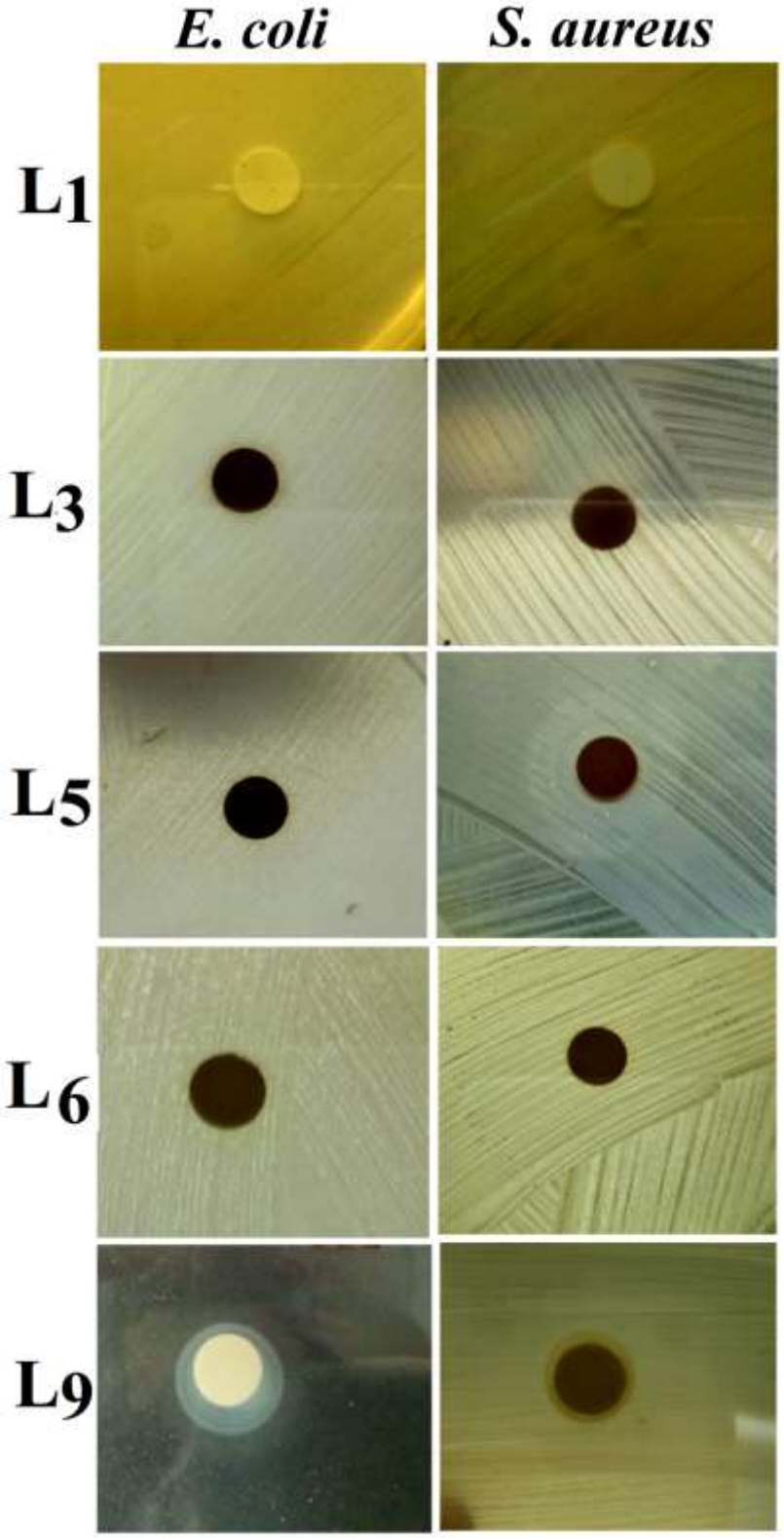

Fig. 4.25 Agar diffusion test of the samples of L1, L3, L5, L6 and L9.

4.10 Effect of dopants on dielectric behavior

Figure 4.26a and b show the values of dielectric constant and dissipation factor for the pure HA and multi-ion doped HA, respectively, as a function of increasing frequency from 100 Hz to 100 MHz. It is clearly shown in Fig. 4.26 that the dielectric constant of the samples except L-5 increases significantly at the frequencies below 1 kHz. However, thereafter the dielectric constant of the samples decreases slightly with increasing frequency. For example, the dielectric constant of pure HA is 8.5 (at 100 Hz) which is decreased to 8.05 (at 1 MHz) and to 8.03 (10 MHz). Interestingly, the value of dielectric constant (at 100 Hz) of the doped samples except L-5 increases with change of doping combination, i.e., it is about 12.3 for L-6 sample. With increasing frequency from 100 Hz to about 10 MHz, the dielectric constant of these samples remains either close or higher than that of pure HA. In HA structure, OH^- ions located at the centre of Ca^{2+} triangles along the c-axis of a hexagonal unit cell probably have an important role in ionic conduction [207] which is probably responsible for the dispersion in dielectric constant with increasing frequency. A similar trend in dielectric constant was reported for the cadmium (Cd) doped HA bioceramics by Kargili et al. [172] They reported that the dielectric constant of the Cd-doped HA increased with increasing Cd content from 10 at.% to 30 at.% except 40 at.% Cd, i.e., the values of dielectric constant measured at 1 kHz increased from 6.75 for pure HA to a value between 7.12 and 8.16 for the Cd doped HA with no trend with increasing Cd content in HA structure. The dielectric constant of 40 at.% Cd doped HA was found to be 6.24, i.e., lower than that of pure HA. The decrease in dielectric constant for 40 at.% Cd doped HA sample compared to pure HA was attributed to change in crystal structure from hexagonal structure to monoclinic structure. It was also reported that the dielectric constant increased non-monotonously with decreasing degree of crystallinity of HA and thereafter, it decreased with increase in degree of crystallinity [172]. Similarly, a dielectric constant value of about 10 (at 1 kHz) was reported for pure HA by Prezas et al. [208] and it was found to increase first with increasing Sr content to an optimum level in HA structure but thereafter it decreased on further increasing Sr content[121]. Incontrast to low dielectric dispersion in our samples, Ramya et al. reported a significant dielectric dispersion with increasing frequency for the iron (Fe) and zinc (Zn) doped HA. For example, the value of dielectric constant was found to increase from 150 (for pure HA) to 479 (for doped HA) at 1 kHz and decreased to 10 (for pure HA) and 16 (for doped HA) at 1 MHz [160] The addition of multi-ions into HA structure causes increase in ionic

polarization and thus, the dielectric constant increases with ions content in HA structure. The increased in ionic polarization probably assists the calcification and mineralization of osseous tissue at the fracture site and helps in healing the fractured bone [171,172]. The lower values (i.e., 4 - 4.29) of dielectric constant for L-5 may be attributed to the presence of high amount of porosity. These values are in the reported range of 4.93 (for a sample with 42 vol% porosity) to 13.55 (for a sample with 5 vol.% porosity) [171]. Figure 1b shows the variation in dissipation factor with increasing frequency for the pure HA and multi-ion doped HA. It can be seen that the dissipation factor of the pure HA varies from a value of 0.02 (at 100 Hz) to 0.005 or less with increasing frequency up to 10 MHz. However, thereafter it increases slightly. In case of doped HA samples, the value of dissipation factor increases to about 0.08 at lower frequencies and decreases to about 0.01 at 10 MHz. The increase in dissipation factor may be attributed to the increase in imaginary part of the complex dielectric constant, which is proportional to the ac conductivity.

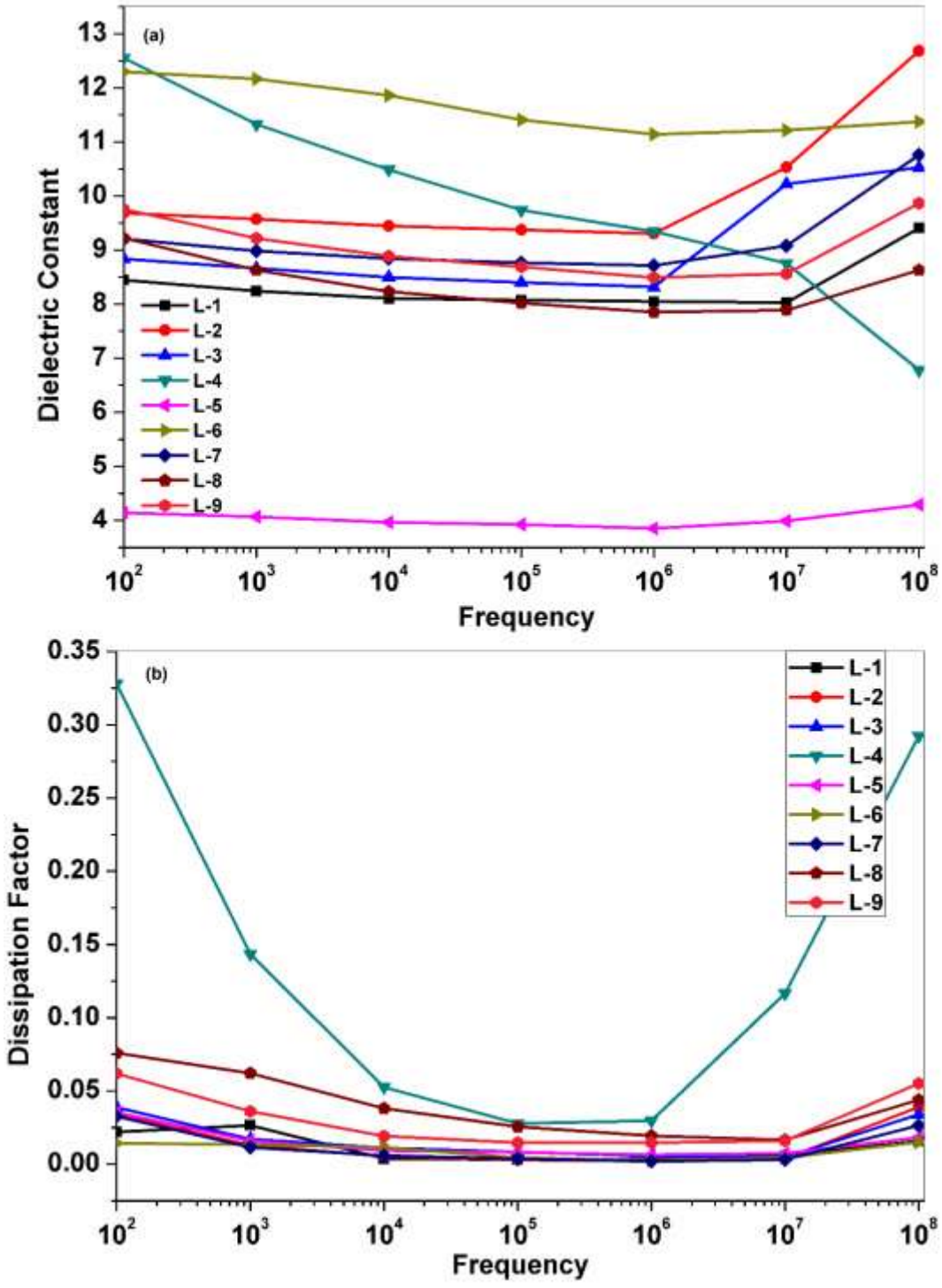

Fig. 4.26 Variation in (a) dielectric constant and (b) dissipation factor as a function of frequency measured at room temperature.

In brief, the dispersion in dielectric constant for the pure HA and doped HA is desirable because the dielectric properties of biological cells and tissues also typically display frequencies dependent behavior, i.e., the dielectric constant decreases from a very high value at lower frequency to a lower value at higher frequency. The frequency dependent dielectric constant permits identification and investigation of a number of completely different underlying mechanisms [171]. It is well known that HA is the matrix for bone cement applications and so its electrical behavior under electrical field is very important to study from the physiological point of view. The dielectric properties of HA are very important for different applications such as sensors and bone substitutes [209]. Under electromagnetic field, HA can accelerate the healing of fractured bones as well as enhance the rate of bone osteobonding and bone growth. The dielectric constant measured at 1 kHz at room temperature of both undoped and doped HA samples is summarized in Table 4.9.

Table 4.9 Dielectric constant of undoped and doped HA compositions and % contributions of each doping elements towards change in the dielectric constant

	L1	**L2**	**L3**	**L4**	**L5**	**L6**	**L7**	**L8**	**L9**
Dielectric constant	8.11	9.24	8.64	9.08	4.51	11.79	8.83	9.16	10.76
Contribution of doping elements towards change in the dielectric constant									
		Sr	Zn	Ag	F				
		5.25	34.09	34.46	20.46				

As shown in Table 4.9, sample L1 (undoped HA) is considered as reference or control sample. As compared to control sample, all other samples (except L5) showed higher values of dielectric constant. The sample L4 (i.e., 2.5Sr-2.5Zn-5.0Ag-0.0F-HA) exhibited minimum dielectric constant as compared to other samples. The maximum dielectric constant of 11.79 was observed in sample L6 (i.e., 2.5Sr-5.0Zn-0.0Ag-2.5F-HA). The second highest dielectric constant of 10.76 was observed in case of sample L9 (i.e., 5.0Sr-5.0Zn-2.5Ag-0.0F-HA) as compared with other samples. These changes in dielectric constant are expected to enhance current flow in natural hard tissues which leads to healing of fractured bone. However, the dielectric constant values of all the doped samples (except L5) are very close to that of natural bone (9.20). **Table 4.9** also shows the % contribution of different dopants towards the enhancement of dielectric constant when larger is better condition applied. It can be noted that

Ag had maximum influence (34.46 %) followed by Zn (34.09%), F (20.46%) and Sr (5.25%) on dielectric constant of HA.

4.10.1 Main effect of dopants on dielectric constant

The results shown in Table 4.9 are used to determine the effects of the selected factor namely (Sr, Zn, Ag and F) on the calculated response (i.e., dielectric constant). The main effects of various doping elements on dielectric constant of HA were determined considering "larger is better" condition. This condition is selected because higher dielectric constant is expected to favour osteogenic capacity of HA. The main effects of dopants thus determined are displayed in Fig. 4.27.It can be seen from Fig. 4.27that 5% Sr doping into HA structure results in marginal increase in dielectric constant, while the addition of Zn upto 2.5 % decreased the same slightly but when its concentration increased from 2.5 to 5 % then a significant increment can be noted. Further, doping of 2.5% Ag ions decreases dielectric constant very marginally but with increased concentration to5.0 %, dielectric constant decreases significantly. Doping with F^-ion up to 2.5% resulted in significant increase in dielectric constant but on further increase to 5%, dielectric constant decreased moderately.

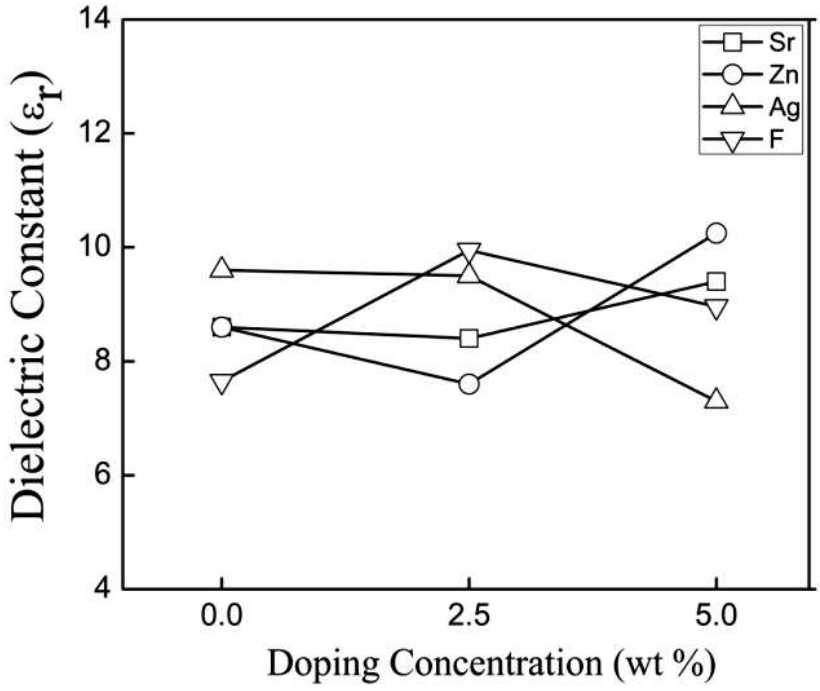

Fig. 4.27 Influence of different dopants and their concentration on dielectric constant

4.10.2 Influence of multi-ion dopants in binary combination on dielectric constant

The influence of binary co-doping of multi-ions on dielectric constant of HA is shown in Fig. 4.28 (a-f). As stated previously that crossing lines in the interaction plots suggests interaction among different parameters but when lines are parallel to each other then relation does not exist between them. From all the six binary plots shown in Fig. 4.28 (a-f), it can be seen that all lines are crossing to each other at some composition indicating that interaction exists between Sr, Zn, Ag and F dopants in HA. The binary interaction plots of Zn and Sr doping for dielectric constant,(shown in Fig. 4.28a) indicates that the relationship between Sr doping and dielectric constant strongly depends on the concentration of Zn. From this binary plot it can be seen that doped HA exhibits the highest dielectric constant (approx 11.50) when both the ions (elements) are co-doped at higher concentration (≥2.5%/ 2.5% Sr and 5% Zn) i.e.5% into HA. Further, the lowest dielectric constant (4.51) noticed when both the elements are doped with 2.5% into HA. So higher concentrations of these two dopants into HA, leads to increase of dielectric constant which in turn ultimately expected to contribute to improved osteoblast reaction during tissue material interaction.

Fig. 4.28b shows the binary interaction plots of Ag and Sr co-doping, indicating that the addition of Ag either at 0.0 or 2.5 % (Ag 0.0, Ag 2.5 lines) displayed maximum dielectric constant as compared to higher concentration of Ag (Ag 5.0 line) with presence of Sr into HA. The highest dielectric constant(approx 10.33) can be noted when HA is doped with 2.5 % Ag and 5% Sr. On the contrary a combination of higher content of Ag (5%) and lower concentration of Sr (2.5%) leads to lowest value of dielectric constant. So from this binary co-doping plot it is suggested that lower concentrations of Ag and higher concentration of Sr can be recommended to achieve significantly higher dielectric constant as compared with undoped HA samples.

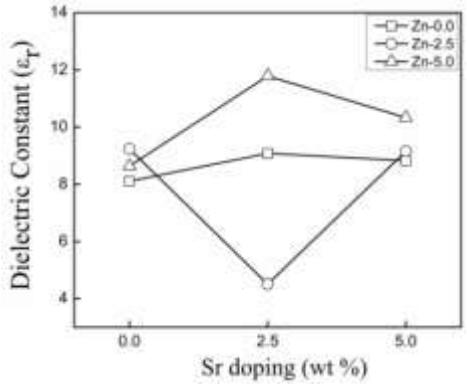

(a)

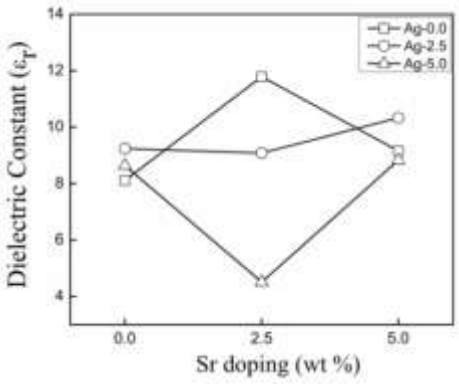

(b)

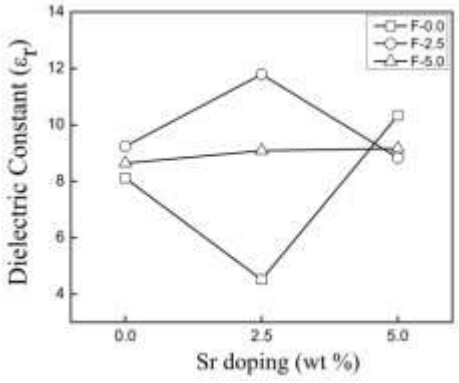

(c)

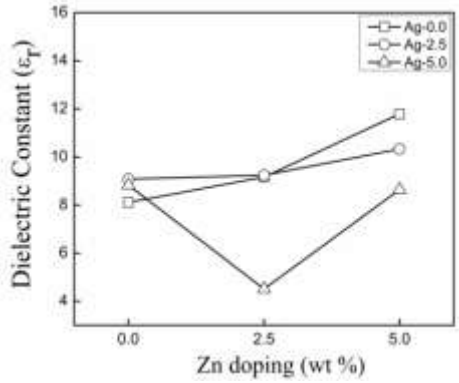

(d)

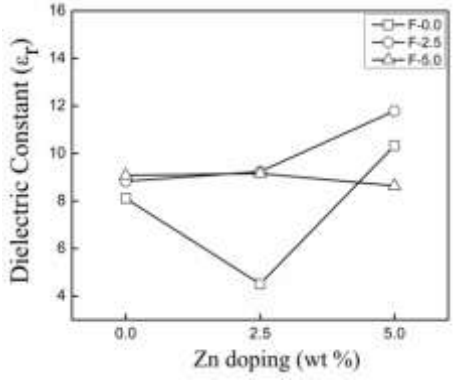

(e)

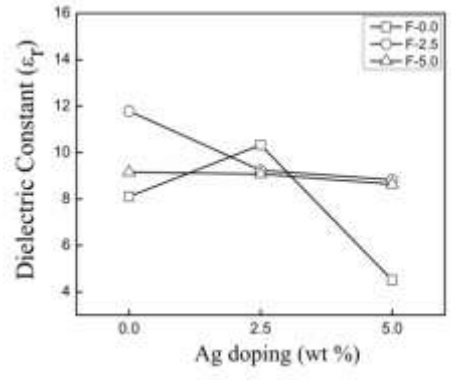

(f)

Fig. 4.28 Influence of binary ion doping on dielectric constant of HA (a) Zn-Sr HA (b) Ag-Sr HA (c) F-Sr HA (d) Ag-Zn HA (e) F-Zn HA (f) F-Ag.

The binary interaction plots between F and Sr co-doping for dielectric constant of HA shown in Fig. 4.28c indicates that the highest dielectric constant (11.79) can be achieved when both the elements are doped with 2.5 % in HA. However, the lines corresponding to 0.0 and 5.0 % F are showing lower dielectric constant as compared to F-2.5% line when Sr varying from 0 to 5%. Further, the binary co-doping plot between Ag and Zn shown in Fig. 4.28d, indicates that Ag-2.5 line favors to increase the dielectric constant as compared to Ag-5.0 line when it incorporated into Zn doped HA. The highest dielectric constant (9.69) observed when Ag-2.5 and Zn-5.0 doped into HA. The lowest dielectric constant (4.71) from this co-doping plot observed when Ag-5.0 and Zn-2.5 doped into HA. The highest dielectric constant (11.79) was observed in case of co-doping with F-2.5% and Zn-5.0 % into HA (Fig. 4.28e). Relatively a lower dielectric constant (7.07) was obtained for the F-5.0% and Zn-2.5% doped HA. The binary interactive effect of Ag and F co-doped HA is shown in Fig. 4.28f, indicating that both F and Ag upto 2.5 only provides higher dielectric constant as compared to undoped HA.

4.10.3 Influence of multi-ion dopants in ternary and quaternary combination on dielectric constant

Analyzing the effects of multiple ion doping (ternary and quaternary) on dielectric constants is quite complex and there is no another way to identify the same using standard DOE analysis. Therefore, assessment is done on the basis of binary interaction plots (shown in Fig. 4.28a-f) and ANOVA (Table 4.9) that doping of Sr and Zn $\geq$ 2.5 % and Ag and F $\leq$ 2.5 % provide enhanced dielectric constant. Further, these binary compositions were used to assess the effect of other two dopants in ternary and quaternary combinations. The effect of Ag and F addition on dielectric behavior of Sr-Zn doped HA, are presented in Fig. 4.29a-b in the form of ternary interaction plot. Furthermore, the influence of F and Ag as ternary and quaternary dopant to HA is very similar to the respective individual element effect on dielectric constant shown in Fig. 4.27. The ternary interaction plot shown in Fig. 4.29a indicates that when Ag concentration increases from 0 to 5 % then all four binary doped with Sr and Zn lines showed decrement trend in dielectric constant of HA. Apart from Ag-0.0 points, (shown in Fig. 4.29a) the highest dielectric constants 10.33 and 9.35 were observed when Ag doped at 2.5 % into 5.0Sr-5.0Zn and 2.5Sr-5.0Zn doped HA respectively. From Fig. 4.29b the highest dielectric constants 12.77 and

11.79 would be obtained if F ion doped at 2.5 % into 5.0Sr-5.0Zn doped followed by 2.5Sr-5.0Zn doped HA samples respectively. Further it can be seen from this ternary plot that if F concentration increases from 2.5 % to 5 % then it would be expected that dielectric constant of HA decreases in case of all binary doped (Sr-Zn doped) HA samples as shown in Fig. 4.29b.

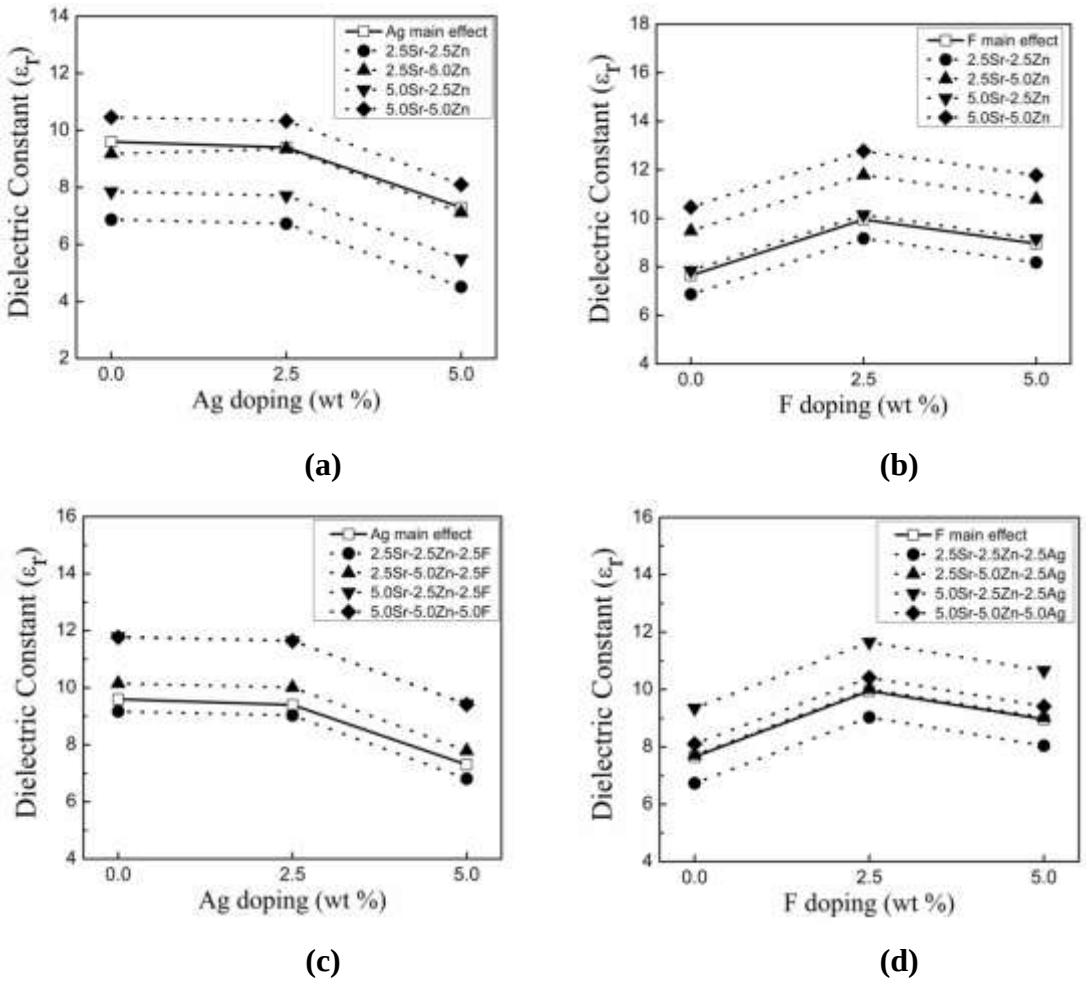

Fig. 4.29 (a-b) Influence of ternary ion on dielectric constant of binary ion doped HA (a) F+Sr-Zn, (b) Ag+Sr-Zn, (c-d) effect of quaternary ion on dielectric constant of ternary ion doped HA (c) F+Sr-Zn-Ag, (d) Ag+Sr-Zn-F.

Further the effect of Ag and F on dielectric behavior of Sr-Zn-Ag and Sr-Zn-F doped HA are presented in Fig. 4.29c-d in the form of quaternary interaction plot respectively. The influence of F and Ag as quaternary dopant (shown in Fig. 4.29c-d) to HA is similar to ternary

interaction plot (Fig. 4.29a-b), binary plots (Fig. 4.28f) and main/individual effect plot Fig. 4.27. Form this quaternary interaction plot it can be observed that doping of Ag ≤ 2.5 %, Sr ≥ 2.5 % and Zn 2.5 % favor to increase the dielectric constant as compared to undoped HA samples. In contrast, the highest dielectric constant (11.65) was observed for the quaternary system (i.e., when Ag is added as fourth dopant), as shown in Fig. 4.29c. Similarly, a highest dielectric constant (11.65) was observed in case of F as fourth dopant (Fig. 4.29d).

4.11 Effect of dopants on photoluminescence (PL) behavior

Photoluminescence (PL) spectroscopy is widely used technique for characterization of optical and electronic properties of ceramic or bioceramic. The PL is light emission from any form of matter after the absorption of electromagnetic radiation (i.e., photons). The PL intensities calculated from PL spectroscopy data at 520 nm wavelength are summarized in Table 4.10. These results shows that doping of (Sr^{+2}, Zn^{+2}, Ag^{+} and F^{-}) ions into HA increases the PL intensity in all compositions, except 2.5Sr-2.5Ag-5.0F (L4) composition. The L-4 composition shows lowest intensity of about 1187. The second lowest PL intensity is 2929 for the 5.0Sr-5.0Ag-2.5F (L7) composition. The highest PL intensities obtained from 5.0Sr-5.0Zn-2.5Ag (L9), 2.5Sr-5.0Zn-2.5F (L6) and 2.5Zn-2.5Ag-2.5F (L2) compositions are 33,655, 31,696 and 25,696, respectively. However, 5Sr-2.5Zn-5.0F composition (L8) exhibits intensity of 18,874 which is much higher than that of undoped HA. However, it is difficult to conclude that which elements among four elements increase or decrease the PL intensity of HA. So for better understanding and optimized effect of dopants on current response such as PL intensity we used design of experiment (DOE). By using this DOE technique, individual or main effect of dopants on PL can be evaluated. Furthermore, apart from main effect, binary, ternary and quaternary interactive effects of multi-ion dopants have been assessed to identify the optimal concentrations to achieve target properties.

4.11.1 Main effect of dopants on PL intensity of HA

In this section, the main effects of various dopants on PL intensity of HA were determined using “larger is better” condition. Here larger is better condition is selected because higher PL intensity leads to absorbance of higher electromagnetic radiations which are ultimately increase the optical properties of HA for various biomedical applications such target drug delivery, bioimaging, biosensing, cancer treatment etc. It is well reported that PL is an important

technique for measuring the purity and crystalline quality of doped and undoped HA compositions. The increase in ionic polarization due to dopants HA [41] lead to creation of population of electrons and holes in conductor and valence band, respectively. PL is also useful to know the structural defects such as lattice distortions due to variation of chemical composition. The change in PL intensity by lattice distortion occurs due to doping which leads to localization of charge carriers.

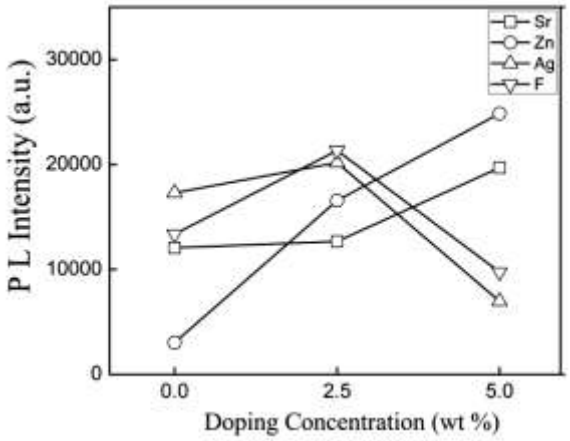

Fig. 4.30 Influence of different dopants (main effect plot) and their concentration on PL intensity

Table 4.10 shows the effects of the individual dopants (Sr, Zn, Ag and F) on PL intensity (emission energy). The main/individual effects of dopants on PL intensity of undoped and doped HA samples are displayed in Fig. 4.30. From Fig. 4.30, it is found that doping of Sr ion increases the PL intensity gradually while the addition of Zn increases the PL intensity significantly. From the main effect plot the highest PL intensity of 24856 can be obtained when Zn is doped at 5 % as compared to other three dopants (Sr, Ag and F) into HA structure. Further, as shown in Fig. 4.26a,it can be seen that addition of Ag and F ions up to 2.5 % increased the PL intensity while their 5 % concentration decreased significantly the response factor. From the main effect plot it can be revealed that F and Ag upto 2.5 %, and Sr and Zn up to 5% favors the increment in PL intensity of HA samples.

4.11.2 Influence of multi-ion dopants in binary combination on PL intensity

The influence of binary co-doping of multi-ions on PL intensity of HA is showing in Fig. 4.31a-f. As explained in previous section, crossed lines indicate interaction among different elements while parallel lines do not.

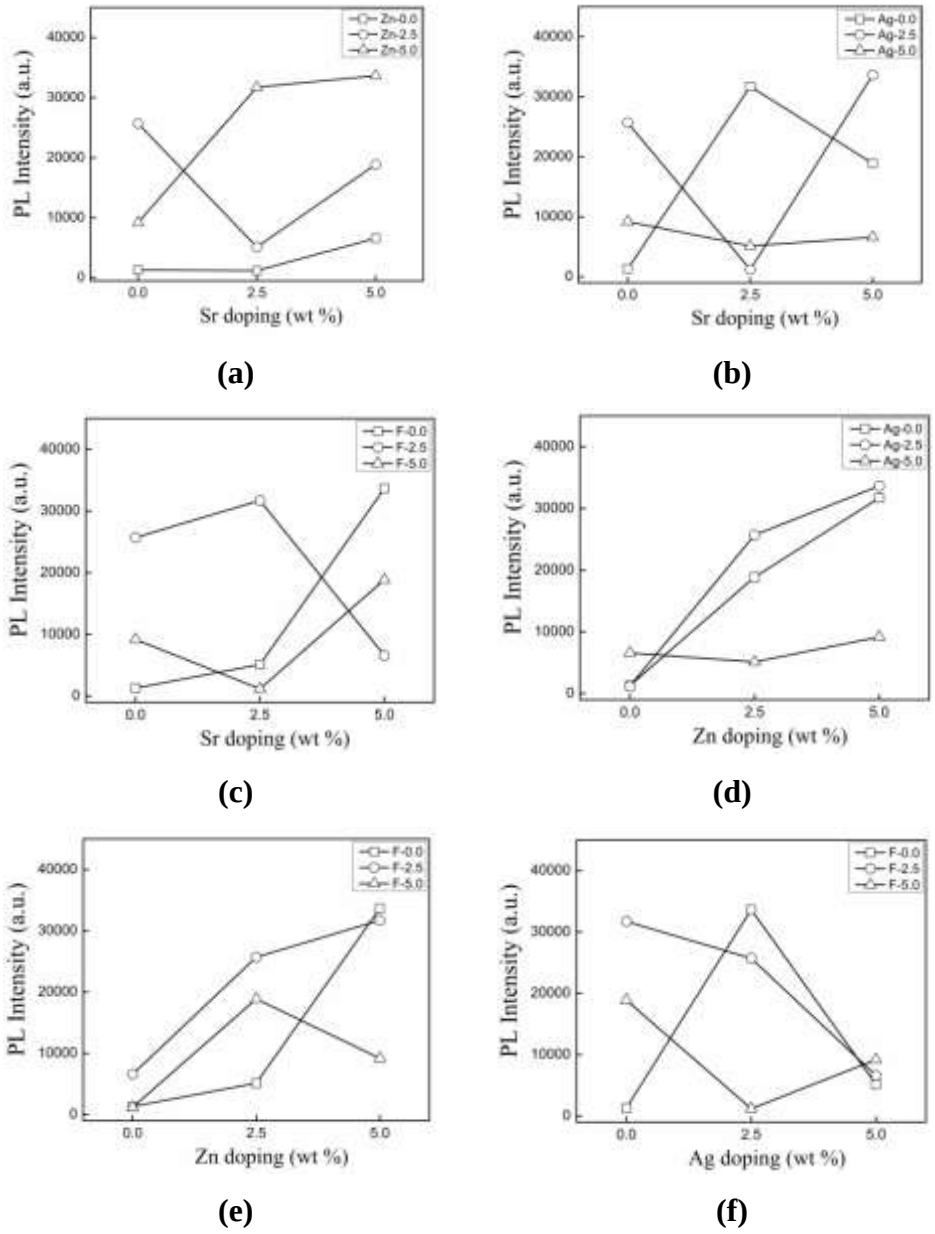

Fig. 4.31 Influence of binary ion doping on PL intensity of HA (a) Zn-Sr, (b) Ag-Sr, (c) F-Sr, (d) Ag-Zn, (e) F-Zn, (f) F-Ag.

As shown in Fig. 4.31a-f, all lines are crossing to each other, i.e., the interaction exist between Sr, Zn, Ag and F doped HA throughout the concentration range studied. The binary interaction plots of Zn and Sr doped HA is shown in Fig. 4.31a. It can be seen that highest PL intensity of 33655 is observed when both Zn and Sr ions are co-doped with concentration of 5% into HA. As shown in Fig. 4.31a, Zn-5.0 line shows continuous increment trend with increasing Sr concentration while Zn-2.5 line shows decreasing trend. The binary interaction plot between Ag and Sr co-doping is shown in Fig. 4.31b. The Ag 0 and Ag 2.5 lines displayed maximum PL intensity as compare to higher concentration of Ag with Sr doped HA, i.e., highest PL intensity of 32117 is observed for the 2.5% Ag co doped with 5 % Sr. Hence, it is suggested from the binary co-doping plot that lower concentrations of Ag with higher concentration of Sr is better to achieve significantly higher PL intensity compare to that of undoped HA sample.

Table 4.10 Photoluminescence intensity of different HA compositions and contributions (%) of each doping elements towards change in the PL intensity.

	L1	**L2**	**L3**	**L4**	**L5**	**L6**	**L7**	**L8**	**L9**
Density	1307	25696	9191	1187	5127	31721	2930	18874	33655
Contribution (%) of doping elements towards change in the PL intensity									
		Sr	Zn	Ag	F				
		5.35	58.09	11.23	27.77				

The binary interaction plots between Sr and F co-doping for PL intensity is shown in Fig. 4.31c. This indicates that F-5.0 lines have lower PL intensity as compare to F-2.5 line when Sr varies from 0 to 5%. The highest PL intensity is observed for the 2.5% F co doped with 2.5 Sr% compare to other concentrations. The lowest PL intensity of 1691 is observed for the 5 % F co doped with 2.5% Sr. Furthermore, the binary co-doping plot between Ag and Zn is shown in Fig. 4.31d. This shows that the Ag-2.5 line is favorable to increase the PL intensity as compare to Ag-5.0 line when it is incorporated into Zn doped HA. As shown in Fig. 4.31e, the highest PL intensity of 30776 is observed in case of co-doping when addition of F at 2.5 % into 5.0% Zn doped HA. The binary interactive effect of Ag and F co-doped into HA for PL intensity is shown in Fig.4.31f indicating that both F and Ag upto 2.5 provides higher PL intensity as compare to undoped HA. This can be well correlated with main effect plot (shown in Fig. 4.27a). The

highest PL intensity of 27847 is observed for the 2.5% F codoped with 2.5% Ag doped HA. The F-5.0 line shows minimum PL intensities at all Ag concentrations.

4.11.3 Influence of multi-ion dopants in ternary and quaternary combination on PL intensity

Analyzing the effects of ternary and quaternary ions on PL intensity is quite complex and there is no another way to identify the same using standard DOE analysis. Therefore, we assessed from binary interaction plot (shown in Fig. 4.31a-f) and ANOVA (Table 4.10) that doping of Sr and Zn ≥ 2.5 % and Ag and F ≤ 2.5 % provide enhanced PL intensity. Further, these binary compositions were used to assess the effect of other two dopants in ternary and quaternary combinations as shown in Fig. 4.32.

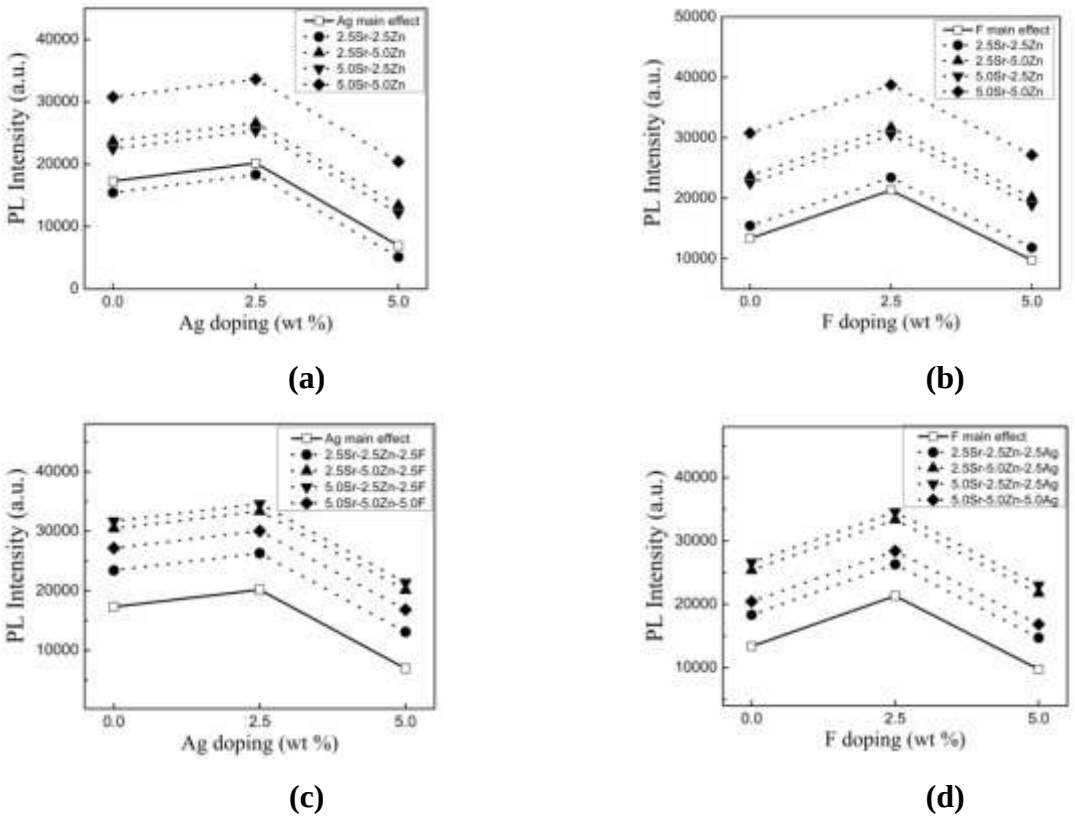

Fig. 4.32 Influence of ternary ion (a-b) on PL intensity of binary ion doped HA; (a) F+Sr-Zn and (b) Ag+Sr-Zn. Effect of quaternary ion (c-d) on PL intensity of ternary ion doped HA; (c) F+Sr-Zn-Ag and (d) Ag+Sr-Zn-F.

The effects of Ag and F addition on PL behavior of Sr-Zn doped HA are presented in Fig. 4.32a and b, respectively. Since, there are three elements involved in doping HA, hence such systems are called ternary interaction plot. The influence of F and Ag as ternary and quaternary dopant to HA is similar to those of individual element effect on PL intensity as shown in Fig. 4.30. As shown in Fig. 4.32a, the highest PL intensities of 33655 and 25365 are obtained for the 2.5 % Ag ion doped into 5.0Sr-5.0Zn doped HA and 2.5Sr-5.0Zn doped HA. Further, it can be seen from this ternary plot that if Ag concentration increases from 2.5 % to 5 %, then the PL intensity of HA decreases in case of all Sr-Zn doped HA ternary systems (Fig. 4.32a).The ternary interaction plot shown in Fig. 4.32b indicates that the addition of F ion (0 to 2.5 %) in all four binary systems doped with Sr and Zn lines increases PL intensity while more than 2.5% F addition decreases Pl intensity. The highest PL intensities of 37528 and of 29238 are observed when 2.5 % Ag ion is doped into 5.0Sr-5.0Zn and 2.5Sr-5.0Zn doped HA, respectively. Further, the effect of Ag and F on PL intensity of Sr-Zn-Ag and Sr-Zn-F doped HA are presented in Fig. 4.32c-d. These systems are involving four elements hence, called quaternary interaction plot. The influence of Ag and F as quaternary dopant to HA is very similar to that of ternary interaction plot (Fig. 4.32a-b), binary plots (Fig. 4.31a-f) and main/individual effect plot (Fig. 4.30). The highest PL intensities of 40407 and 34600are obtained for the Ag doped in (Fig. 4.32c) 2.5Sr-5.0Zn-2.5F and 5.0Sr-5.0Zn-2.5F doped HA samples, respectively.

The quaternary interaction plot indicates that doping of Ag $\leq$ 2.5 %,Sr $\geq$ 2.5 % and Zn > 2.5 % favors to increase the PL intensity as compare to undoped HA sample. Whereas the highest PL intensities of 40410 and 32117 are obtained for the F doped (Fig. 4.32d) in 2.5Sr-5.0Zn-2.5 Ag and 5.0Sr-5.0Zn-5.0 Ag doped HA samples. In both the cases the positive influence of Zn doping in the presence of other dopants ions is dominating more so contributes to increase higher values of PL intensifies as compare to undoped HA samples. In summary based on the main effect, binary, ternary and quaternary interaction plots of doping elements, higher PL intensity can be achieved with high concentrations of Zn and Sr with intermediate concentration of Ag and F into HA. Table 4.10 shows the % contribution of different dopants towards the change in PL intensity when larger is better condition applied. The PL study shows that the order of ion on PL intensity is Zn (58.09 %) > F (27.77%)> Ag (11.23%) >Sr (2.91 %) at room temperature. As shown in Fig. 4.30, the addition of Zn from 0 to 5.0 % increases the PL intensity

which is followed by Fin terms of increasing PL intensity. The addition of F and Ag ions upto 2.5% contributes more positive influence as compare to Sr ions upto 2.5%. Although the % contribution of Sr (2.91 %) is low but it can be expected that Sr alone can also increase PL intensity if it is incorporated into HA lattice.

CHAPTER 5

CONCLUSIONS

Based on the results obtained following conclusions can be drawn:

1. The synthesis of pure HA by wet precipitation method followed by multi-ion doping of HA with Sr, Zn, Ag and F ions using high energy ball milling was done successfully.
2. The crystallinity of as synthesized HA was about 52% and increased to 93% after calcinations at 1250 °C. However, the crystallinity and crystallite size of HA decreased due to multi-ions doping.
3. Among the doping elements studied, Sr followed by Zn showed maximum influence on crystallinity and crystallite size of HA. Compared to F, Ag doping had relatively more effect on crystallite size than on crystallinity.
4. The concentration of Ag and Zn close to 2.5% resulted in nominal crystallinity, while Sr and F concentrations <2.5% or close to 5.0% showed similar crystallinity in HA. The crystallite size of HA decreased with Sr concentration and other dopants had mixed influence. To achieve smaller crystallite size in HA dopant concentration must be ≤ 2.5%.
5. DOE analysis showed clear interaction between dopants at binary level doping, while ternary and quaternary doping of elements did not exhibit any interaction.
6. The influence of Sr^{+2}, Zn^{+2}, Ag^{+} and F^{-}ion doping on *in vitro* cytotoxicity and ion release of HA was systematically analyzed using DOE. During early culture period of 3 days all concentrations of doping elements showed significantly higher cell viability than pure HA, except 5 wt.% F.
7. However, for long-term cytocompatibility the concentration of dopants must be reduced and multi-ion doping found to compensate inhibitory effect of some of the dopants.
8. Interestingly, strong binary interaction was observed between cation dopants (Sr, Zn and Ag) than between cation and anion dopant (F). HA with binary ion doping with ≤ 2.5 wt.%F, ≤ 2.5 wt.% Ag, 2.5-5 wt.% Sr and Zn can provide up to 2-fold increase in the early-stage cell proliferation compared to pure HA.

9. Similarly, the composition of multi-ion doped HA to achieve excellent cell viability during initial culture period would be 5Sr-5Zn-2.5Ag and 5Sr-2.5Zn-2.5Ag with or without 2.5 wt.% F. However, for stable and positive later-stage cell proliferation on binary ion doped HA, the concentration of all dopants appears to be ≤ 2.5 wt.%.
10. Finally, for enhanced long-term cytocompatibility the compositions of multi-ion doped HA would be 2.5Sr-2.5Zn-2.5Ag, 2.5Sr-5Zn-2.5Ag and 5Sr-2.5Zn-2.5Ag with up to 5 wt.% F. *In vitro* bioactivity experiments revealed that HA compositions with high Sr and Zn concentration exhibit excellent bone-like apatite layer formation.
11. However, high concentration of Ag and F found to have limited bioactivity. The dopants also increased the sintered density of HA and refined its grain size as well. These results can be used to tailor the composition of multi-ion doped HA to achieve desired early-stage and long-term biological performance.

Future Scope

1. Apart from the compositions selected in this work that is from L2-L9 the more compositions proposed based on taguchi method can be validated for best combinations of properties.
2. Further in-vitro studies including bone mineralization, osteogenic potential for current optimized or best compositions.
3. *In-vivo* animals' trials are required to confirm the benefits of these compositions.

REFERENCES:

[1] A.K. BHARGAVA, Engineering Materials : Polymers, Ceramics and composites, 2nd ed., PHI Learning Private Limited , New Delhi, 2012.

[2] Z. Li, M. Kawashita, Current progress in inorganic artificial biomaterials, J. Artif. Organs. 14 (2011) 163–170.

[3] M. Geetha, A.K. Singh, R. Asokamani, A.K. Gogia, Ti based biomaterials, the ultimate choice for orthopaedic implants - A review, Prog. Mater. Sci. 54 (2009) 397–425.

[4] K. Okamoto, T. Matsuura, R. Hosokawa, Y. Akagawa, RGD peptides regulate the specific adhesion scheme of osteoblasts to hydroxyapatite but not to titanium, J. Dent. Res. 77 (1998) 481–487.

[5] M. Mucalo, Hydroxyapatite for biomedical application, 1st Edition, Woodhead Publishing , Elsevier, Cambridge, 2015.

[6] A. Haider, S. Haider, S.S. Han, I.K. Kang, Recent advances in the synthesis, functionalization and biomedical applications of hydroxyapatite: a review, RSC Adv. 7 (2017) 7442–7458.

[7] A. El-Ghannam, Bone reconstruction: From bioceramics to tissue engineering, Expert Rev. Med. Devices. 2 (2005) 87–101.

[8] M. Šupová, Substituted hydroxyapatites for biomedical applications: A review, Ceram. Int. 41 (2015) 9203–9231.

[9] S. Bose, A. Banerjee, S. Dasgupta, A. Bandyopadhyay, Synthesis, processing, mechanical, and biological property characterization of hydroxyapatite whisker-reinforced hydroxyapatite composites, J. Am. Ceram. Soc. 92 (2009) 323–330.

[10] G. Graziani, M. Bianchi, E. Sassoni, A. Russo, M. Marcacci, Ion-substituted calcium phosphate coatings deposited by plasma-assisted techniques: A review, Mater. Sci. Eng. C. 74 (2017) 219–229.

[11] S. Bose, G. Fielding, S. Tarafder, A. Bandyopadhyay, Understanding of dopant-induced

osteogenesis and angiogenesis in calcium phosphate ceramics, Trends Biotechnol. 31 (2013) 594–605.

[12] J.-Y. Reginster, M.-P. Lecart, R. Deroisy, C. Lousberg, Strontium ranelate: a new paradigm in the treatment of osteoporosis, Expert Opin. Investig. Drugs. 13 (2004) 857–864.

[13] D. Shepherd, Zinc-substituted hydroxyapatite for the inhibition of osteoporosis, in: Hydroxyapatite Biomed. Appl., 2015: pp. 107–126.

[14] A. Bianco, I. Cacciotti, M. Lombardi, L. Montanaro, E. Bemporad, M. Sebastiani, F-substituted hydroxyapatite nanopowders: Thermal stability, sintering behaviour and mechanical properties, Ceram. Int. 36 (2010) 313–322.

[15] M. Navarro, A. Michiardi, O. Castaño, J.A. Planell, J.R.S. Interface, M. Navarro, A. Michiardi, O. Castan, Biomaterials in orthopaedics Biomaterials in orthopaedics, (2008) 1137–1158.

[16] Buddy Ratner Allan Hoffman Frederick Schoen Jack Lemons., Biomaterials Science: An introduction to materials in medicine, 2nd Edition , Elsevier Academic Press, 2004.

[17] N. Huebsch, D.J. Mooney, Inspiration and application in the evolution of biomaterials, Nature. 462 (2009) 426–432.

[18] S. Sahoo, M. Goel, P. Gandhi, S. Saxena, Biological aspects of dental implant ; Current knowledge and perspectives in oral implantology, 4 (2018) 87–91.

[19] E.S. Thian, J. Huang, S.M. Best, Z.H. Barber, W. Bonfield, Silicon-substituted hydroxyapatite: The next generation of bioactive coatings, Mater. Sci. Eng. C. 27 (2007) 251–256.

[20] Roger Narayan , Materials for Medical Devices ASM Handbook, Volume 23, 2012.

[21] M.L. Wang, P.F. Sharkey, R.S. Tuan, Particle bioreactivity and wear-mediated osteolysis., J. Arthroplasty. 19 (2004) 1028–1038.

[22] Y. Yang, K.H. Kim, J.L. Ong, A review on calcium phosphate coatings produced using a

sputtering process - An alternative to plasma spraying, Biomaterials. 26 (2005) 327–337.

[23] C. Combes, C. Rey, Amorphous calcium phosphates: Synthesis, properties and uses in biomaterials, Acta Biomater. 6 (2010) 3362–3378.

[24] Y. Yang, K. Kim, J.L. Ong, A review on calcium phosphate coatings produced using a sputtering process — an alternative to plasma spraying, 26 (2005) 327–337.

[25] C. Schmidt, D. Kaspar, M.R. Sarkar, L.E. Claes, A.A. Ignatius, A scanning electron microscopy study of human osteoblast morphology on five orthopedic metals, J. Biomed. Mater. Res. 63 (2002) 252–261.

[26] P.D. Brown, H.K. Edwards, M.W. Fay, Microscopy at the life sciences / physical sciences interface, J. Phys. Conf. Ser. 241 (2010).

[27] M. Navarro, A. Michiardi, O. Castaño, J.A. Planell, Biomaterials in orthopaedics, J. R. Soc. Interface. 5 (2008) 1137–1158.

[28] P.D. Brown, H.K. Edwards, M.W. Fay, Microscopy at the life sciences / physical sciences interface Microscopy at the life sciences / physical sciences interface, (2010).

[29] M. Vandrovcova, J. Hanus, M. Drabik, O. Kylian, H. Biederman, V. Lisa, L. Bacakova, Effect of different surface nanoroughness of titanium dioxide films on the growth of human osteoblast-like MG63 cells, J. Biomed. Mater. Res. - Part A. 100 A (2012) 1016–1032.

[30] Z. Evis, T.J. Webster, Z. Evis, T.J. Webster, Nanosize hydroxyapatite : doping with various ions Nanosize hydroxyapatite : doping with various ions, 6753 (2013).

[31] R. Nirmala, R. Navamathavan, R. Afeesh, H.-M. Park, H.-S. Kang, H.Y. Kim, Characterisation of bioresourced hydroxyapatite containing silver nanoparticles, Mater. Res. Innov. 16 (2012) 249–256.

[32] A. Hoppe, N.S. Güldal, A.R. Boccaccini, A review of the biological response to ionic dissolution products from bioactive glasses and glass-ceramics, Biomaterials. 32 (2011) 2757–2774.

[33] A. Bansiddhi, T.D. Sargeant, S.I. Stupp, D.C. Dunand, Porous NiTi for bone implants: A review, Acta Biomater. 4 (2008) 773–782.

[34] K.M.R. Nuss, B. von Rechenberg, Biocompatibility Issues with Modern Implants in Bone - A Review for Clinical Orthopedics, Open Orthop. J. 2 (2008) 66–78.

[35] V.P. Mantripragada, B. Lecka-Czernik, N.A. Ebraheim, A.C. Jayasuriya, An overview of recent advances in designing orthopedic and craniofacial implants, J. Biomed. Mater. Res. - Part A. 101 (2013) 3349–3364.

[36] J. Rho, Mechanical properties and the hierarchical structure of bone, 20 (1998) 92–102.

[37] 1989 R. Bruce Martin and David B Burr, Structure function and adaptation of compact bone, in: New York: Raven Press, 1989: p. 275.

[38] J.W. L.L. Hench, An Introduction to Bioceramics, World Scientific, 1993.

[39] M. Niinomi, Recent metallic materials for biomedical applications, Metall. Mater. Trans. A. 33 (2002) 477–486.

[40] F.H. Netter, Atlas of Human Anatomy, New York: Elsevier, New york, 2013.

[41] Z. Schwartz, B.D. Boyan, Underlying Mechanisms at the Bone-Biomaterial Interface, 347 (1994) 340–347.

[42] P.E.A. Ugat, S.A.S. Chorlemmer, The role of cortical bone and its microstructure in bone strength, (2006) 27–31.

[43] J. Currey, Incompatible mechanical properties in compact bone, J. Theor. Biol. 231 (2004) 569–580.

[44] H.D. Weiner, S. and Wagner, The Material Bone: Structure-Mechanical Function Relations, Annu. Rev. Mater. Sci. 28 (1988) 271–298.

[45] C. Hellmich, F. Ulm, M. Asce, Micromechanical Model for Ultrastructural Stiffness of Mineralized Tissues, 128 (2003) 898–908.

[46] V.P. Orlovskii, V.S. Komlev, S.M. Barinov, Hydroxyapatite and Hydroxyapatite-Based

Ceramics, 38 (2002) 973–984.

[47] R.B. Martin, Skeletal Tissue Mechanics, Springer, New York, NY, 1998.

[48] E.H. Burger, Experiments on Cell Mechanosensitivity: Bone Cells as Mechanical Engineers, 2nd ed., CRC Press, New York, 2001.

[49] S. Weiner, H.D. Wagner, THE MATERIAL BONE: Structure-Mechanical Function Relations, Annu. Rev. Mater. Sci. 28 (1998) 271–298.

[50] Gundtoft P.H., Prosthetic Joint Infection following Total Hip Arthroplasty - Incidence, Mortality and Validation of the Diagnosis in the Danish Hip Arthroplasty Register. Dan Med J. 2017 Sep; 64(9).

[51] S.A. Broos PL1, From unstable internal fixation to biological osteosynthesis. A historical overview of operative fracture treatment., Acta Chir Belg. 104 (2004) 396–400.

[52] Reviews and notices of books, (1965) 1965.

[53] M.W.M.W.S.L.C. Rockwood, Rockwood and Matsen's The Shoulder, 2009.

[54] S.-P. MN., The classic: Evolution of mould arthroplasty of the hip joint by M. N. Smith-Petersen, J. Bone Jt. Surg. 134 (1978) 5–11.

[55] S. Kovac, Case Report Fifty-One-Year Survival of a Judet Polymethylmethacrylate Hip Prosthesis, 19 (2004) 664–667.

[56] F. Street, The History of the Royal Society of Medicine, (2002) 105–109.

[57] B. Walldius, Arthroplasty of the Knee Using an Endoprosthesis ARTHROPLASTY OF TI-fE KNEE, 6470 (2014).

[58] G. FH., Polycentric knee arthroplasty. Prosthetic simulation of normal knee movement, J Bone Jt. Surg Br. 53 (1971) 272–279.

[59] R.C. Insall J, Scott WN, The total condylar knee prosthesis. A report of two hundred and twenty cases, J Bone Jt. Surg Am. 61 (1979) 173–180.

[60] R. Trebše, A. Miheli, Joint Replacement : Historical Overview, (2012). doi:10.1007/978-1-4471-2482-5.

[61] Vamsi Krishna Balla, Mitun Das, Someswar Datta and Biswanath Kundu, Processing Techniques and Tribological Behavior of Composite Materials, in: 2015.

[62] B.V. Krishna, S. Bose, A. Bandyopadhyay, Low stiffness porous Ti structures for load-bearing implants, Acta Biomater. 3 (2007) 997–1006.

[63] S.R. Knight, R. Aujla, S.P. Biswas, Total Hip Arthroplasty - over 100 years of operative history, 3 (2011) 2–4.

[64] D.J.W. McMinn, J. Daniel, H. Ziaee, The best bearing couple for hip arthroplasty, Ann. R. Coll. Surg. Engl. 87 (2005) 411–418.

[65] G.P. Amstutz HC1, Metal on metal bearings in hip arthroplasty, Amstutz HC1, Grigoris P. 329 (1996) 11–34.

[66] S.L. Bizot P1, Nizard R, Hamadouche M, Hannouche D, Prevention of wear and osteolysis: alumina-on-alumina bearing, Clin Orthop Relat Res. 393 (2001) 85–93.

[67] C. JM, The rationale for metal-on-metal total hip arthroplasty, Clin Orthop Relat Res. 441 (2005) 132–138.

[68] G.T. Archibeck MJ1, Jacobs JJ, Roebuck KA, The basic science of periprosthetic osteolysis, Instr Course Lect. 50 (2001) 185–195.

[69] B. P., Total arthroplasty of the hip by fritted alumina prosthesis. Experimental study and 1st clinical applications, Orthop. Traumatol. Surg. Res. 100 (2014) 15–21.

[70] S.T. Tharani R1, Dorey FJ, The risk of cancer following total hip or knee arthroplasty, J Bone Jt. Surg Am. 83 (2001) 774–780.

[71] W.D. ierbaum BE, Nairus J, Kuesis D, Morrison JC, Ceramic-on-ceramic bearings in total hip arthroplasty, Clin Orthop Relat Res. 405 (2002) 158–163.

[72] C. PS, Biocompatibility of surgical-grade dense polycrystalline alumina, Clin Orthop

Relat Res. 282 (1992) 10–18.

[73] E.W. Paxton, O. Furnes, R.S. Namba, M.C. Inacio, A.M. Fenstad, L.I. Havelin, Comparison of the Norwegian Knee Arthroplasty Register and a United States Arthroplasty Registry, J. Bone Jt. Surgery-American Vol. 93 (2011) 20–30.

[74] G.X. Ni, W.W. Lu, K.Y. Chiu, Review article : Cemented or uncemented femoral component in primary total hip replacement ? A review from a clinical and radiological perspective, 13 (2005) 96–105.

[75] I.H.F. Reininga, W. Zijlstra, R. Wagenmakers, A.L. Boerboom, B.P. Huijbers, J.W. Groothoff, S.K. Bulstra, M. Stevens, Minimally invasive and computer-navigated total hip arthroplasty : a qualitative and systematic review of the literature, (2010).

[76] W.R.J. Archibeck MJ1, Learning curve for the two-incision total hip replacement., Clin Orthop Relat Res. 429 (2004) 232–240.

[77] K. Kieswetter, S. Antonio, Z. Schwartz, H. Hospital, S. Antonio, D.D. Dean, B.D. Boyan, S. Antonio, THE ROLE OF IMPLANT SURFACE CHARACTERISTICS, 7 (1996) 329–345.

[78] R.Z. Legeros, J.P. Legeros, Dense Hydroxyapatite, An Introd. to Bioceram. (1971) 139–179.

[79] S. Rujitanapanich, P. Kumpapan, P. Wanjanoi, Synthesis of hydroxyapatite from oyster shell via precipitation, Energy Procedia. 56 (2014) 112–117.

[80] P. Duheyne, J. Beight, J. Cuckler, B. Evans, S. Radin, Effect of calcium phosphate coating characteristics on early post-operative bone tissue ingrowth, Biomaterials. 11 (1990) 531–540.

[81] P. Buma, P.J.M. Van Loon, H. Versleyen, H. Weinans, T.J.J.H. Slooff, K. De Groot, R. Huiskes, Histological and biomechanical analysis of bone and interface reactions around hydroxyapatite-coated intramedullary implants of different stiffness: A pilot study on the goat, Biomaterials. 18 (1997) 1251–1260.

[82] K. Yamada, K. Imamura, H. Itoh, H. Iwata, S. Maruno, Bone bonding behavior of the hydroxyapatite containing glass-titanium composite prepared by the Cullet method, Biomaterials. 22 (2001) 2207–2214.

[83] F. Fazan, P.M. Marquis, Dissolution behavior of plasma-sprayed hydroxyapatite coatings, J. Mater. Sci. Mater. Med. 11 (2000) 787–792.

[84] P. A.E., H. L.W., R. V.B., S. M., The ultrastructure of the plasma-sprayed hydroxyapatite-bone interface predisposing to bone bonding, Biomaterials. 23 (2002) 725–733.

[85] G. William, Coating of implant with HA-material connections between bone and metal, Adv. Eng. Mater. 1 (1999) 95–105.

[86] Y. Cao, J.Y. Chen, J.M. Feng, X.D. Li, W.D. Tong, Z.J. Yang, X.D. Zhang, Effect of particle size on molten states of starting powder and degradation of the relevant plasma-sprayed hydroxyapatite coatings, Biomaterials. 17 (1996) 1507–1513.

[87] M.K.S.& D.B. A. Dey, A. K. Mukhopadhyay, S. Gangadharan, Development of Hydroxyapatite Coating by Microplasma Spraying, Mater. Manuf. Process. 24 (2009) 1321–1330.

[88] G.J.D. Shi, Coating of hydroxyapatite on highly porous Al2O3 substrate for bone substitutes, J. Biomed. Mater. Res. 43 (1998) 77–81.

[89] B.G.X. Zhang, D.E. Myers, G.G. Wallace, M. Brandt, P.F.M. Choong, Bioactive coatings for orthopaedic implants-recent trends in development of implant coatings, Int. J. Mol. Sci. 15 (2014) 11878–11921.

[90] M.T. Manley, J.R. Feinberg, Hydroxyapatite in Total Hip Arthroplasty, (1998) 200–211.

[91] J.P. Mcauley, E.S. Szuszczewicz, A. Young, C.A. Engh, Total Hip Arthroplasty in Patients 50 Years and Younger, 22306 (2004) 119–125.

[92] M.M. D'Antonio JA1, Capello WN, Crothers OD, Jaffe WL, Early clinical experience with hydroxyapatite-coated femoral implants, J Bone Jt. Surg Am. 74 (1992) 995–1008.

[93] B.Y.J.A.D. Antonio, M. Township, W.N. Capello, F. Lakes, Remodeling of Bone around

Hydroxyapatite-Coated Femoral Stems *, (1996) 1226–1234.

[94] Joanna Maggs and Matthew Wilson, The Relative Merits of Cemented and Uncemented Prostheses in Total Hip Arthroplasty, Indian J Orthop. 2017 Jul-Aug; 51(4): 377–385.

[95] Edword J Mcpheron, Hydroxyapatite-coated proximal ingrowth femur stem, clinical othopeaadics and realted resaerch, June 1995, PP, 315.

[96] O. Rahbek, S. Overgaard, M. Lind, K. Bendix, C. Bünger, K. Soballe, Sealing effect of hydroxyapatite coating on peri-implant migration of particles. An experimental study in dogs., J. Bone Jt. Surg. Br. Vol. 83 (2001) 441–447.

[97] O. Kaygili, S. Keser, Zr / Mg , Zr / Sr and Zr / Zn co-doped hydroxyapatites : Synthesis and characterization, 42 (2016) 9270–9273.

[98] N. Patel, S.M. Best, W. Bonfield, R.F. Campus, R.H. Street, <Patel 2002 Fluorochrome Bone Labelling.Pdf>, 3 (2002) 1199–1206.

[99] A.E. Porter, C.M. Botelho, M.A. Lopes, J.D. Santos, S.M. Best, W. Bonfield, Ultrastructural comparison of dissolution and apatite precipitation on hydroxyapatite and silicon-substituted hydroxyapatite in vitro and in vivo, J. Biomed. Mater. Res. - Part A. 69 (2004) 670–679.

[100] T. Leventouri, C.E. Bunaciu, V. Perdikatsis, Neutron powder diffraction studies of silicon-substituted hydroxyapatite, Biomaterials. 24 (2003) 4205–4211.

[101] 3 W. Bonfield C.M. Botelho,1,2 R.A. Brooks,3 S.M. Best,4 M.A. Lopes,1,2 J.D. Santos,1,2 N. Rushton, Human osteoblast response to silicon-substituted hydroxyapatite, Wiley Intersci. (2006).

[102] G. Gasquères, C. Bonhomme, J. Maquet, F. Babonneau, S. Hayakawa, T. Kanaya, A. Osaka, Revisiting silicate substituted hydroxyapatite by solid-state NMR, Magn. Reson. Chem. 46 (2008) 342–346.

[103] A. Aminian, M. Solati-Hashjin, A. Samadikuchaksaraei, F. Bakhshi, F. Gorjipour, A. Farzadi, F. Moztarzadeh, M. Schmücker, Synthesis of silicon-substituted hydroxyapatite

by a hydrothermal method with two different phosphorous sources, Ceram. Int. 37 (2011) 1219–1229.

[104] E. Zhang, C. Zou, S. Zeng, Preparation and characterization of silicon-substituted hydroxyapatite coating by a biomimetic process on titanium substrate, Surf. Coatings Technol. 203 (2009) 1075–1080.

[105] H.M. da Silva, M. Mateescu, C. Damia, E. Champion, G. Soares, K. Anselme, Importance of dynamic culture for evaluating osteoblast activity on dense silicon-substituted hydroxyapatite, Colloids Surfaces B Biointerfaces. 80 (2010) 138–144.

[106] E. Landi, G. Logroscino, L. Proietti, A. Tampieri, M. Sandri, S. Sprio, Biomimetic Mg-substituted hydroxyapatite: From synthesis to in vivo behaviour, J. Mater. Sci. Mater. Med. 19 (2008) 239–247.

[107] Robert K.RudeaHelen E.Gruberb, Magnesium deficiency and osteoporosis: animal and human observations, Https://Www.Sciencedirect.Com/Science/Journal/09552863. 15 (2004) 710–716.

[108] W.L. Suchanek, K. Byrappa, P. Shuk, R.E. Riman, V.F. Janas, K.S. Tenhuisen, Preparation of magnesium-substituted hydroxyapatite powders by the mechanochemical-hydrothermal method, Biomaterials. 25 (2004) 4647–4657.

[109]K.Yasukawa1*T.Akihisa2Y.Kasahara3M.Ukiya2K.Kumaki3T.Tamura2S.Yamanouchi1M. Takido1, Inhibitory effect of heliantriol C; a component of edible Chrysanthemum, on tumor promotion by 12-O-tetradecanoylphorbol-13-acetate in two-stage carcinogenesis in mouse skin, Phytomedicine. 5 (1998) 215–218.

[110] F. Ren, Y. Leng, R. Xin, X. Ge, Synthesis, characterization and ab initio simulation of magnesium-substituted hydroxyapatite, Acta Biomater. 6 (2010) 2787–2796.

[111] M. Mehrjoo, J. Javadpour, M.A. Shokrgozar, M. Farokhi, S. Javadian, S. Bonakdar, Effect of magnesium substitution on structural and biological properties of synthetic hydroxyapatite powder, Mater. Express. 5 (2015) 41–48.

[112] I.R. Gibson, W. Bonfield, Preparation and characterization of magnesium / carbonate co-

substituted hydroxyapatites, 3 (2002) 685–693.

[113] Z.Y. Li, W.M. Lam, C. Yang, B. Xu, G.X. Ni, S.A. Abbah, K.M.C. Cheung, K.D.K. Luk, W.W. Lu, Chemical composition, crystal size and lattice structural changes after incorporation of strontium into biomimetic apatite, Biomaterials. 28 (2007) 1452–1460.

[114] E. Landi, S. Sprio, M. Sandri, G. Celotti, A. Tampieri, Development of Sr and CO3co-substituted hydroxyapatites for biomedical applications, Acta Biomater. 4 (2008) 656–663.

[115] C. Rey, C. Combes, C. Drouet, H. Sfihi, A. Barroug, Physico-chemical properties of nanocrystalline apatites: Implications for biominerals and biomaterials, Mater. Sci. Eng. C. 27 (2007) 198–205.

[116] C.M. Mardziah, I. Sopyan, S. Ramesh, Strontium-doped hydroxyapatite nanopowder via sol-gel method: Effect of strontium concentration and calcination temperature on phase behavior, Trends Biomater. Artif. Organs. 23 (2009) 105–113.

[117] Sooboo Singh and Sreekanth B. Jonnalagadda, Synthesis and thermally stable metal substituted hydroxyapatites for the selective oxidation of light paraffins, Bull. Chem. Soc. Ethiop. 27 (2013) 57–68.

[118] E. Boanini, M. Gazzano, A. Bigi, Ionic substitutions in calcium phosphates synthesized at low temperature, Acta Biomater. 6 (2010) 1882–1894.

[119] M.J.J. Kashmira P. Tank, Bhoomika V. Jogiya, Dinesh K. Kanchan, Dielectric Properties of Pure and Strontium Doped Nano-Hydroxyapatite, Solid State Phenom. 209 (2013).

[120] K. P. Tank P. Sharma D. K. Kanchan M. J. Joshi, FTIR, powder XRD, TEM and dielectric studies of pure and zinc doped nano-hydroxyapatite, Cryst. Res. Technol. 46 (2011) 1309–1316.

[121] R. AL-Wafi, Ferroelectric properties of Sr doped hydroxyapatite bioceramics for biotechnological applications, J. Alloys Compd. 689 (2016) 169–173.

[122] E. Landi, A. Tampieri, G. Celotti, S. Sprio, M. Sandri, G. Logroscino, Sr-substituted

hydroxyapatites for osteoporotic bone replacement, Acta Biomater. 3 (2007) 961–969.

[123] H.W. Kim, Y.H. Koh, Y.M. Kong, J.G. Kang, H.E. Kim, Strontium substituted calcium phosphate biphasic ceramics obtained by a powder precipitation method, J. Mater. Sci. Mater. Med. 15 (2004) 1129–1134.

[124] O. Kaygili, S. Keser, M. Kom, Y. Eroksuz, S. V. Dorozhkin, T. Ates, I.H. Ozercan, C. Tatar, F. Yakuphanoglu, Strontium substituted hydroxyapatites: Synthesis and determination of their structural properties, in vitro and in vivo performance, Mater. Sci. Eng. C. 55 (2015) 538–546.

[125] V. Stanić, S. Dimitrijević, J. Antić-Stanković, M. Mitrić, B. Jokić, I.B. Plećaš, S. Raičević, Synthesis, characterization and antimicrobial activity of copper and zinc-doped hydroxyapatite nanopowders, Appl. Surf. Sci. 256 (2010) 6083–6089.

[126] D.R. Ergun C1, Webster TJ, Bizios R, Hydroxylapatite with substituted magnesium, zinc, cadmium, and yttrium. I. Structure and microstructure., J Biomed Mater Res. 59 (2002) 305–311.

[127] S.S. and E.K.G. G. Suresh Kumar, A. Thanizhavel, Y. Yokogawa, Synthesis and characterization and in vitro studies of zinc and carbonate co-substituted mono-hydroxyapatite for biomedical applications, Mater. Chem. Phy. 134 (2012) 1127–1135.

[128] F. Miyaji, Y. Kono, Y. Suyama, Formation and structure of zinc-substituted calcium hydroxyapatite, Mater. Res. Bull. 40 (2005) 209–220.

[129] A. Bigi, Inhibiting Effect of Zinc on Hydroxyapatite Crystallization, J. Inorg. Biochem. 58 (1995) 49–58.

[130] T.T. Ito A1, Ojima K, Naito H, Ichinose N, Preparation, solubility, and cytocompatibility of zinc-releasing calcium phosphate ceramics, J Biomed Mater Res. 50 (2000) 178–183.

[131] F. Ren, R. Xin, X. Ge, Y. Leng, Characterization and structural analysis of zinc-substituted hydroxyapatites, Acta Biomater. 5 (2009) 3141–3149.

[132] I. Uysal, F. Severcan, A. Tezcaner, Z. Evis, Co-doping of hydroxyapatite with zinc and

fluoride improves mechanical and biological properties of hydroxyapatite, Prog. Nat. Sci. Mater. Int. 24 (2014) 340–349.

[133] Y. Tang, H.F. Chappell, M.T. Dove, R.J. Reeder, Y.J. Lee, Zinc incorporation into hydroxylapatite, Biomaterials. 30 (2009) 2864–2872.

[134] A. Bandyopadhyay, E.A. Withey, J. Moore, S. Bose, Influence of ZnO doping in calcium phosphate ceramics, Mater. Sci. Eng. C. 27 (2007) 14–17.

[135] J. Terra, M. Jiang, D.E. Ellis, Characterization of electronic structure and bonding in hydroxyapatite: Zn substitution for Ca, Philos. Mag. A Phys. Condens. Matter, Struct. Defects Mech. Prop. 82 (2002) 2357–2377.

[136] T.J. Webster, E.A. Massa-Schlueter, J.L. Smith, E.B. Slamovich, Osteoblast response to hydroxyapatite doped with divalent and trivalent cations, Biomaterials. 25 (2004) 2111–2121.

[137] M. Li, X. Xiao, R. Liu, C. Chen, L. Huang, Structural characterization of zinc-substituted hydroxyapatite prepared by hydrothermal method, J. Mater. Sci. Mater. Med. 19 (2008) 797–803.

[138] S.C. Cox, P. Jamshidi, L.M. Grover, K.K. Mallick, Preparation and characterisation of nanophase Sr, Mg, and Zn substituted, 35 (2014) 106–114.

[139] H. Esfahani, E. Salahi, A. Tayebifard, M.R. Rahimipour, M. Keyanpour-Rad, Structural and morphological analysis of zinc incorporated non-stoichiometric hydroxyapatite nano powders, Rev. Mater. 21 (2016) 569–576.

[140] M. Mirzaee, M. Vaezi, Y. Palizdar, Synthesis and characterization of silver doped hydroxyapatite nanocomposite coatings and evaluation of their antibacterial and corrosion resistance properties in simulated body fluid, Mater. Sci. Eng. C. 69 (2016) 675–684.

[141] C.S. Ciobanu, S.L. Iconaru, I. Pasuk, B.S. Vasile, A.R. Lupu, A. Hermenean, A. Dinischiotu, D. Predoi, Structural properties of silver doped hydroxyapatite and their biocompatibility, Mater. Sci. Eng. C. 33 (2013) 1395–1402.

[142] B.J.H. In Deok Kim, Paeoniflorin protects RAW 264.7 macrophages from LPS-induced cytotoxicity and genotoxicity, Toxicol. Vitr. 23 (2009) 1014–1019.

[143] V.Y.I. a A.A. Yanovska a,□ , A.S. Stanislavov a, L.B. Sukhodub c, V.N. Kuznetsov a, L.F.S. S.N. Danilchenko a, Silver-doped hydroxyapatite coatings formed on Ti–6Al–4V substrates and their characterization, Mater. Sci. Eng. C. 36 (2014) 215–220.

[144] 4 K. Prasad Rao N. Rameshbabu, 1 T.S. Sampath Kumar, 1 T.G. Prabhakar, 2 V.S. Sastry, 3 K.V.G.K. Murty, Antibacterial nanosized silver substituted hydroxyapatite: Synthesis and characterization, Wiley Intersci. (2006).

[145] H.R. Bakhsheshi-Rad, E. Hamzah, M. Daroonparvar, M.A.M. Yajid, M. Kasiri-Asgarani, M.R. Abdul-Kadir, M. Medraj, In-vitro degradation behavior of Mg alloy coated by fluorine doped hydroxyapatite and calcium deficient hydroxyapatite, Oral Oncol. 50 (2014) 2516–2528.

[146] C.J. Tredwin, A.M. Young, E.A. Abou Neel, G. Georgiou, J.C. Knowles, Hydroxyapatite, fluor-hydroxyapatite and fluorapatite produced via the sol-gel method: Dissolution behaviour and biological properties after crystallisation, J. Mater. Sci. Mater. Med. 25 (2014) 47–53.

[147] A. Joseph Nathanael, D. Mangalaraj, S.I. Hong, Y. Masuda, Y.H. Rhee, H.W. Kim, Influence of fluorine substitution on the morphology and structure of hydroxyapatite nanocrystals prepared by hydrothermal method, Mater. Chem. Phys. 137 (2013) 967–976.

[148] H. Eslami, M. Solati-Hashjin, M. Tahriri, The comparison of powder characteristics and physicochemical, mechanical and biological properties between nanostructure ceramics of hydroxyapatite and fluoridated hydroxyapatite, Mater. Sci. Eng. C. 29 (2009) 1387–1398.

[149] I. Zofkova, M. Davis, J. Blahos, Trace elements have beneficial, as well as detrimental effects on bone homeostasis., Physiol. Res. 66 (2017) 391–402. doi:10.1007/978-3-319-59387-6_28.

[150] S. V. Dorozhkin, Nanodimensional and Nanocrystalline Calcium Orthophosphates, Am. J. Biomed. Eng. 2 (2012) 48–97.

[151] D.G. Anderson, D. Putnam, E.B. Lavik, T.A. Mahmood, R. Langer, Biomaterial microarrays: Rapid, microscale screening of polymer-cell interaction, Biomaterials. 26 (2005) 4892–4897.

[152] N.D. Ravi, R. Balu, T.S. Sampath Kumar, Strontium-substituted calcium deficient hydroxyapatite nanoparticles: Synthesis, characterization, and antibacterial properties, J. Am. Ceram. Soc. 95 (2012) 2700–2708.

[153] I. Uysal, F. Severcan, A. Tezcaner, Z. Evis, Co-doping of hydroxyapatite with zinc and fluoride improves mechanical and biological properties of hydroxyapatite, Prog. Nat. Sci. Mater. Int. 24 (2014) 340–349.

[154] C.F. Kim TN1, Feng QL, Kim JO, Wu J, Wang H, Chen GC, Antimicrobial effects of metal ions (Ag+, Cu2+, Zn2+) in hydroxyapatite., Med., J Mater Sci Mater. 9 (1998) 129–134.

[155] A. Khan, M.H. Shah, M. Nauman, I. Hakim, G. Shahid, P. Niaz, H. Sethi, S. Aziz, M. Arabdin, Clinical manifestations of patients with Systemic Lupus Erythematosus (SLE) in Khyber Pakhtunkhwa, J. Pak. Med. Assoc. 67 (2017) 1180–1185.

[156] K.& T. Sygnatowicz, M., Keyshar, Antimicrobial properties of silver-doped hydroxyapatite nano-powders and thin films, A. JOM. 62 (2010) 65–70.

[157] G.A. Fielding, M. Roy, A. Bandyopadhyay, S. Bose, Antibacterial and biological characteristics of silver containing and strontium doped plasma sprayed hydroxyapatite coatings, Acta Biomater. 8 (2012) 3144–3152.

[158] MasayoshiYamaguchiRieYamaguchi, Action of zinc on bone metabolism in rats: Increases in alkaline phosphatase activity and DNA content, Biochem. Pharmacol. 35 (1986) 773–777.

[159] M. Turkoz, A.O. Atilla, Z. Evis, Silver and fluoride doped hydroxyapatites: Investigation by microstructure, mechanical and antibacterial properties, Ceram. Int. 39 (2013) 8925–8931.

[160] J.R. Ramya, K.T. Arul, K. Elayaraja, S.N. Kalkura, Physicochemical and biological

properties of iron and zinc ions co-doped nanocrystalline hydroxyapatite, synthesized by ultrasonication, Ceram. Int. 40 (2014) 16707–16717.

[161] T.T. Kawamura H1, Ito A, Miyakawa S, Layrolle P, Ojima K, Ichinose N, Stimulatory effect of zinc-releasing calcium phosphate implant on bone formation in rabbit femora, J Biomed Mater Res. 50 (2000) 184–190.

[162] and S.N.K. V. Sarath Chandra, Ganga Baskar, R. V. Suganthi, K. Elayaraja, M. I. Ahymah Joshy, W. Sofi Beaula, R. Mythili, Ganesh Venkatraman, Blood Compatibility of Iron-Doped Nanosize Hydroxyapatite and Its Drug Release, ACS Appl. Mater. Interfaces. 4 (2012) 1200–1210.

[163] M.H. Chen, T. Yoshioka, T. Ikoma, N. Hanagata, F.H. Lin, J. Tanaka, Photoluminescence and doping mechanism of theranostic Eu3+/Fe3+dual-doped hydroxyapatite nanoparticles, Sci. Technol. Adv. Mater. 15 (2014).

[164] S. Bodhak, S. Bose, A. Bandyopadhyay, Bone cell-material interactions on metal-ion doped polarized hydroxyapatite, Mater. Sci. Eng. C. 31 (2011) 755–761.

[165] J. Gao, M. Wang, C. Shi, L. Wang, Y. Zhu, D. Wang, A facile green synthesis of trace Si, Sr and F multi-doped hydroxyapatite with enhanced biocompatibility and osteoconduction, Mater. Lett. 196 (2017) 406–409. doi:10.1016/j.matlet.2017.03.054.

[166] M. Furko, V. Havasi, Z. Kónya, A. Grünewald, R. Detsch, A.R. Boccaccini, C. Balázsi, Development and characterization of multi-element doped hydroxyapatite bioceramic coatings on metallic implants for orthopedic applications, Bol. La Soc. Esp. Ceram. y Vidr. 57 (2018) 55–65.

[167] D. Gopi, E. Shinyjoy, L. Kavitha, Influence of ionic substitution in improving the biological property of carbon nanotubes reinforced hydroxyapatite composite coating on titanium for orthopedic applications, Ceram. Int. 41 (2015) 5454–5463.

[168] K.Y. Soichiro Itoh, Satoshi Nakamura, Takayuki Kobayashi, Kenichi Shinomiya, The Effects of Electrically Polarized Hydroxyapatite on Osteogenic Cell Activity and Bone Formation, Key Eng. Mater. 309–311 (2006) 15.

[169] P.M. Meaney, T. Zhou, D. Goodwin, A. Golnabi, E.A. Attardo, K.D. Paulsen, Bone dielectric property variation as a function of mineralization at microwave frequencies, Int. J. Biomed. Imaging. 2012 (2012).

[170] S. Grimnes, O. Rikshospitalet, N.H.P. Schwan, Interface phenomena and dielectric properties of biological tissue, Encycl. Surf. Colloid Sci. 20 (2002) 2643–2653. doi:10.1081/E-ESCS-120000618.

[171] Timothy P. Hoepfner Eldon D. Case, The porosity dependence of the dielectric constant for sintered hydroxyapatite, J. Biomed. Mater. Res. 60 (2002) 643–650.

[172] O. Kaygili, S. Keser, T. Ates, A.A. Al-Ghamdi, F. Yakuphanoglu, Controlling of dielectrical and optical properties of hydroxyapatite based bioceramics by Cd content, Powder Technol. 245 (2013) 1–6.

[173] C. Zhang, C. Li, S. Huang, Z. Hou, Z. Cheng, P. Yang, C. Peng, J. Lin, Self-activated luminescent and mesoporous strontium hydroxyapatite nanorods for drug delivery, Biomaterials. 31 (2010) 3374–3383.

[174] P. Yang, Z. Quan, C. Li, X. Kang, H. Lian, J. Lin, Bioactive, luminescent and mesoporous europium-doped hydroxyapatite as a drug carrier, Biomaterials. 29 (2008) 4341–4347. doi:10.1016/j.biomaterials.2008.07.042.

[175] D.G. Guo, A.H. Wang, Y. Han, K.W. Xu, Characterization, physicochemical properties and biocompatibility of La-incorporated apatites, Acta Biomater. 5 (2009) 3512–3523.

[176] S. Han, Yingchao; Wang, Xinyu; Li, Biocompatible Europium Doped Hydroxyapatite Nanoparticles as a Biological Fluorescent Probe, Curr. Nanosci. 6 (2010) 178–183.

[177] F. Chen, P. Huang, Y.J. Zhu, J. Wu, C.L. Zhang, D.X. Cui, The photoluminescence, drug delivery and imaging properties of multifunctional Eu3+/Gd3+dual-doped hydroxyapatite nanorods, Biomaterials. 32 (2011) 9031–9039.

[178] M.P. Mahabole, M.M. Bahir, N. V Kalyankar, R.S. Khairnar, Effect of incubation in simulated body fluid on dielectric and photoluminescence properties of nano-hydroxyapatite ceramic doped with strontium ions, J. Biomed. Sci. Eng. 5 (2012) 396–

405.

[179] G. Gonzalez, C. Costa-Vera, L.J. Borrero, D. Soto, L. Lozada, J.I. Chango, J.C. Diaz, L. Lascano, Effect of carbonates on hydroxyapatite self-activated photoluminescence response, J. Lumin. 195 (2018) 385–395.

[180] P. J. Ross, Taguchi Techniques for quality Engineering, McGraw-Hill, New York, 1988.

[181] Y.W. G. Taguchi, S. Chowdhury, Taguchi's Quality Engineering Handbook, 2004. doi:doi:10.1002/9780470258354.

[182] B. Vamsi Krishna, P. Venugopal, K. Prasad Rao, Analysis of deformation during simultaneous plastic deformation of dissimilar powder metallurgical preforms, Powder Technol. 146 (2004) 137–146.

[183] S. Athreya, Y.D. Venkatesh, Application Of Taguchi Method For Optimization Of Process Parameters In Improving The Surface Roughness Of Lathe Facing Operation, Int. Ref. J. Eng. Sci. 1 (2012) 13–19.

[184] W. Turning, E.N. Steel, Taguchi Method and Anova: an Approach for Process Parameters Optimization of Wet Turning Operation While Turning En 353 Steel, Int. J. Adv. Res. Eng. Technol. 68 (2013) 1–7.

[185] B. Kundu, M.K. Sinha, M.K. Mitra, D. Basu, Fabrication and characterization of porous hydroxyapatite ocular implant followed by an in vivo study in dogs, Bull. Mater. Sci. 27 (2004) 133–140.

[186] Y.X. Pang, X. Bao, Influence of temperature, ripening time and calcination on the morphology and crystallinity of hydroxyapatite nanoparticles, J. Eur. Ceram. Soc. 23 (2003) 1697–1704.

[187] J.H. Kim, S.H. Kim, H.K. Kim, T. Akaike, S.C. Kim, Synthesis and characterization of hydroxyapatite crystals: A review study on the analytical methods, J. Biomed. Mater. Res. 62 (2002) 600–612.

[188] Z.S. Tao, W.S. Zhou, X.W. He, W. Liu, B.L. Bai, Q. Zhou, Z.L. Huang, K.K. Tu, H. Li,

T. Sun, Y.X. Lv, W. Cui, L. Yang, A comparative study of zinc, magnesium, strontium-incorporated hydroxyapatite-coated titanium implants for osseointegration of osteopenic rats, Mater. Sci. Eng. C. 62 (2016) 226–232.

[189] M. Turkoz, A.O. Atilla, Z. Evis, Silver and fluoride doped hydroxyapatites: Investigation by microstructure, mechanical and antibacterial properties, Ceram. Int. 39 (2013) 8925–8931.

[190] G. Taguchi, S. Chowdhury, Y. Wu, Taguchi's Quality Engineering Handbook, 2004.

[191] W. Zhang, Y. Shen, H. Pan, K. Lin, X. Liu, B.W. Darvell, W.W. Lu, J. Chang, L. Deng, D. Wang, W. Huang, Effects of strontium in modified biomaterials, Acta Biomater. 7 (2011) 800–808.

[192] S.C. Cox, P. Jamshidi, L.M. Grover, K.K. Mallick, Preparation and characterisation of nanophase Sr, Mg, and Zn substituted hydroxyapatite by aqueous precipitation, Mater. Sci. Eng. C. 35 (2014) 106–114.

[193] A. Bigi, E. Boanini, C. Capuccini, M. Gazzano, Strontium-substituted hydroxyapatite nanocrystals, Inorganica Chim. Acta. 360 (2007) 1009–1016.

[194] A.K. Panda, R.K. Singh, Optimization of Process Parameters by Taguchi Method : Catalytic degradation of polypropylene to liquid fuel, Int. J. Multidiscip. Curr. Res. (2013) 50–58.

[195] B. Basar, A. Tezcaner, D. Keskin, Z. Evis, Improvements in microstructural, mechanical, and biocompatibility properties of nano-sized hydroxyapatites doped with yttrium and fluoride, Ceram. Int. 36 (2010) 1633–1643.

[196] Z. Zhang, B. Gu, W. Zhang, G. Kan, J. Sun, The enhanced characteristics of osteoblast adhesion to porous Zinc-TiO 2 coating prepared by plasma electrolytic oxidation, Appl. Surf. Sci. 258 (2012) 6504–6511.

[197] S. Dasgupta, S.S. Banerjee, A. Bandyopadhyay, S. Bose, Zn- and Mg-doped hydroxyapatite nanoparticles for controlled release of protein, Langmuir. 26 (2010) 4958–4964.

[198] N.C. Reger, A.K. Bhargava, R. Itishree, B. Kundu, V.K. Balla, Structural and phase analysis of multi-ion doped hydroxyapatite for biomedical applications, Ceram. Int. (2018).

[199] J.R. Nilsson, How cytotoxic is zinc? A study on effects of zinc on cell proliferation, endocytosis, and fine structure of the ciliate Tetrahymena, Acta Protozool. 42 (2003) 19–29.

[200] N. Hanagata, H. Morita, Calcium ions rescue human lung epithelial cells from the toxicity of zinc oxide nanoparticles., J. Toxicol. Sci. 40 (2015) 625–635.

[201] Y. Liu, H. Zhu, H. Hong, W. Wang, F. Liu, Can zinc protect cells from the cytotoxic effects of cobalt ions and nanoparticles derived from metal-on-metal joint arthroplasties?, Bone Jt. Res. 6 (2017) 649–655.

[202] Z. Saidak, P.J. Marie, Strontium signaling: Molecular mechanisms and therapeutic implications in osteoporosis, Pharmacol. Ther. 136 (2012) 216–226.

[203] M.D. O'Donnell, P.L. Candarlioglu, C.A. Miller, E. Gentleman, M.M. Stevens, Materials characterisation and cytotoxic assessment of strontium- substituted bioactive glasses for bone regeneration, J. Mater. Chem. 20 (2010) 8934–8941.

[204] Y. Huang, X. Zhang, H. Qiao, M. Hao, H. Zhang, Z. Xu, X. Zhang, X. Pang, H. Lin, Corrosion resistance and cytocompatibility studies of zinc-doped fluorohydroxyapatite nanocomposite coatings on titanium implant, Ceram. Int. 42 (2016) 1903–1915.

[205] A. Peetsch, C. Greulich, D. Braun, C. Stroetges, H. Rehage, B. Siebers, M. Köller, M. Epple, Silver-doped calcium phosphate nanoparticles: Synthesis, characterization, and toxic effects toward mammalian and prokaryotic cells, Colloids Surfaces B Biointerfaces. 102 (2013) 724–729.

[206] D.R. Monteiro, L.F. Gorup, A.S. Takamiya, A.C. Ruvollo-Filho, E.R. de Camargo, D.B. Barbosa, The growing importance of materials that prevent microbial adhesion: antimicrobial effect of medical devices containing silver, Int. J. Antimicrob. Agents. 34 (2009) 103–110.

[207] J.P. Gittings, C.R. Bowen, A.C.E. Dent, I.G. Turner, F.R. Baxter, J.B. Chaudhuri, Electrical characterization of hydroxyapatite-based bioceramics, Acta Biomater. 5 (2009) 743–754.

[208] M.P.F. Prezas, P. R.; Melo, B. M. G.; Costa, L. C.; Valente, M. A.; Lança, M. C.; Ventura, J. M. G.; Pinto, L. F. V.; Graça, TSDC and impedance spectroscopy measurements on hydroxyapatite, β-tricalcium phosphate and hydroxyapatite/β-tricalcium phosphate biphasic bioceramics, Appl. Surf. Sci. 424 (2017) 28–38.

[209] T.G.M. Bonadio, V.F. Freitas, T.T. Tominaga, R.Y. Miyahara, J.M. Rosso, L.F. Cótica, M.L. Baesso, W.R. Weinand, I.A. Santos, R. Guo, A.S. Bhalla, P.R. Prezas, B.M.G. Melo, L.C. Costa, M.A. Valente, M.C. Lança, J.M.G. Ventura, L.F.V. Pinto, M.P.F. Graça, TSDC and impedance spectroscopy measurements on hydroxyapatite, β-tricalcium phosphate and hydroxyapatite/β-tricalcium phosphate biphasic bioceramics, Appl. Surf. Sci. 424 (2017) 1–7.

APPENDICES

Table 1 ANOVA table for density measurement

Factor	DF	Adj SS	Adj MS	F value	P value	% contribution (R square)
Sr	2	0.002756	0.001378	0.69	0.536	18.76
Zn	2	0.001622	0.000811	0.37	0.704	11.04
Ag	2	0.000156	0.000078	0.03	0.969	1.06
F	2	0.010156	0.005078	6.72	0.029	69.14

Table 2 ANOVA table for hardness measurement

Factor	DF	Adj SS	Adj MS	F value	P value	% contribution (R square)
Sr	2	2.376	1.1878	2.71	0.145	47.69
Zn	2	0.2756	0.1378	0.17	0.844	5.66
Ag	2	0.08222	0.04111	0.05	0.952	1.45
F	2	2.276	1.1378	2.50	0.163	45.21

Table 3 ANOVA table for crystallinity optimization

Factor	DF	Adj SS	Adj MS	F value	P value	% contribution (R square)
Sr	2	116.2	58.11	2.51	0.161	19.97
Zn	2	67.56	33.78	1.08	0.397	7.93
Ag	2	20.22	10.11	0.26	0.780	26.50
F	2	50.89	25.44	0.75	0.513	19.97

Table 4 ANOVA table for crystallite size optimization

Factor	DF	Adj SS	Adj MS	F value	P value	% contribution (R square)
Sr	2	294.9	147.44	1.84	0.238	38.06
Zn	2	168.2	84.11	0.83	0.480	21.71
Ag	2	180.2	90.11	0.91	0.452	23.26
F	2	131.6	65.78	0.61	0.572	16.98

Table 5 ANOVA table for Cell proliferation optimization for 03 days

Factor	DF	Adj SS	Adj MS	F value	P value	% contribution (R square)
Sr	2	5514	2757	0.44	0.663	12.81
Zn	2	2083	1041	0.15	0.862	4.84
Ag	2	1307	653.4	0.09	0.912	3.09
F	2	34147	17073	11.51	0.009	79.32

Table 6 ANOVA table for Cell proliferation optimization 05 days

Factor	DF	Adj SS	Adj MS	F value	P value	% contribution (R square)
Sr	2	13856	6928	0.75	0.510	20.09
Zn	2	24841	12420	1.69	0.262	36.02
Ag	2	4813	2406	0.23	0.805	6.98
F	2	25459	12729	1.76	0.251	36.91

Table 7 ANOVA table for Cell proliferation optimization 07 days

Factor	DF	Adj SS	Adj MS	F value	P value	% contribution (R square)
Sr	2	1393	696.4	1.96	0.221	39.56
Zn	2	278.2	139.1	0.26	0.781	7.90
Ag	2	1563	781.4	2.39	0.172	44.39
F	2	286.9	143.4	0.27	0.775	8.15

Table 8 ANOVA table for optimization of dielectric constant

Factor	DF	Adj SS	Adj MS	F value	P value	% contribution (R square)
Sr	2	1.605	0.8025	0.17	0.851	5.25
Zn	2	10.42	5.209	1.55	0.286	34.46
Ag	2	10.53	5.266	1.58	0.282	34.06
F	2	8.008	4.004	1.07	0.402	26.20

Table 9 ANOVA table for optimization of photoluminescence (PL) intensity

Factor	DF	Adj SS	Adj MS	F value	P value	% contribution (R square)
Sr	2	75347254	37673627	0.17	0.848	5.35
Zn	2	817707764	408853882	4.15	0.074	58.03
Ag	2	349944924	174972462	0.99	0.425	24.83
F	2	166080684	83040342	0.40	0.686	11.79

BRIEF BIO-DATA OF NIMU CHAND REGER

1. Details of Educational Qualification

Degrees	Specialization	Board/University	Passing	Class/Division	Marks /CGPA
UG (B.Tech)	Metallurgical Engineering	Malaviya National Institute of Technology (MNIT) Jaipur	2008	I	6.99~7.0
PG (M.Tech)	Metallurgical and materials Engineering	Malaviya National Institute of Technology (MNIT) Jaipur	2014	I	8.80
Ph.D.	Metallurgical and materials Engineering	Malaviya National Institute of Technology (MNIT) Jaipur	2014-2019	I	8.33

2. Research Activities: Paper publications in National / International Journals

S.No.	Title of paper	Author(s)	Name of the Journal	Vol. & Year	Pages
1	Structural and phase analysis of multi-ion doped hydroxyapatite for biomedical applications	Nimu Chand Reger, Anil Kumar Bhargava, Itishree Ratha, Biswanath Kundu, Vamsi Krishna Balla	Ceramics International	45 (2019)	252-263
2	Wear and corrosion properties of in-situ grown zirconium nitride layers for implant applications	Nimu Chand Reger, Vamsi Krishna Balla, Mitun Das, Anil Kumar Bhargava,	Surface & Coatings Technology	334 (2018)	357–364
3	In vitro cytotoxicity and ion release of multi-ion doped hydroxyapatite	Nimu Chand Reger, Biswanath Kundu, Vamsi Krishna Balla, Anil Kumar Bhargava	International Journal of Applied Ceramic Technology 16 (2), 503-516	1(2018)	1-14

3. Paper Publications in Conference

S.No.	Title of paper	Co-author(s), if any	Name of the Conference	Date
1.	Synthesis Techniques for Hydroxyapatite :an overview	Nimu Chand Reger, Bhawna Jarwal, A. K. Bhargava	Advanced functional Materials & their application (AFMA)	Dec,11-12, 2015
2	Techniques for Hydroxyapatite synthesis	Nimu Chand Reger, Bhawna jarwal, A K Bhargava	Advanced Materials & Processing	December 2-4, 2015
3	"Wear Behaviour of *In-situ* grown ceramic film on Zirconium for orthopadeic implants	Nimu Chand Reger, A. K. Bhargva, Vamsi Krishna Balla	Advanced Materials & Processing	December 2-4, 2015

4. Short term courses attended during Ph.D. (2014-2019)

S.No.	From	To	Institute/ Organization	Sponsored by	Name of the course
1	07-12-2015	11-12-2015	Dept of Material Science and Engineering IIT Kanpur	QIP	Biomaterials and its Applications
2	04-05-2015	08-05-2015	Dept of MME, MNIT Jaipur	ASM Materials Education foundation	ASM Materials Camp
3	09-10-2017	13-10-2017	Dept of Chemical and Mechanical, MNIT Jaipur	TEQIP-III	Applied Statistics for Experiments"
4	29-01-2018	02-02-2018	Dept of Mechanical Engg	TEQIP-III	Protective Coatings: Low friction and wear
5	19-02-2018	23-02-2018	Dept of MME &MRC, MNIT Jaipur	TEQIP-III	Electron Microscopy
6	11-02-2019	15-02-2019	MRC, MNIT Jaipur	TEQIP-III	Nanostructure-Nanoparticles & thin films :synthesis and characterization